FACULTY OF SCIENCE
UNIVERSITY OF COPENHAGEN

Unforced climate transitions as a scenario for Dansgaard-Oeschger events

Hannah Kleppin

PhD thesis supervised by
Prof. Dr. Markus Jochum

This thesis has been submitted to the PhD School of
The Faculty of Science, University of Copenhagen, February 4th 2016

Fuata mto uone bahari

Abstract

An unforced pre-industrial control simulation of the Community Climate System Model 4 (CCSM4) is found to have Greenland warming and cooling events that resemble Dansgaard-Oeschger-cycles in pattern and magnitude. With the caveat that only 3 transitions were available to be analyzed, we find that the transitions are triggered by stochastic atmospheric forcing. The atmospheric anomalies change the strength of the subpolar gyre, leading to a change in Labrador Sea sea-ice concentration and meridional heat transport. The changed climate state is maintained over centuries through the feedback between sea-ice and sea-level pressure in the North Atlantic. The full evolution of the anomalous climate state depends crucially on the climatic background state

We present evidence for a El Niño Southern Oscillation (ENSO) -like mode that varies in tandem with the Greenland cooling and warming phases. Greenland cold phases correspond to dominant El Niño-like conditions, increased variance of ENSO and a displacement of El Niños (La Niñas) farther to the east (west). This ENSO-like mode is correlated with sea-level pressure anomalies over the Labrador Sea. ENSO-like variability with said characteristics on centennial scales is also present in a different pre-industrial control simulation. The absence of Greenland climate transitions in this simulation suggest that the the centennial scale climate variability presented here, originates in the tropics.

In the southern hemisphere the only significant changes in association with the Greenland cooling and warming phases are out-of-phase sea level pressure anomalies over the Weddell and Ross Sea. We explore why a strong interhemispheric coupling is absent and demonstrate that increased atmospheric CO_2 - as observed for the cold phases of Dansgaard-Oeschger-cycles - improves the southern hemisphere temperature response.

Net snow accumulation changes between the Greenland cold and warm phases are comparable in pattern and magnitude to those induced by orbital changes. This suggests that internal climate variability has the potential to favour a glacial inception even though orbital conditions might not yet be in optimal conditions - based on Milankovitch theory.

We discuss potential effects of glacial boundary conditions for the above described climate changes.

Abstrakt

En uforceret, præindustriel klimasimulation med Community Climate System Model 4 (CCSM4) viser opvarmnings- og nedkølingshændelser i Grønland som ligner Dansgaard-Oeschger-begivenheder i deres mønster og størrelse. Med forbehold for at kun tre overgange mellem et koldt og et varmt klima er tilgængelige for analyse, opdager vi at overgangene bliver udløst af et stokastisk signal i atmosfæren. Signalet påvirker styrken af den subpolare gyre, som fører til en ændring i Labradorhavets haviskoncentration og den meridionale varmetransport. Den nye klimatilstand er bibeholdt over flere århundreder gennem en tilbagekobling mellem havis og lufttryk over Nordatlanten. Den fulde udvikling af den anomale klimatilstand afhænger kraftigt af den klimatiske baggrundstilstand.

I vores analyse finder vi en svingningstype der ligner El Niño Southern Oscillation (ENSO) og som svinger i takt med de Grønlandske kold- og varme-faser. Kolde faser svarer til stærke El Niño-forhold, øget varians af ENSO og forskydning af El Niños (La Niñas) mod øst (vest). Den ENSO-lignende modus er korreleret med lufttryksanomalier over Labradorhavet. En anden præindustriel kørsel viser den samme modus med hundredårssvingninger, men uden klimaskifte i Grønland, hvilket tyder på at hundredårsklimavariationen har sin oprindelse i troperne.

På den sydlige halvkugle er de eneste større ændringer, der står i sammenhæng med de grønlandske nedkølings- og opvarmingsfaser, lufttryks-anomalier af modsat fase over Weddellhavet og Rosshavet. Vi undersøger hvorfor der ingen stærk kobling er mellem den nord- og sydlige halvkugle. Vi viser at den øgede CO_2-koncentration i atmosfæren – som optræder under de kolde Dansgaard-Oeschger-faser – fører til en stærkere respons i temperaturen på den sydlige halvkugle. Ændringer i sne-akkumulation mellem de grønlandske varme og kolde faser har samme mønster og størrelse som under orbitale ændringer. Dette tyder på at intern klimavariabilitet kan begunstige begyndelse af istider, selvom de orbitale betingelser ikke er optimale efter Milankovićs teori.

Vi diskuterer mulige effekter af de glaciale randbetingelser for klimaforandringerne.

Contents

1 Introduction

Abrupt climate transitions occurring in the North Atlantic (NA) region and in particular in Greenland during the last glacial period, spanning the period from about 120,000 to 12,000 years ago, are well documented in various climate proxy archives, the most frequent ones being Dansgaard-Oeschger events (D-O events, Dansgaard et al. (1993)). D-O events are associated with global scale climate changes of full glacial-interglacial amplitudes. The northern hemisphere (NH) high latitude temperature changes are characterised by a sawtooth shape, consisting of an abrupt warming and subsequent gradual cooling. Southern hemisphere (SH) temperature changes are gradual, symmetric and anti-correlated with the NH temperature changes. In the tropics D-O events manifest as changes in the monsoon strength and shifts in the Intertropical Convergence Zone (ITCZ). we present in this thesis evidence for centennial scale internal climate variability in a pre-industrial control simulation (CONT) of the Community Climate System Model Version 4 (CCSM4) that features several characteristics of D-O events. Motivated by these model results we raise the following question:

Can internal climate variability account for the observed millennial scale climate changes during the last glacial?

The NA climate changes in CONT involve the subpolar gyre (SPG) circulation, sea ice-atmosphere interactions in the Labrador Sea (LS) and cessation of deep water convection. Chapter 2 is identical to the manuscript “Stochastic Atmospheric Forcing as a Cause of Greenland Climate Transitions”, published in the Journal of Climate, 28, 7741-7763 (Kleppin et al., 2015). Except for the introduction, which is embedded in a slightly modified version in the general introduction (Chapter 1). The tropical Pacific climate changes are associated with dominant El-Niño-like conditions during NA cold phases, involving changes in the hydrological cycle and enhanced ENSO variability. We suggest that the centennial scale climate variability in CONT originates in the tropics (Chapter 3). In the SH, we find no significant centennial scale temperature changes. We review possible ocean and atmosphere pathways of inter-hemispheric coupling and discuss why they fail in CONT. Furthermore, it is shown that an increase in atmospheric CO_2 - as reconstructed for D-O events - improves the SH temperature response to NA cooling (Chapter 4). In Chapter 5 we show that net snow accumulation changes associated with the NA cold phases are comparable in pattern and magnitude to those induced by changed orbital conditions. Implications for a glacial inception scenario are discussed.

Three feedback mechanisms are identified in this study:

- SPG circulation -LS deep water convection- salinity feedback
- LS sea ice -atmosphere feedback
- interaction of tropical mean climate anomalies and ENSO variability

They are essential in particular for the high amplitude changes simulated in the NA region and sensitive to the mean background climate. Thus, two key-questions should be addressed by further research in order to determine, whether the proposed mechanism is a realistic scenario for contributing to millennial scale climate variability during the last glacial.

(1) Can the proposed mechanism work as well under different boundary conditions? Can different boundary conditions possibly lengthen the time scales or amplify the magnitude of changes?

(2) Can the centennial scale climate variability in CONT apply in the real world?

These questions are discussed in Chapter 6 and we conclude, with the constraint of the aforementioned background climate and model dependency, that internal climate variability can account for several important aspects of millennial scale climate variability.

The remaining Introduction is structured as follows.
In Sec. 1.1 we summarize the observational evidence for NA millennial scale climate variability and review dynamics that are suggested to explain D-O events. We emphasize the potential role of internal climate variability (Sec. 1.1.2). This is followed by a summary of tropical millennial scale hydrological changes in Sec. 1.2.1 and in Sec. 1.2.2

hypotheses regarding a potential role for tropical dynamics in triggering millennial scale climate variability are presented. An overview of SH millennial scale climate variability is given in Sec. 1.3.1, and a brief review of inter-hemispheric coupling theories in Sec. 1.3.2. A summary of the most recent developments in relative timing between tropical, SH and NH millennial scale climate variability completes the introduction (Sec. 1.4).

1.1 North Atlantic millennial scale climate variability during the last glacial

1.1.1 Observations

D-O events feature a distinct pattern of abrupt warming of 8 to 16 $°C$ (e.g., Landais and Coauthors (2004), Huber and Coauthors (2006)) followed by gradual cooling of the same amplitude, completing a so called D-O cycle. The cold and warm phases are called Greenland stadials (GSs) and Greenland interstadials (GIs), respectively (Fig. 1.1 (a)). D-O cycles occur most frequently in Marine Isotope Stage 3 (MIS3) and are also associated with a reorganization in atmospheric circulation as inferred from various dust and deuterium excess measurements of Greenland ice cores (e.g., Steffensen et al. (2008)). Consistent with warming during Greenland interstadials, snow accumulation rate is 50-100% increased relative to stadials (Andersen et al., 2006). D-O cycles coincide with changes in the tropics and large parts of the northern hemisphere (an overview of paleo-climatic proxies indicating coinciding shifts with Greenland temperature can be found in Rahmstorf (2002), Seager and Battisti (2007) and Clement and Peterson (2008)). Antarctic temperature changes are gradual and in antiphase with Greenland temperature (Barbante et al., 2006).
Interestingly, there is also evidence for abrupt warmings at Greenland in the instrumental record, although they are smaller in amplitude: around 1920 a warming of about $4°C$ at several meteorological stations at Greenland is reported by Cappelen (2013). The warming lasted over a decade and was followed by a slight cooling until the mid-eighties. Furthermore Bond et al. (1997) suggest “mini-D-O events ” during the Holocene based on ice rafted debris (IRD) changes in two marine sediment cores from the NA (Bond-events). These align with geochemical composition changes in the Greenland Ice Sheet Project 2 ice core, indicating atmospheric circulation changes over Greenland (O’Brien, 1995).
It has been often suggested, that Holocene climate is stable and that the underlying dynamics of D-O events thus require the presence of ice sheets (or glacial boundary condi-

tions, e.g., Wunsch (2006)). However, another possibility is that the underlying dynamics of Holocene and last glacial climate variability are the same, but the amplitude and time scale are dependent on boundary conditions.

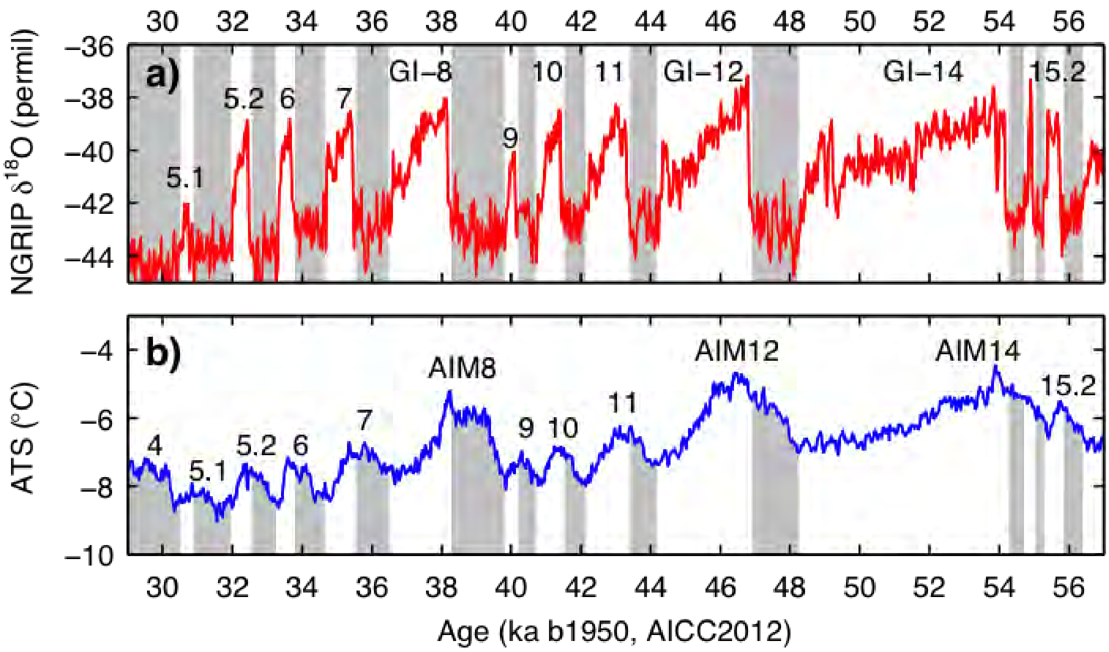

Figure 1.1.: (a) $\delta^{18}O$ variations during D-O cycles, spanning the period from 57 to 29 kyrs before 1950, from the North Greenland Ice Sheet Project (NGRIP) ice core. (b) The corresponding temperature changes for Antarctic Isotope Maximum events, both kindly provided by Dr. Joel Pedro.

1.1.2 State-of-art hypothesis for D-O events

Early hypotheses trying to explain D-O cycles were based on an abrupt shutdown of the Atlantic Meridional Overturning Circulation (AMOC), initiated by fresh water input into the NA (e.g., Broecker et al. (1990)), although the cooling phase of D-O cycles is not necessarily abrupt. More recent model studies revealed that the amount of fresh water necessary to slow down the AMOC sufficiently to produce temperature changes at Greenland comparable to D-O cycles depends on model details (Kageyama et al. (2013), Manabe and Stouffer (1999), Dijkstra (2007)), as well as on the location of the freshwater forcing (Mignot et al., 2007) and its timing (Bethke et al., 2012). Bethke et al. (2012) demonstrate that different models produce a wide range of outcomes for the deglaciation, given the same forcing. Furthermore, the evidence for freshwater input into the NA during D-O cycles is still subject to discussion. Based on sea level reconstructions from the Red Sea, Arz et al. (2007) suggest up to 25 ±12 *m* global sea level rise at the onset of Greenland interstadials. On the other hand Siddall et al. (2003) and Rohling et al. (2008) suggest an increase of sea level of 30 ±12 *m* during GSs.

Other mechanisms invoked to play a role in centennial to millennial scale AMOC variability and possibly in the dynamics behind D-O cycles are salt oscillators of the NA. Jackson and Vellinga (2013) find a salt-oscillator due to interaction of tropical salinity anomalies (induced by a southward (northward) Inter Tropical Convergence Zone (ITCZ) shift associated with AMOC weakening (strengthening)), and subpolar salinity anomalies due to decadal fluctuations of freshwater export through the Fram Strait. Peltier and Vettoretti (2014) find, by decreasing diapycnal diffusivity in a model simulation, that a salt oscillator of the glacial NA causes D-O-like temperature changes and AMOC variability. However, this contrasts with recent findings that suggest vertical diffusivities were larger by a factor of 3 during Last Glacial Maximum (LGM) compared to pre-industrial climate (Schmittner et al., 2015). Furthermore, evidence for AMOC shut down during D-O cycles is ambiguous. A recent study finds instead that a strong AMOC prevailed during most parts of the last glacial period and shut down of the AMOC occurred only during Heinrich events close to LGM (Böhm et al., 2015). Similarly, Lynch-Stieglitz et al. (2014) find that there was little change in AMOC in association with Heinrich events 2 and 3, suggesting that the AMOC was already in a weak state previous to the onset of these Heinrich events. However, low latitude climate changes are observed during all Greenland cooling events, which leads the authors to suggest that said climate changes are not directly linked to AMOC variations.

Some of the more recent hypotheses trying to explain D-O events invoke sea ice - atmosphere interactions. Li et al. (2005) find that a reduction of NA sea-ice extent can cause a climatic response consistent with D-O event signals of temperature and accumulation measured from Greenland ice cores. The authors point out, that in addition to the well known ice-albedo feedback, sea ice strongly influences regional air temperatures by insulating the atmosphere from the ocean heat reservoir. The possibility of "switching the ocean-atmosphere heat exchange off" due to extensive sea ice cover provides a plausible mechanism for abrupt and large local temperature changes, even though the initial forcing might be relatively small. Far-field signals and ocean-atmosphere feedbacks are not represented in their study, due to prescribed sea surface temperatures (SST) and an inactive ocean component. In their study the mechanism causing the displacement of the sea ice edge remains unexplored. Li et al. (2010) extends this by implementing more realistic sea ice retreat scenarios. They find that the displacement of the sea ice edge in the Nordic

Seas causes a 10 $^{\circ}C$ warming and 50 % increase in snow accumulation at Greenland summit, whereas sea ice changes in the western NA have less effect.

Rasmussen and Thomsen (2004) find a subsurface warming during GSs based on the analysis of eight marine sediment cores taken from the Nordic Seas and the NA. A new high resolution sediment core from the Nordic Seas confirms this subsurface warming (Dokken et al., 2013). They suggest a sequence of events that could explain a sudden melt of sea ice. In combination with the results of Li et al. (2005) this provides a possible mechanism for D-O events. During the stadial phase warm Atlantic inflow is separated from surface and sea ice by a strong halocline, allowing for an extensive ice cover to persist. The mechanism proposed to initiate the abrupt melting involves a slow subsurface warming during stadials due to the separation of the warm Atlantic inflow from the surface. Eventually this subsurface warming destabilises the water column, the halocline collapses and warm subsurface water is reaching the surface and melting the sea ice (e.g., Dokken et al. (2013) and Kim et al. (2012)). Other hypothesis invoke ice sheet height variations as a trigger of D-O events. For instance Zhang et al. (2014) demonstrates that by varying the height of the Laurentide ice sheet a positive ocean-atmosphere-sea ice feedback is initiated eventually leading to D-O-like climate shifts.

Studying the climate response to highly idealised scenarios of prescribed external forcing (e.g., freshwater-hosing experiments, prescribing sea ice cover or ice sheet changes) gives insight into the particular process and helps to determine its potential influence on Greenland temperatures. However, the origin of the prescribed external forcing remains unclear. To our knowledge there are only five examples of abrupt climate changes arising spontaneously in coupled climate models, i.e., without having been triggered by variations in external forcing. Hall and Stouffer (2001) describe a cooling event around Greenland in a fully coupled climate model with coarse resolution. The event lasts for a period of only 30-40 years and is caused by a persistent northwesterly wind anomaly transporting cold and fresh water into the NA and causing a shutdown of deep water convection. Goosse et al. (2002) describe cooling events occurring in an Earth System Model of Intermediate Complexity (EMIC). The cold events are attributed to a displacement of the oceanic deep water convection sites to a more southern location. Just as in Hall and Stouffer (2001) the shut down of deep water convection is induced by stochastic atmospheric forcing, but in addition Goosse et al. (2002) demonstrate that such an event could also be triggered by appropriate changes in solar irradiance. The remaining three examples of spontaneous climate transitions occur in state-of-the-art fully coupled climate models. Sidorenko et al. (2014) report several events of sudden decrease of deep water convection and increase of LS ice extent. The mechanism behind them is not studied in detail, but the authors attribute them to anomalously saline and warm water inflow into the deep LS. The anomalous light deep water weakens the SPG circulation causing a change in the upper-LS fresh water budget. The warm and saline bias in the deep NA is mainly attributed to overly strong surface winds in the subtropical NA, modifying the path of Gibraltar Strait outflow in the NA. Martin et al. (2014) report on centennial-scale variability of the AMOC and other changes in the NA (e.g., SPG strength and NA heat content) driven by Southern Ocean deep water convection variability. The signal transmission to the NA occurs through an enhanced meridional density gradient between deep (below 1200 m) NA and South Atlantic and a compensation of Antarctic Bottom Water (AABW) by increased NA deep water extent. Drijfhout et al. (2013) describe a spontaneous cold event with a duration of about 100 years. The authors attribute the cold event to a period of anomalous high atmospheric blocking above the eastern subpolar gyre. The blocking causes the sea ice edge to progress farther south in the Greenland Sea and eventually excites a cold core high pressure anomaly at the south western tip of Greenland. The anomalous anticyclone advects cold air through enhanced northerly winds to the sea ice edge, causing the sea ice extent to grow even farther. Additional sea ice is transported southwards by ocean currents and causes a fresh surface anomaly in the LS. As a consequence deep water convection shuts off and due to longer exposure of the ocean surface to the atmosphere sea ice growth commences, reinforcing the atmospheric anomaly. The anticyclonic anomaly, now centered above the LS, causes a change from northerly to more southerly winds, advecting warm air, melting the sea ice and returning the system to normal.

1.2 The role of the tropics in global climate variability

1.2.1 Observational evidence for tropical millennial scale climate variability

There exist a variety of paleo-proxy records that suggest significant changes in the global tropics in tandem with the above described NA changes. They suggest global scale rearrangements in the atmospheric circulation and associated hydrological changes. We review in the following some of the existing evidence for

- ITCZ shifts
- global monsoon changes
- changes to ENSO and equatorial Pacific climate

In the second part of this Section, we summarize existing hypotheses on how the tropics could play an active rather than a passive role in millennial scale climate variability. Motivated by two studies, we hypothesize that a mode of ENSO-like variability, characterised by an east-west displacement of SST anomalies and changes in ENSO amplitude, can account for the model results presented in Chapter 3.

1.2.1.1 ITCZ shifts

A southward migration of the Atlantic ITCZ is observed during GSs. Peterson et al. (2000) present evidence for changes in sediment reflectance in a sediment core from Cariaco basin (off the coast of Venezuela), that are interpreted as changes in the amount of terrestrial sediments brought into the basin by rivers. The reconstructed amount of terrestrial sediments carried into Cariaco Basin reflects changes in the precipitation-evaporation balance north of the Amazon Basin. The authors suggest that GSs are associated with decreased precipitation in northern South America, probably as a consequence of a southward migration of the Atlantic ITCZ. This is further supported by an analysis of speleothems, indicating wetter conditions during GSs in north eastern Brazil (Wang et al., 2004). The authors further find that the southward migration of the Atlantic ITCZ occurs simultaneous with a weakening of the East Asian summer monsoon, documented by Wang et al. (2001) (see next section), suggesting a rapid and global scale change of the ocean-atmosphere system in association with D-O events.
ITCZ migration to the warmer hemisphere is a consequence of angular momentum conservation of the rising branch of the Hadley cell (Lindzen and Hou, 1988). The altered Hadley circulation allows further for increased atmospheric heat transport into the colder hemisphere (Chiang and Bitz, 2005). Support also comes from modelling studies. The southward migration of the Atlantic ITCZ is a robust response in a variety of climate models to strong NA cooling, either linked to LGM boundary conditions, fresh water hosing or sea ice anomalies (e.g., Chiang et al. (2003); Braconnot et al. (2007); Zhang and Delworth (2005); Dong and Sutton (2002); Chiang and Bitz (2005)) and is estimated to occur within 2 years (Chiang et al., 2008). At present the ITCZ migration in association with D-O cycles is considered to arise from NA cooling. However, a southward migration of the Atlantic ITCZ can also be caused or amplified by South Atlantic warming (e.g., Cvijanovic et al. (2013)). Alternatively, Peterson et al. (2000) suggests that the southward ITCZ migration in South America could also be the consequence of tropical Pacific convection changes. During present El Niño events the SST pattern in the tropical Pacific becomes more equatorial symmetric, resulting in a southward migration of the ITCZ in the Pacific (Rasmusson and Carpenter, 1982; Fedorov and Philander, 2000; Peterson

et al., 2000).
Additionally a southward migration of the ITCZ provides a plausible mechanism by which a NH cooling signal can be fast propagated to the southern Hemisphere ((Chiang et al., 2008; Lee et al., 2011), see Sec. 1.3.2).

1.2.1.2 Monsoonal changes and the Global Paleo Monsoon System

The variations in monsoon strength of the different monsoonal systems (the most important ones being the East Asian summer monsoon (EASM), Indian summer monsoon (ISM), South American summer monsoon (SASM) and African monsoon) are proposed to be a manifestation of global scale seasonal changes in atmospheric overturning (Trenberth et al., 2000). These changes are characterized by a reversal of surface winds and a shift in the rain belts, associated with the seasonal migration of the ITCZ and changes of the land-sea temperature contrast. Cheng et al. (2012) proposes that millennial and orbital scale variability in the different paleo-monsoon systems should also be considered as a response to global scale seasonal differences, rather than as regional circulation anomalies (the global paleo monsoon).
$\delta^{18}O$ variations of speleothem calcite, recording precipitation changes on local (ISM; e.g., Burns et al. (1998); Shakun et al. (2007)) to regional scales (EASM; Cheng et al. (2006)), are widely used as an indicator of variations in the paleo monsoon system. $\delta^{18}O$ variations of speleothem calcite in the EASM domain feature a precessional signal, reflecting the change in ratio between summer and winter precipitation (Wang et al., 2001). Seasonal changes in $\delta^{18}O$ of precipitation reaching eastern Asia are anti-correlated with summer monsoon intensity since enhanced atmospheric circulation brings moisture from more distant sources. Through a larger fractionation during the longer moisture transport trajectory the $\delta^{18}O$ of precipitation reaching eastern Asia is less enriched (Yuan et al., 2004; Cheng et al., 2012).
Modelling studies further support the interpretation of $\delta^{18}O$ speleothem calcite variations in the EASM domain as changes in the overall Asian summer monsoon intensity (including the ISM domain, Pausata et al. (2011)). In the SASM domain variations of $\delta^{18}O$ in speleothems are mainly interpreted as a change of moisture originating from the Pacific or the Atlantic (Cruz et al., 2005; Wang et al., 2006). A strengthened SASM is linked to enhanced transport of Pacific moisture, associated with low $\delta^{18}O$ of precipitation, towards south eastern Brazil.
Periods of strong ASM occur during GIs (e.g., Wang et al. (2001); Cheng et al. (2006); Burns et al. (1998)) and are anti-correlated to changes in SASM (e.g., Cruz et al. (2005); Wang et al. (2004)). This interhemispheric anti-correlation is likely a result of the afore-

mentioned meridional migration of the ITCZ.
Cheng et al. (2012) suggest further that complex changes in the Walker circulation (e.g., through changes in ENSO or deep monsoonal convection) may have occurred during the GI-1 to GS-1 transition. This suggestion is based on the discrepancy between equatorial Asian (Griffiths et al., 2009; Partin et al., 2007) and equatorial American (Van Breukelen et al., 2008; Cruz et al., 2009) $\delta^{18}O$ speleothem records. The former two are located in opposite hemispheres and positively correlated, whereas the latter two are located in the same hemisphere and negatively correlated.
Cheng et al. (2012) and Wang et al. (2001) among others find that the changes in monsoon intensity are conform with a NH trigger. However, substantial contributions to the changes in EASM strength from SH climate changes are suggested by Rohling et al. (2009).

1.2.1.3 El Niño-like conditions during Greenland stadials

Several reconstructions suggest changes in ENSO variability and the mean climate state of the equatorial Pacific, in association with D-O cycles. However, We are aware of only few reconstructions of ENSO variability on millennial scales during the last glacial. Changes in ENSO variability during the Holocene are better documented, but information from different paleo-proxies are partially conflicting (e.g., Karamperidou et al. (2015)). Thus the studies summarized in the following need to be confirmed by further reconstructions.
Stott et al. (2002) analyse magnesium/calcium composition and $\delta^{18}O$ of planctonic foraminifera, which show that GSs are correlated with decreased salinity in the west Pacific warm pool (WPWP), likely the result of precipitation changes associated with dominant El Niño-like conditions. The authors further suggest that dominant El Niño-like conditions could account for many reconstructed changes that are linked to D-O cycles, as for example lower atmospheric CH_4 concentrations during GSs. Koutavas et al. (2002) also find El Niño-like conditions during past cold NA events over the past 30 $kyrs$, based on magnesium/calcium compositions of foraminifera in sediment cores from the eastern Pacific cold tongue region. Sadekov et al. (2013) find that over the past 22 $kyrs$ increased zonal SST gradients during the (warm) early Holocene are associated with decreased ENSO variability, while the opposite is true for the (cold) deglaciation. This is contrary to the findings of Tudhope et al. (2001), who suggest, based on $\delta^{18}O$ of fossil corals from the WPWP area, decreased ENSO variability during past cold and warm intervals relative to present day. The authors further attribute the decreased ENSO variability to the cold glacial conditions and precessional forcing.
The low ENSO activity during the early Holocene, however, is supported by the reconstruction of Moy et al. (2002), who further find millennial scale variability in ENSO vari-

ance (on top of the orbital induced trends) that are possibly linked to Bond events (Bond et al., 1997). The authors suggest that cold NA Bond events tend to occur immediately after a transition from intervals of high to low ENSO variability.

Dominant El Niño-like conditions can explain several of the changes around the globe that are associated with D-O events. For example, decreased convective heating over the western Pacific in association with El Niño-like conditions can weaken the ISM (Lau and Nath, 2000). In addition a southward migration of the Pacific ITCZ can be the result of more equatorial symmetric SST pattern during El Niño-like conditions (Peterson et al., 2000). El Niño-like conditions imply decreased upwelling in the eastern equatorial Pacific and hence decrease the flux of CO_2 into the atmosphere (Stott et al., 2002; Feely et al., 1999). Tropical soil CH_4 emissions are effected by changes in the strength and structure of tropical convection systems, both associated with ENSO variability and monsoonal changes and could therefore amplify millennial-scale climate changes (Stott et al., 2002; Ivanochko et al., 2005).

However, under present day conditions the impact of ENSO variability itself in the NA is too minor to explain D-O events and a process that could amplify NA changes in response to ENSO variability has yet to be identified. It is conceivable that a change of the mean tropical climate has different impacts than interannual ENSO variability. The modelling results of Barreiro et al. (2006) show that tropospheric net vapour content increases significantly, when forcing an atmospheric GCM with tropical Pacific SSTs that have no longitudinal variations. The increased vapour content increases surface temperature and causes an amplified warming over northern America, with a maximum amplitude at $\sim 50°N$ of $6°C$ compared to a present day control simulation. It should be noted however, that Barreiro et al. (2006)'s study aimed at studying atmospheric circulation anomalies associated with the early and mid-Pliocene (5 to 3 million years ago), and for the last glacial period only weakened zonal gradients are consistent with reconstructions.

1.2.2 Potential role of the tropical climate system in triggering D-O events

The idea that the tropics could play an active role in past abrupt climate changes comes from several considerations. However, this ideas have been mainly explored hypothetically and not yet been tested.

Firstly, as pointed out by Seager and Battisti (2007), tropical hydrological changes be-

tween GSs and GIs have full glacial-interglacial amplitudes. Thus the signal of millennial scale climate variability is not muted, when moving away from the NA.
Secondly, energy budget considerations suggest at least an amplifying role of the tropics in millennial scale climate variability (Clement and Peterson (2008) and references therein): Radiative energy gain occurs in the tropics and is exported from here to the extra-tropics. The amount of energy available for export is dependent on the outgoing longwave radiation that is decreased by higher water vapour content. Thus changes in the tropics that alter the water vapour content, through for example surface warming or cooling, provide a strong positive feedback and could lead to synchronous cooling or warming of the globe as a whole. Vavrus et al. (2006) suggest a mechanism by which slowly increasing atmospheric CO_2 concentrations can lead to rapid warming after tropical deep convection reaches a certain amplitude. Cloud and water vapour feedbacks are essential to their mechanism and depend to some extent on cloud parameterizations, which are generally one of the largest uncertainties in climate models (e.g., Chapter 7 of Stocker et al. (2013)).

Effects of tropical Pacific SST changes on NA atmosphere and ocean changes

Under present day conditions the tropical SST variability plays an important role in driving long-term atmospheric circulation changes in the NA. A recent study by Ding et al. (2014) shows that the warming trend during the last three decades in eastern Canada, the Baffin Bay area and parts of Greenland is associated with distinct geopotential height anomalies ($\sim$ 15 m) over the same area. The geopotential height anomalies are the result of anomalous Rossby wave activity in response to Pacific SST trends. Furthermore, Hurrell et al. (2004) attribute the big share of NAO trends since the 1950ies to tropical forcing, based on the results of a multi-model ensemble forced with observed tropical SSTs.
Also, under LGM boundary conditions tropical Pacific SST pattern have been shown to play a major role in forcing NA atmospheric circulation anomalies. Yin and Battisti (2001) find that differences in tropical SST pattern result in large geopotential height anomalies ($\mathbf{O}$(300 m) at 500 hPa (their Figure 3a)) in the northern mid- to high latitudes. The changes are most pronounced during winter and are associated with surface temperature changes in the area of the Fennoscandian and Laurentide ice sheets by more than 8°C (with opposite signs for the two areas). This alters the mass balance of the ice sheets considerably. The spatial pattern of tropical SSTs is found to be very important. In fact, the authors find that a uniform cooling of tropical SSTs by 3°C effects the NH atmospheric circulation less, than a 1°C mean decrease together with a non-uniform pattern of SST

cooling in the tropics. Yin and Battisti (2001) suggest furthermore that the mechanism connecting the NH atmospheric circulation changes and the tropical Pacific SST changes can be explained by the effect of tropical convection changes on the subtropical circulation by interacting with transients. Decreased (increased) tropical convection causes cyclonic (anticyclonic) anomalies poleward of the convection regions. The associated changes in upper level zonal winds then affect Rossby wave propagation.

Seager and Battisti (2007) advance the hypothesis that small changes in tropical heating can cause a change between two possible states of the subtropical jets, with important impacts for atmospheric heat transport in the NA:
Lee and Kim (2003) suggest that the northern hemisphere subtropical and polar front jets are dynamically different. The existence of the subtropical jet follows from angular momentum conservation of the poleward flow of the Hadley cell (Held and Hou, 1980), whereas the polar jet is characterised as an eddy-generated jet (Lee and Kim, 2003). As Seager and Battisti (2007) point out, this is an idealized scenario and in reality both jets are characterised by the interaction of eddies and thermal wind balance. Lee and Kim (2003) demonstrate that strong tropical heating causes a strong Atlantic subtropical jet, eventually resulting in one merged jet, due to the strengthened temperature gradients and the associated eddy activity. Under certain conditions of tropical heating (or northern hemisphere cooling) a small change in tropical heating can lead to mergence and demergence of the two jets (Lee and Kim, 2003; Son and Lee, 2005). This would in turn reorient the NA storm-track and thus provide a plausible mechanism by which tropical heating changes could abruptly regulate the atmospheric heat transport brought into the northern parts of the NA. Furthermore, it could effect the gyre circulation and eventually deep water formation, through the associated wind stress changes (Seager and Battisti, 2007).
Furthermore ENSO-like variability can influence the strength of the AMOC through differences in moisture transport between the Atlantic and the Pacific. Resulting salinity anomalies in the tropical surface Atlantic are advected downstream into the deep water formation sites, causing enhanced/decreased convection there and hence alter one of the key drivers of the AMOC (e.g., (Latif, 2001; Schmittner et al., 2000; Latif, 2003)).

Abruptness

The abruptness that characterises the warming transition between one GS into a GI followed by gradual cooling is among the major aspects that any theory for D-O events should be able to explain. Abruptness in the tropics has been proposed to arise as a re-

sponse to slowly varying external forcing, either through nonlinear interaction with ENSO variability or through thresholds in tropical convection and the super greenhouse effect (Clement et al. (2001); Vavrus et al. (2006), respectively).
Clement et al. (2001) identify a mechanism by which slowly varying orbital forcing can abruptly alter ENSO behaviour and thus can give rise to abrupt millennial scale climate variability on a global scale. Using a Zebiak and Cane (ZC, Zebiak and Cane (1987)) model they demonstrate that under certain orbital conditions - and when ENSO transitions from one dominant period regime to an other - ENSO variability can lock completely to the annual forcing. This complete phase lock of ENSO (annual Niño 3.4 SST anomalies do not exceed 0.5 $°C$ for a minimum of 5 years) lasts for several centuries. It is argued that changes in the seasonality - dominated by the precession cycle - produce the two very different modes of ENSO variability, associated with different amplitudes, periods and irregularity of ENSO. Clement et al. (2001) identified a La Niña-like pattern in SST as the response to the phase lock events. The periods of completely muted ENSO variability reoccur after half a precession cycle ($\sim 11\ kyrs$) and it should be noted that such a pacing of D-O events is not observed. This mechanism is supported by the results from a coupled GCM simulation (Timmermann et al., 2007). The authors suggest that when the seasonal cycle is strong, ENSO variability locks in phase to the frequency of the forcing (i.e., the seasonal cycle).
The recent shift in ENSO properties (e.g., Zhang et al. (1997); Fedorov and Philander (2000); Wang and An (2002)) in the late 1970ies might be an indication that abrupt changes in the tropics can also arise through internal dynamics. However, the cause of this shift is still matter of debate and for example Fedorov and Philander (2000) conclude that the shift could be the result of decadal background climate variations, random perturbances and even a contribution of global warming cannot be excluded.

1.2.2.1 ENSO amplitude modulation and east-west displacement of ENSO activity

In particular during the mid-Holocene paleo-proxies from the eastern Pacific disagree with proxies from the central to western Pacific on the amplitude of decreased ENSO variability (Karamperidou et al., 2015). The authors suggest that a shift between dominant east Pacific (EP) and central Pacific (CP) ENSO flavours could resolve this conflicting information. Teleconnections differ distinctly between CP and EP ENSO variability (e.g., Ashok et al. (2007), Wang et al. (2012)) and it seems thus likely that paleo-proxies record EP and CP ENSO flavours differently, depending on their location (Wang et al., 2012; Karamperidou et al., 2015). Altered teleconnections are even observed in the NA, that is an increased frequency of tropical north Atlantic cyclones in association with the CP

ENSO flavour (Kim et al., 2009).
The frequency of CP ENSO events might have increased over the past decades (e.g., Giese and Ray (2011); Lee and McPhaden (2010)) and could be related to the aforementioned major shift in other ENSO properties (amplitude, period) and mean climate changes in the tropical Pacific (e.g., Fedorov and Philander (2000)). Plenty of mechanism have been invoked to explain the two distinct ENSO flavours and it is beyond the scope of this study to explore these theories. In particular since there is even still debate on whether CP and EP El Niño events are indeed a different phenomena (Takahashi et al., 2011). The reader is referred to the review by Wang et al. (2012).
However, we elaborate on one theory because it is linked to the centennial scale tropical changes in CONT (Chapter 3). Timmermann (2003) suggest a mechanism by which an east-west displacement of ENSO's center of action could be generated by internal tropical dynamics alone, a mode of decadal ENSO amplitude modulation (DEAM) that is associated with the second Empirical Orthogonal function (EOF) mode of (sub-) surface temperature anomalies and is characterised by the same spatial pattern of SST anomalies as El Niño Modoki (this is one amongst several names for CP types of ENSO, Ashok et al. (2007)). Timmermann (2003) finds that ENSO variability is strong when El Niño events are displaced towards the eastern and La Niña events towards the western Pacific. DEAMs are accompanied by decadal oscillations of a temperature dipole extending from the surface to depth of about 150 m. A reduction of the thermocline slope and a deepening of the thermocline in the eastern equatorial Pacific go along with intervals of increased ENSO variability. The author suggest that the decadal mean climate changes (i.e., thermocline depth anomalies and SSTs) and the variations in ENSO amplitude can not be separated into cause and effect, but are instead the result of coupled nonlinear dynamics within the tropical Pacific.
In chapter 3 we demonstrate that in the pre-industrial control run of CCSM4 there is evidence for an east-west displacement of ENSO activity that is correlated with the NA climate transitions. Based on several indications, we speculate further that the centennial changes in ENSO behaviour are intrinsic to the tropics and thus not caused by the NA climate transitions.

1.3 The southern Hemisphere

1.3.1 Observations

The European Programme for Ice Coring in Antarctica (EPICA) Dronning Maud Land (EDML) ice core is characterised by high accumulation (and hence resolution) compared to most other Antarctic sites, owed to its coastal location. The synchronization with the NGRIP ice core made it possible to relate each D-O event with a corresponding Antarctic Isotope Maximum (AIM) event. The inferred Antarctic temperature changes are gradual and in anti-phase with Greenland temperature over a D-O cycle (Barbante et al., 2006). In Antarctica the magnitude of temperature changes is distinctly lower than in Greenland and ranges between $1°C$ to $3°C$ (e.g.,WAIS Divide Project Members et al. (2015) and Fig. 1.1 (b)). The change in Greenland temperature is further highly anti-correlated with the rate of change of Antarctic temperatures thus also linking the amplitude of GSs to the length of AIM events (Stocker and Johnsen, 2003; Schmittner et al., 2003). This is consistent with a simple thermodynamic seesaw concept (see next Sec. 1.3.2). Based on benthic carbon isotopes and neodymium isotopes from several sediment cores across the South Atlantic Piotrowski et al. (2008) find that AABW northward extent increases as Antarctica warms and decreases as Antarctica cools. A partial control of SH climate changes on the AABW extent lead the authors to suggest that rapid switchs between southern and northern dominated deep ocean ventilation occurred in association with D-O events.

Pedro et al. (2015) compiled 84 terrestrial and marine paleo-records in the SH for the Antarctic cold reversal (the SH equivalent of the Bølling-Allerød). Strongest cooling occurs in the South Atlantic sector and globally poleward of $40°S$. The South Atlantic and Southern Ocean records all show a transition that is unambiguously characterised by the more gradual cooling associated with Antarctic temperature changes. The terrestrial records (from $0 - 20°S$) however are correlated with the abrupt northern Hemisphere climate changes. The spatial pattern of changes is compared with a transient model simulation with applied fresh water flux in the NA and the Gulf of Mexico, changing greenhouse gases and orbital configurations (Liu et al., 2009). The said characteristics of terrestrial and marine reconstructions are reproduced by the model simulations. The authors show that the increased northward ocean heat transport in the Atlantic, amplified by sea ice anomalies in the Southern Ocean can account for amplitude and spatial extent of observed changes. The increased ocean heat transport (associated with the recovery of the AMOC) is found to be only partly compensated by a decreased atmospheric heat transport (contrary to suggestions by e.g., Wunsch (2006)). However, the decreased northward heat transport of the atmosphere is responsible for the terrestrial hydrology changes, that are characterised by the fast and abrupt northern Hemisphere changes (through an adjustment of the Hadley circulation). The proxy evidence suggest that both atmospheric and oceanic heat transport anomalies are required to explain SH millennial scale climate variability (Pedro et al., 2015).

1.3.2 Bipolar seesaw concepts and their limits

The leading hypotheses explaining the antiphased inter-hemispheric millennial scale climate changes invoke ocean heat transport changes associated with AMOC variations. we summarize in this section the two leading hypotheses that relate to the ocean overturning circulation. In the second part we present a recently suggested interhemispheric coupling mechanism, relying on atmosphere-surface ocean interaction.

- the "classical" bipolar seesaw (Crowley, 1992), extended by Stocker and Johnsen (2003) by adding a SH heat reservoir to account for the different interhemispheric phasing
- a competition between AABW and North Atlantic Deep Water (NADW) formation and a seesaw of heat release to the atmosphere between SH and NH, in conjunction with deep water ventilation in the respective hemisphere (Broecker, 1998)

In the former the southern Hemisphere cooling is a direct consequence of the decreased northward heat transport, associated with a shut down of the AMOC. When the AMOC is active, the southern Atlantic is cooled, consistent with observations of a northward heat transport at $30°S$ (e.g., Talley (2003)). A shut down of the AMOC causes directly a reduced northward heat transport and subsequent warming of the southern Atlantic. The resulting relationship between SH and NH is an anti-phased 0-lag relationship, contrary to reconstructions. Further it cannot account for the different time scales of transitions in Antarctica and Greenland. To account for these obvious inadequacies Stocker and Johnsen (2003) construct a thermodynamic bipolar seesaw by coupling the classical bipolar seesaw model to a Southern Ocean heat reservoir and find improved realism in the timing of the Greenland-Antarctic temperature seesaw. Stocker and Johnsen (2003); Schmittner et al. (2003) suggest that the long timescale of SH-NH coupling arises from the combination of fast signal transmission along the western boundaries in the North Atlantic by coastal Kelvin waves and an adjustment of the interior by westward propagating Rossby waves (following the ideas of Kawase (1987)), and a slow thermal adjustment in the Southern Ocean due to the absence of meridional boundaries.

The southern Atlantic warming in response to AMOC shut down is a common climate model feature. However, the Antarctic response to fresh water hosing differs distinctly between the models (Kageyama et al., 2013). It has been argued, that the strong zonal flow of the Antarctic Circumpolar Current (ACC) acts as a dynamical barrier for signal transmission from the southern Atlantic to Antarctica (Ferrari and Nikurashin, 2010; Marshall et al., 2006). A hampered signal transmission across the ACC potentially provides

an explanation for the absence of warming in Antarctica in some of the simulations analysed by Kageyama et al. (2013). This implies that further investigation is necessary to determine whether such a bipolar seesaw mechanism was at play in the real world.
In the latter enhanced formation of AABW occurs when NADW formation is reduced. Radiocarbon ratio reconstructions show a rapid increase during the onset of the Younger Dryas followed by a gradual decline over the rest of the cold event (Hughen et al., 1998). The initial increase is interpreted as the response to a shut down of NADW formation, causing the cooling in the NA. However, temperatures in the NA stayed cold even though the radiocarbon ratio decreases steadily, suggesting the emergence of a radiocarbon sink elsewhere.
Based on these observations and on modelling studies by Wright (1996); Mikolajewicz (1996); Schiller et al. (1997), showing that radiocarbon sequestration shifts to the Southern Ocean when the AMOC shuts down, Broecker (1998) suggest a different bipolar seesaw concept that is based on a compensation by enhanced AABW formation when NADW formation is reduced. This process is hypothesized to work as follows. When NADW production ceases, downward mixing of heat continues, resulting in less dense water in the deep ocean. This creates a tendency for dense surface waters in the southern ocean to sink, simultaneously allowing for heat release to the atmosphere in the Southern Ocean, causing warming there when Greenland is cold. The radiocarbon trend can then be explained by sequestration in the Southern Ocean. In this conceptual model NA warming involves increased heat release from the ocean and NADW production in the north and Antarctic warming involves increased heat release and production of AABW in the south.
The two above described hypotheses for interhemispheric coupling during D-O events rely both on a severe reduction of the AMOC. Although several studies suggest that such weakening of the AMOC occurred (e.g., Kissel et al. (2008); Gottschalk et al. (2015)), during D-O events, there exist as well several studies drawing the opposite conclusion (e.g., Böhm et al. (2015); Lynch-Stieglitz et al. (2014)).

1.3.2.1 Atmospheric-surface ocean interhemispheric coupling

Chiang et al. (2014); Lee et al. (2011) propose an atmospheric-surface ocean coupling mechanism for connecting the two hemispheres. The proposed mechanism is thought to work in addition to possible deep ocean circulation pathways.
A southward migration of the ITCZ in response to NH cooling weakens the SH Hadley cell. This results in a weaker south Pacific subtropical jet and consequently the south Pacific split jet weakens, which is associated with more zonally symmetric westerlies. The

south Pacific subtropical front subsequently moves farther south, resulting in warming equatorward of its new position. This is consistent with terrestrial paleo-proxies from these sites that indicate climate changes that are in phase with NH climate changes (Pedro et al., 2015; Chiang et al., 2014). Lee et al. (2011) show further that the weakened subtropical jet in the Pacific causes an intensification of the eddy-driven SH mid-latitude westerlies. The strengthened westerlies in turn lead to enhanced northward Ekman transport, which is compensated by enhanced upwelling from depth (Toggweiler and Samuels, 1998). The results of Lee et al. (2011) suggest further that the enhanced Southern Ocean ventilation can result in increased outgasing of CO_2, consistent with reconstructions of increased upwelling rates in association with increased atmospheric CO_2 concentrations during the last deglaciation (Anderson et al., 2009).

1.3.2.2 Internal centennial scale climate variability in Weddell Sea deep water convection

A series of recent modelling studies by Martin et al. (2013, 2014, 2015) demonstrate that internal centennial scale variability in open ocean deep convection in the Weddell Sea impacts the strength of the AMOC. The signal transmission to the NA occurs through an enhanced meridional density gradient between the deep (below 1200 m) NA and South Atlantic and a compensation of AABW by increased NADW extent. The changes in the overturning are accompanied by changes in the NA gyre circulation and temperature anomalies in both hemispheres. This study shows that, at least on centennial time scales, a "Broecker-type" bipolar seesaw can be initiated in the SH and can arise from internal dynamics, without relying on external forcing.

1.4 Timing of global changes relative to Greenland stadials and interstadials

A question that arises naturally is whether the relative timing of changes around the globe can give some information about the cause of D-O events. The relative timing of southern Hemisphere, tropical and northern Hemisphere millennial scale climate variability is notoriously difficult, because of different age models and different uncertainties in timing, associated with different paleo- proxies. Hence the timing is still subject to discussion. However, there exist some recent advancements (e.g., Rosen et al. (2014); WAIS Divide Project Members et al. (2015)) that we briefly summarize in the following.

1.4.1 Tropics

Methane concentrations - trapped in air bubbles of ice cores - provide a possibility to compare tropical changes with high-latitude changes, while avoiding different uncertainties in timing. During GIs methane concentration increased by ~ 200 *ppb* during ~ 200 *years*, distinctly slower than Greenland warming occurred. This time delay could reflect the response time of ecosystems to abrupt climate changes (Brook et al., 2000).
Rosen et al. (2014) compare methane concentration of the high resolution North Greenland Eemian (NEEM) Ice core that give information about low-latitude hydrological changes, with $\delta^{15}N$ of N_2, which is a measure for Greenland surface temperature. The authors suggest a lead of Greenland temperature by 4.5^{+21}_{-24} years for the Bølling-Allerød. However, the amount to which changing methane concentrations reflect a tropical signal is still subject to discussion. At present the most important methane source are tropical wetlands (Bergamaschi et al., 2009) and some of them are influenced by the Asian monsoon systems, that varied together with D-O events (see Sec. 1.2.1.2). During glacial boundary conditions methane production from boreal sources was probably even further reduced, due to ice sheets and permafrost in the high latitudes (e.g., Brook et al. (2000)). However, boreal contributions are in general non-negligible (e.g., Brook et al. (2000); Chappellaz et al. (1997)). Rosen et al. (2014) estimate a boreal contribution over the Bølling-Allerød transition of up to ~ 22%. If boreal methane increases were to precede those of the tropics, a maximum lag of tropical sources of 40 years behind methane concentration in NEEM is estimated.
This is in good agreement with the findings of Steffensen et al. (2008), who suggest a tropical lead for two Greenland warming transitions by 10 ± 5 years, based on the relative timing between Ca^{2+} and dust concentrations and deuterium excess (see Sec. 1.1.1). However, the findings contrast with previous analysis of methane concentration, suggesting a lag of tropical climate changes behind Greenland temperature changes by 20 to 80 years (e.g., Severinghaus and Brook (1999) also for the Bølling-Allerød transition and Huber and Coauthors (2006) for D-O events).

1.4.2 Southern Hemisphere

Recent methane based synchronization of the NGRIP ice core and the newly drilled high resolution West Antarctica Ice Divide (WAIS) ice cores reveal a lead of abrupt Greenland temperature increase by 218 ± 92 years over Antarctic cooling (in average over a stack of all D-O events, WAIS Divide Project Members et al. (2015)). A similar lead is found for Greenland cooling events. This time scale confirms that ocean dynamics must play an important role in the interhemispheric coupling of millennial scale climate variability and supports the classical view of an oceanic bipolar seesaw, associated with major changes in the AMOC. The authors further argue that this anti-correlation with a 200 year lead of Greenland temperature suggests a north-south directionality. However, changes in deuterium excess in the same ice core occur abrupt and at the same time as Greenland climate changes (Markle, Pedro, 2015, personal communication). Deuterium excess changes reflect source changes of precipitation arriving in Antarctica, suggesting that a global scale atmospheric reorganization is associated with D-O events and was fast mediated to the high southern latitudes.

The remaining thesis is structured as follows. In Chapter 2 we focus on the NA climate changes in CONT. We show that an atmospheric anomaly triggers a switch between a strong and a weak circulation mode of the SPG. The weak mode is maintained over centuries through the positive feedback between (a) fresh water convergence into the LS, deep water convection and circulation strength and (b) a sea ice - and SLP. In Chapter 3 we document changes of the tropical Pacific mean climate, ENSO variance and an east-west displacement of ENSO activity that covary with the NA phases. Furthermore, we suggest that the tropical changes are the origin of the centennial scale variability in CONT. In Chapter 4 we analyse why possible ocean and atmosphere mechanisms do not trigger any significant temperature changes. We show further that increased atmospheric CO_2, as observed during GSs, improves the SH response. Motivated by the similarity of net snow accumulation changes between the NA warm and cold phases and orbital induced changes, we discuss the potential role of internal climate variability for a glacial inception scenario in Chapter 5. This thesis finishes with a discussion about implications of MIS 3 boundary conditions for the scenario drawn here (Chapter 6).

Bibliography

Andersen, K. K., and Coauthors, 2006: The Greenland ice core chronology 2005, 15–42ka. Part 1: Constructing the time scale. *Quaternary Science Reviews*, **25 (23)**, 3246–3257.

Anderson, R., S. Ali, L. Bradtmiller, S. Nielsen, M. Fleisher, B. Anderson, and L. Burckle, 2009: Wind-driven upwelling in the Southern Ocean and the deglacial rise in atmospheric CO2. *science*, **323 (5920)**, 1443–1448.

Arz, H. W., F. Lamy, A. Ganopolski, N. Nowaczyk, and J. Pätzold, 2007: Dominant Northern Hemisphere climate control over millennial-scale glacial sea-level variability. *Quaternary Science Reviews*, **26 (3)**, 312–321.

Ashok, K., S. K. Behera, S. A. Rao, H. Weng, and T. Yamagata, 2007: El Niño Modoki and its possible teleconnection. *Journal of Geophysical Research: Oceans (1978–2012)*, **112 (C11)**.

Barbante, C., and Coauthors, 2006: One-to-one coupling of glacial climate variability in Greenland and Antarctica. *Nature*, **444 (7116)**, 195–198.

Barreiro, M., G. Philander, R. Pacanowski, and A. Fedorov, 2006: Simulations of warm tropical conditions with application to middle Pliocene atmospheres. *Climate Dynamics*, **26 (4)**, 349–365.

Bergamaschi, P., and Coauthors, 2009: Inverse modeling of global and regional CH4 emissions using SCIAMACHY satellite retrievals. *Journal of Geophysical Research: Atmospheres (1984–2012)*, **114 (D22)**.

Bethke, I., C. Li, and K. H. Nisancioglu, 2012: Can we use ice sheet reconstructions to constrain meltwater for deglacial simulations? *Paleoceanography*, **27 (2)**.

Böhm, E., and Coauthors, 2015: Strong and deep Atlantic meridional overturning circulation during the last glacial cycle. *Nature*, **517 (7532)**, 73–76.

Bond, G., and Coauthors, 1997: A pervasive millennial-scale cycle in North Atlantic Holocene and glacial climates. *Science*, **278 (5341)**, 1257–1266, doi:10.1126/science.278.5341.1257.

Braconnot, P., and Coauthors, 2007: Results of PMIP2 coupled simulations of the Mid-Holocene and Last Glacial Maximum–Part 2: feedbacks with emphasis on the location of the ITCZ and mid-and high latitudes heat budget. *Climate of the Past*, **3 (2)**, 279–296.

Broecker, W. S., 1998: Paleocean circulation during the last deglaciation: a bipolar seesaw? *Paleoceanography*, **13 (2)**, 119–121.

Broecker, W. S., G. Bond, M. Klas, G. Bonani, and W. Wolfli, 1990: A salt oscillator in the glacial Atlantic? 1. The concept. *Paleoceanography*, **5 (4)**, 469–477.

Brook, E. J., S. Harder, J. Severinghaus, E. J. Steig, and C. M. Sucher, 2000: On the origin and timing of rapid changes in atmospheric methane during the Last Glacial Period. *Global Biogeochemical Cycles*, **14 (2)**, 559–572.

Burns, S. J., A. Matter, N. Frank, and A. Mangini, 1998: Speleothem-based paleoclimate record from northern Oman. *Geology*, **26 (6)**, 499–502.

Cappelen, J., 2013: Greenland-DMI historical climate data collection 1873-2012 - with Danish abstracts. *DMI Technical Report 13-04. Copenhagen*, [http://www.dmi.dk/laer-om/generelt/dmi-publikationer/2013/].

Chappellaz, J., and Coauthors, 1997: Changes in the atmospheric CH_4 gradient between Greenland and Antarctica during the Holocene. *Journal of Geophysical Research*, **102**, 15–987.

Cheng, H., A. Sinha, X. Wang, F. W. Cruz, and R. L. Edwards, 2012: The Global Paleomonsoon as seen through speleothem records from Asia and the Americas. *Climate Dynamics*, **39 (5)**, 1045–1062.

Cheng, H., and Coauthors, 2006: A penultimate glacial monsoon record from Hulu Cave and two-phase glacial terminations. *Geology*, **34 (3)**, 217–220.

Chiang, J. C., M. Biasutti, and D. S. Battisti, 2003: Sensitivity of the Atlantic intertropical convergence zone to last glacial maximum boundary conditions. *Paleoceanography*, **18 (4)**.

Chiang, J. C., W. Cheng, and C. M. Bitz, 2008: Fast teleconnections to the tropical Atlantic sector from Atlantic thermohaline adjustment. *Geophysical Research Letters*, **35 (7)**.

Chiang, J. C., S.-Y. Lee, A. E. Putnam, and X. Wang, 2014: South Pacific Split Jet, ITCZ shifts, and atmospheric North–South linkages during abrupt climate changes of the last glacial period. *Earth and Planetary Science Letters*, **406**, 233–246.

Chiang, J. C. H., and C. M. Bitz, 2005: Influence of high latitude ice cover on the marine Intertropical Convergence Zone. *Clim. Dynam.*, **25 (5)**, 477–496, doi: 10.1007/s00382-005-0040-5.

Clement, A. C., M. A. Cane, and R. Seager, 2001: An Orbitally Driven Tropical Source for Abrupt Climate Change. *Journal of Climate*, **14 (11)**, 2369–2375.

Clement, A. C., and L. C. Peterson, 2008: Mechanisms of abrupt climate change of the last glacial period. *Reviews of Geophysics*, **46 (4)**.

Crowley, T. J., 1992: North Atlantic deep water cools the southern hemisphere. *Paleoceanography*, **7 (4)**, 489–497.

Cruz, F. W., and Coauthors, 2005: Insolation-driven changes in atmospheric circulation over the past 116,000 years in subtropical Brazil. *Nature*, **434 (7029)**, 63–66.

Cruz, F. W., and Coauthors, 2009: Orbitally driven east–west antiphasing of South American precipitation. *Nature Geoscience*, **2 (3)**, 210–214.

Cvijanovic, I., P. L. Langen, E. Kaas, and P. D. Ditlevsen, 2013: Southward intertropical convergence zone shifts and implications for an atmospheric bipolar seesaw. *Journal of Climate*, **26 (12)**, 4121–4137.

Dansgaard, W., and Coauthors, 1993: Evidence for general instability of past climate from a 250-kyr ice-core record. *Nature*, **364 (6434)**, 218–220.

Dijkstra, H. A., 2007: Characterization of the multiple equilibria regime in a global ocean model. *Tellus*, **59A (5)**, 695–705.

Ding, Q., J. M. Wallace, D. S. Battisti, E. J. Steig, A. J. Gallant, H.-J. Kim, and L. Geng, 2014: Tropical forcing of the recent rapid Arctic warming in northeastern Canada and Greenland. *Nature*, **509 (7499)**, 209–212.

Dokken, T. M., K. H. Nisancioglu, C. Li, D. S. Battisti, and C. Kissel, 2013: Dansgaard-Oeschger cycles: Interactions between ocean and sea ice intrinsic to the Nordic seas. *Paleoceanography*, **28 (3)**, 491–502, doi:10.1002/palo.20042.

Dong, B.-W., and R. Sutton, 2002: Adjustment of the coupled ocean–atmosphere system to a sudden change in the thermohaline circulation. *Geophysical Research Letters*, **29 (15)**, 18–1.

Drijfhout, S., E. Gleeson, H. A. Dijkstra, and V. Livina, 2013: Spontaneous abrupt climate change due to an atmospheric blocking–sea-ice–ocean feedback in an unforced climate model simulation. *Proc. Nat. Acad. Sci. USA*, **110 (49)**, 19 713–19 718, doi:10.1073/pnas.1304912110.

Fedorov, A. V., and S. G. Philander, 2000: Is El Niño changing? *Science*, **288 (5473)**, 1997–2002.

Feely, R. A., R. Wanninkhof, T. Takahashi, and P. Tans, 1999: Influence of El Nino on the equatorial Pacific contribution to atmospheric CO2 accumulation. *Nature*, **398 (6728)**, 597–601.

Ferrari, R., and M. Nikurashin, 2010: Suppression of eddy diffusivity across jets in the Southern Ocean. *Journal of Physical Oceanography*, **40 (7)**, 1501–1519.

Giese, B. S., and S. Ray, 2011: El Niño variability in simple ocean data assimilation (SODA), 1871–2008. *Journal of Geophysical Research: Oceans (1978–2012)*, **116 (C2)**.

Goosse, H., H. Renssen, F. M. Selten, R. J. Haarsma, and J. D. Opsteegh, 2002: Potential causes of abrupt climate events: A numerical study with a three-dimensional climate model. *Geophys. Res. Lett.*, **29 (18)**, 7–1–7–4, doi:10.1029/2002GL014993.

Gottschalk, J., L. C. Skinner, S. Misra, C. Waelbroeck, L. Menviel, and A. Timmermann, 2015: Abrupt changes in the southern extent of North Atlantic Deep Water during Dansgaard-Oeschger events. *Nature Geoscience*.

Griffiths, M., and Coauthors, 2009: Increasing Australian–Indonesian monsoon rainfall linked to early Holocene sea-level rise. *Nature Geoscience*, **2 (9)**, 636–639.

Hall, A., and R. J. Stouffer, 2001: An abrupt climate event in a coupled ocean–atmosphere simulation without external forcing. *Nature*, **409 (6817)**, 171–174.

Held, I. M., and A. Y. Hou, 1980: Nonlinear axially symmetric circulations in a nearly inviscid atmosphere. *Journal of the Atmospheric Sciences*, **37 (3)**, 515–533.

Huber, C., and Coauthors, 2006: "Isotope calibrated Greenland temperature record over Marine Isotope Stage 3 and its relation to CH_4". *Earth and Planetary Science Letters*, **243 (4)**, 504–519, doi:10.1016/j.espl.2006.01.002.

Hughen, K. A., J. T. Overpeck, S. J. Lehman, M. Kashgarian, J. Southon, L. C. Peterson, R. Alley, and D. M. Sigman, 1998: Deglacial changes in ocean circulation from an extended radiocarbon calibration. *Nature*, **391 (6662)**, 65–68.

Hurrell, J. W., M. P. Hoerling, A. Phillips, and T. Xu, 2004: Twentieth century North Atlantic climate change. Part I: assessing determinism. *Climate Dynamics*, **23 (3-4)**, 371–389.

Ivanochko, T. S., R. S. Ganeshram, G.-J. A. Brummer, G. Ganssen, S. J. Jung, S. G. Moreton, and D. Kroon, 2005: Variations in tropical convection as an amplifier of global climate change at the millennial scale. *Earth and Planetary Science Letters*, **235 (1)**, 302–314.

Jackson, L., and M. Vellinga, 2013: Multidecadal to centennial variability of the AMOC: HadCM3 and a perturbed physics ensemble. *J. Climate*, **26 (7)**, 2390–2407.

Kageyama, M., and Coauthors, 2013: Climatic impacts of fresh water hosing under Last Glacial Maximum conditions: a multi-model study. *Climate of the Past*, **9 (2)**, 935–953.

Karamperidou, C., P. N. Di Nezio, A. Timmermann, F.-F. Jin, and K. M. Cobb, 2015: The response of ENSO flavors to mid-Holocene climate: Implications for proxy interpretation. *Paleoceanography*.

Kawase, M., 1987: Establishment of deep ocean circulation driven by deep-water production. *Journal of Physical Oceanography*, **17 (12)**, 2294–2317.

Kim, H.-M., P. J. Webster, and J. A. Curry, 2009: Impact of shifting patterns of Pacific Ocean warming on North Atlantic tropical cyclones. *Science*, **325 (5936)**, 77–80.

Kim, J.-H., O. E. Romero, G. Lohmann, B. Donner, T. Laepple, E. Haam, and J. S. S. Damste, 2012: Pronounced subsurface cooling of North Atlantic waters off Northwest Africa during Dansgaard–Oeschger interstadials. *Earth and Planetary Science Letters*, **339**, 95–102.

Kissel, C., C. Laj, A. M. Piotrowski, S. L. Goldstein, and S. R. Hemming, 2008: Millennial-scale propagation of Atlantic deep waters to the glacial Southern Ocean. *Paleoceanography*, **23 (2)**.

Kleppin, H., M. Jochum, B. Otto-Bliesner, C. A. Shields, and S. Yeager, 2015: Stochastic Atmospheric Forcing as a Cause of Greenland Climate Transitions. *Journal of Climate*, **28 (19)**, 7741–7763.

Koutavas, A., J. Lynch-Stieglitz, T. M. Marchitto, and J. P. Sachs, 2002: El Nino-like pattern in ice age tropical Pacific sea surface temperature. *Science*, **297 (5579)**, 226–230.

Landais, A., and Coauthors, 2004: A continuous record of temperature evolution over a sequence of Dansgaard-Oeschger events during Marine Isotopic Stage 4 (76 to 62 kyr BP). *Geophys. Res. Lett.*, **31 (22)**, doi:10.1029/2004GL021193.

Latif, M., 2001: Tropical Pacific/Atlantic Ocean interactions at multi-decadal time scales. *Geophysical Research Letters*, **28 (3)**, 539.

Latif, M., 2003: Tropical Pacific influences on the North Atlantic thermohaline circulation. *Marine Science Frontiers for Europe*, Springer, 1–9.

Lau, N.-C., and M. J. Nath, 2000: Impact of ENSO on the variability of the Asian-Australian monsoons as simulated in GCM experiments. *Journal of Climate*, **13 (24)**, 4287–4309.

Lee, S., and H.-k. Kim, 2003: The dynamical relationship between subtropical and eddy-driven jets. *Journal of the atmospheric sciences*, **60 (12)**, 1490–1503.

Lee, S.-Y., J. C. Chiang, K. Matsumoto, and K. S. Tokos, 2011: Southern Ocean wind response to North Atlantic cooling and the rise in atmospheric CO2: Modeling perspective and paleoceanographic implications. *Paleoceanography*, **26 (1)**.

Lee, T., and M. J. McPhaden, 2010: Increasing intensity of El Niño in the central-equatorial Pacific. *Geophysical Research Letters*, **37 (14)**.

Li, C., D. S. Battisti, and C. M. Bitz, 2010: Can North Atlantic Sea Ice Anomalies Account for Dansgaard-Oeschger Climate Signals? *J. Climate*, **23 (20)**, 5457–5475.

Li, C., D. S. Battisti, D. P. Schrag, and E. Tziperman, 2005: Abrupt climate shifts in Greenland due to displacements of the sea ice edge. *Geophys. Res. Lett.*, **32 (19)**, L19 702, doi:10.1029/2005GL023492.

Lindzen, R. S., and A. V. Hou, 1988: Hadley circulations for zonally averaged heating centered off the equator. *Journal of the Atmospheric Sciences*, **45 (17)**, 2416–2427.

Liu, Z., and Coauthors, 2009: Transient simulation of last deglaciation with a new mechanism for Bølling-Allerød warming. *Science*, **325 (5938)**, 310–314.

Lynch-Stieglitz, J., M. W. Schmidt, L. G. Henry, W. B. Curry, L. C. Skinner, S. Mulitza, R. Zhang, and P. Chang, 2014: Muted change in Atlantic overturning circulation over some glacial-aged Heinrich events. *Nature Geoscience*, **7 (2)**, 144–150.

Manabe, S., and R. J. Stouffer, 1999: Are two modes of thermohaline circulation stable? *Tellus*, **51A (3)**, 400–411.

Marshall, J., E. Shuckburgh, H. Jones, and C. Hill, 2006: Estimates and implications of surface eddy diffusivity in the Southern Ocean derived from tracer transport. *Journal of physical oceanography*, **36 (9)**, 1806–1821.

Martin, T., W. Park, and M. Latif, 2013: Multi-centennial variability controlled by Southern Ocean convection in the Kiel Climate Model. *Climate dynamics*, **40 (7-8)**, 2005–2022.

Martin, T., W. Park, and M. Latif, 2014: Southern Ocean forcing of the North Atlantic at multi-centennial time scales in the Kiel Climate Model. *Deep-Sea Res. II*, doi:10.1016/j.dsr2.2014.01.018.

Martin, T., W. Park, and M. Latif, 2015: Southern Ocean forcing of the North Atlantic at multi-centennial time scales in the Kiel Climate Model. *Deep Sea Research Part II: Topical Studies in Oceanography*, **114**, 39–48.

Mignot, J., A. Ganopolski, and A. Levermann, 2007: Atlantic subsurface temperatures: Response to a shutdown of the overturning circulation and consequences for its recovery. *Journal of Climate*, **20 (19)**, 4884–4898.

Mikolajewicz, U., 1996: *A Meltwater Induced Collapse of the" conveyor Belt" Thermohaline Circulation and Its Influence on the Distribution of $\delta^{14}C$ and $\delta^{18}0$ in the Oceans*. Max-Planck-Institut für Meteorologie.

Moy, C. M., G. O. Seltzer, D. T. Rodbell, and D. M. Anderson, 2002: Variability of El Niño/Southern Oscillation activity at millennial timescales during the Holocene epoch. *Nature*, **420 (6912)**, 162–165.

O'Brien, P. M. L. M. D. M. M. T. S. W., S.R., 1995: Complexity of Holocene climate as reconstructed from a Greenland ice core. *Science*, **270**, 1962—-1964, doi:10.1126/science.270.5244.1962.

Partin, J. W., K. M. Cobb, J. F. Adkins, B. Clark, and D. P. Fernandez, 2007: Millennial-scale trends in west Pacific warm pool hydrology since the Last Glacial Maximum. *Nature*, **449 (7161)**, 452–455.

Pausata, F. S., D. S. Battisti, K. H. Nisancioglu, and C. M. Bitz, 2011: Chinese stalagmite $\delta^{18}O$ controlled by changes in the Indian monsoon during a simulated Heinrich event. *Nature Geoscience*, **4 (7)**, 474–480.

Pedro, J. B., and Coauthors, 2015: The spatial extent and dynamics of the Antarctic Cold Reversal. *Nature Geoscience*.

Peltier, W. R., and G. Vettoretti, 2014: Dansgaard-Oeschger oscillations predicted in a comprehensive model of glacial climate: A "kicked" salt oscillator in the Atlantic. *Geophys. Res. Lett.*, **41 (20)**, 7306–7313.

Peterson, L. C., G. H. Haug, K. A. Hughen, and U. Röhl, 2000: Rapid changes in the hydrologic cycle of the tropical Atlantic during the last glacial. *Science*, **290 (5498)**, 1947–1951.

Piotrowski, A. M., S. L. Goldstein, R. H. Sidney, R. G. Fairbanks, and D. R. Zylberberg, 2008: Oscillating glacial northern and southern deep water formation from combined neodymium and carbon isotopes. *Earth and Planetary Science Letters*, **272 (1)**, 394–405.

Rahmstorf, S., 2002: Ocean circulation and climate during the past 120,000 years. *Nature*, **419 (6903)**, 207–214.

Rasmussen, T. L., and E. Thomsen, 2004: The role of the North Atlantic Drift in the millennial timescale glacial climate fluctuations. *Palaeogeography, Palaeoclimatology, Palaeoecology*, **210 (1)**, 101–116.

Rasmusson, E. M., and T. H. Carpenter, 1982: Variations in tropical sea surface temperature and surface wind fields associated with the Southern Oscillation/El Niño. *Monthly Weather Review*, **110 (5)**, 354–384.

Rohling, E., and Coauthors, 2008: New constraints on the timing of sea level fluctuations during early to middle marine isotope stage 3. *Paleoceanography*, **23 (3)**.

Rohling, E. J., Q. Liu, A. Roberts, J. Stanford, S. O. Rasmussen, P. L. Langen, and M. Siddall, 2009: Controls on the East Asian monsoon during the last glacial cycle, based on comparison between Hulu Cave and polar ice-core records. *Quaternary Science Reviews*, **28 (27)**, 3291–3302.

Rosen, J. L., E. J. Brook, J. P. Severinghaus, T. Blunier, L. E. Mitchell, J. E. Lee, J. S. Edwards, and V. Gkinis, 2014: An ice core record of near-synchronous global climate changes at the Bolling transition. *Nature Geoscience*, **7 (6)**, 459–463.

Sadekov, A. Y., R. Ganeshram, L. Pichevin, R. Berdin, E. McClymont, H. Elderfield, and A. W. Tudhope, 2013: Palaeoclimate reconstructions reveal a strong link between El Nino-Southern Oscillation and Tropical Pacific mean state. *Nature communications*, **4**.

Schiller, A., U. Mikolajewicz, and R. Voss, 1997: The stability of the North Atlantic thermohaline circulation in a coupled ocean-atmosphere general circulation model. *Climate Dynamics*, **13 (5)**, 325–347.

Schmittner, A., C. Appenzeller, and T. F. Stocker, 2000: Enhanced Atlantic freshwater export during El Niño. *Geophysical Research Letters*, **27 (8)**, 1163–1166.

Schmittner, A., J. Green, and S. Wilmes, 2015: Glacial ocean over-turning intensified by tidal mixing in a global circulation model. *Geophys. Res. Lett*, **42**, 2.

Schmittner, A., O. Saenko, and A. J. Weaver, 2003: Coupling of the hemispheres in observations and simulations of glacial climate change. *Quaternary Science Reviews*, **22 (5)**, 659–671.

Seager, R., and D. S. Battisti, 2007: Challenges to our understanding of the general circulation: abrupt climate change. *Global Circulation of the Atmosphere*, Princeton Univ. Press, Princeton, N. J., 331–371.

Severinghaus, J. P., and E. J. Brook, 1999: Abrupt climate change at the end of the last glacial period inferred from trapped air in polar ice. *Science*, **286 (5441)**, 930–934.

Shakun, J. D., S. J. Burns, D. Fleitmann, J. Kramers, A. Matter, and A. Al-Subary, 2007: A high-resolution, absolute-dated deglacial speleothem record of Indian Ocean climate from Socotra Island, Yemen. *Earth and Planetary Science Letters*, **259 (3)**, 442–456.

Siddall, M., E. J. Rohling, A. Almogi-Labin, C. Hemleben, D. Meischner, I. Schmelzer, and D. Smeed, 2003: Sea-level fluctuations during the last glacial cycle. *Nature*, **423 (6942)**, 853–858.

Sidorenko, D., and Coauthors, 2014: Towards multi-resolution global climate modeling with ECHAM6-FESOM. Part I: Model formulation and mean climate. *Clim. Dynam., submitted*.

Son, S.-W., and S. Lee, 2005: The response of westerly jets to thermal driving in a primitive equation model. *Journal of the atmospheric sciences*, **62 (10)**, 3741–3757.

Steffensen, J. P., and Coauthors, 2008: High-resolution Greenland ice core data show abrupt climate change happens in few years. *Science*, **321 (5889)**, 680–684, doi:10.1126/science.1156393.

Stocker, T., and Coauthors, 2013: IPCC, 2013: climate change 2013: the physical science basis. Contribution of working group I to the fifth assessment report of the intergovernmental panel on climate change.

Stocker, T. F., and S. J. Johnsen, 2003: A minimum thermodynamic model for the bipolar seesaw. *Paleoceanography*, **18 (4)**.

Stott, L., C. Poulsen, S. Lund, and R. Thunell, 2002: Super ENSO and global climate oscillations at millennial time scales. *Science*, **297 (5579)**, 222–226, doi:10.1126/science.1071627.

Takahashi, K., A. Montecinos, K. Goubanova, and B. Dewitte, 2011: ENSO regimes: Reinterpreting the canonical and Modoki El Niño. *Geophysical Research Letters*, **38 (10)**.

Talley, L. D., 2003: Shallow, intermediate, and deep overturning components of the global heat budget. *Journal of Physical oceanography*, **33 (3)**, 530–560.

Timmermann, A., 2003: Decadal ENSO amplitude modulations: A nonlinear paradigm. *Global and Planetary Change*, **37 (1)**, 135–156.

Timmermann, A., S. J. Lorenz, S.-I. An, A. Clement, and S.-P. Xie, 2007: The effect of orbital forcing on the mean climate and variability of the tropical Pacific. *J. Climate*, **20 (16)**, 4147–4159, doi:10.1175/JCLI4240.1.

Toggweiler, J., and B. Samuels, 1998: On the ocean's large-scale circulation near the limit of no vertical mixing. *Journal of Physical Oceanography*, **28 (9)**, 1832–1852.

Trenberth, K. E., D. P. Stepaniak, and J. M. Caron, 2000: The global monsoon as seen through the divergent atmospheric circulation. *Journal of Climate*, **13 (22)**, 3969–3993.

Tudhope, A. W., and Coauthors, 2001: Variability in the El Niño-Southern Oscillation through a glacial-interglacial cycle. *Science*, **291 (5508)**, 1511–1517.

Van Breukelen, M., H. Vonhof, J. Hellstrom, W. Wester, and D. Kroon, 2008: Fossil dripwater in stalagmites reveals Holocene temperature and rainfall variation in Amazonia. *Earth and Planetary Science Letters*, **275 (1)**, 54–60.

Vavrus, S., M. Notaro, and Z. Liu, 2006: A Mechanism for Abrupt Climate Change Associated with Tropical Pacific SSTs*. *Journal of climate*, **19 (2)**, 242–256.

WAIS Divide Project Members, and Coauthors, 2015: Precise interpolar phasing of abrupt climate change during the last ice age. *Nature*, **520 (7549)**, 661–665.

Wang, B., and S. An, 2002: A mechanism for decadal changes of ENSO behavior: Roles of background wind changes. *Climate Dynamics*, **18 (6)**, 475–486.

Wang, C., C. Deser, J.-Y. Yu, P. DiNezio, and A. Clement, 2012: El Nino and southern oscillation (ENSO): a review. *Coral Reefs of the Eastern Pacific*, 3–19.

Wang, X., A. S. Auler, R. L. Edwards, H. Cheng, P. S. Cristalli, P. L. Smart, D. A. Richards, and C.-C. Shen, 2004: Wet periods in northeastern Brazil over the past 210 kyr linked to distant climate anomalies. *Nature*, **432 (7018)**, 740–743.

Wang, X., A. S. Auler, R. L. Edwards, H. Cheng, E. Ito, and M. Solheid, 2006: Interhemispheric anti-phasing of rainfall during the last glacial period. *Quaternary Science Reviews*, **25 (23)**, 3391–3403.

Wang, Y.-J., H. Cheng, R. L. Edwards, Z. An, J. Wu, C.-C. Shen, and J. A. Dorale, 2001: A high-resolution absolute-dated late Pleistocene monsoon record from Hulu Cave, China. *Science*, **294 (5550)**, 2345–2348.

Wright, D. G., 1996: Rapid changes in ocean circulation and atmospheric radiocarbon. *Paleoceanography*, **11 (6)**, 773–795.

Wunsch, C., 2006: Abrupt climate change: An alternative view. *Quat. Res.*, **65 (2)**, 191–203, doi:10.1016/j.yqres.2005.10.006.

Yin, J. H., and D. S. Battisti, 2001: The importance of tropical sea surface temperature patterns in simulations of Last Glacial Maximum climate. *Journal of Climate*, **14 (4)**, 565–581.

Yuan, D., and Coauthors, 2004: Timing, duration, and transitions of the last interglacial Asian monsoon. *Science*, **304 (5670)**, 575–578.

Zebiak, S. E., and M. A. Cane, 1987: A Model El Niñ-Southern Oscillation. *Monthly Weather Review*, **115 (10)**, 2262–2278.

Zhang, R., and T. L. Delworth, 2005: Simulated tropical response to a substantial weakening of the Atlantic thermohaline circulation. *Journal of Climate*, **18 (12)**, 1853–1860.

Zhang, X., G. Lohmann, G. Knorr, and C. Purcell, 2014: Abrupt glacial climate shifts controlled by ice sheet changes. *Nature*, **512**, 290–294, doi:10.1038/nature13592.

Zhang, Y., J. M. Wallace, and D. S. Battisti, 1997: ENSO-like interdecadal variability: 1900-93. *Journal of climate*, **10 (5)**, 1004–1020.

2 Stochastic atmospheric forcing as cause for Greenland climate transitions

Abstract

An unforced simulation of the Community Climate System Model 4 (CCSM4) is found to have Greenland warming and cooling events that resemble Dansgaard-Oeschger-cycles in pattern and magnitude. With the caveat that only 3 transitions were available to be analyzed, we find that the transitions are triggered by stochastic atmospheric forcing. The atmospheric anomalies change the strength of the subpolar gyre, leading to a change in Labrador Sea sea-ice concentration and meridional heat transport. The changed climate state is maintained over centuries through the feedback between sea-ice and sea-level pressure in the North Atlantic. We discuss indications that the initial atmospheric pressure anomalies are preceded by precipitation anomalies in the West Pacific warm pool. The full evolution of the anomalous climate state depends crucially on the climatic background state.

2.1 Introduction

Here, we document three climate transitions occurring in a 1000 year pre-industrial control simulation of the Community Climate System Model 4 (CCSM4). These are two gradual cooling and one abrupt warming event around Greenland. The analysis is focused on the first cooling event. The atmospheric anomaly during the cold event resembles closely the one described by Drijfhout et al. (2013) (see Sec. 1.1.2). However, the evolution and hence the cause of the cold NA phase is different. It involves a strong positive feedback loop of the SPG circulation. The first weakening of the SPG is caused by decrease in wind stress curl associated with a stochastic atmospheric circulation anomaly. The decreased gyre circulation changes the salinity transport into the highly sensitive deep water convection site in the LS, thus reducing deep water convection and eventually affecting the AMOC. This is followed by an increase of sea ice cover and a drop in Greenland temperature. The increased sea ice cover itself forces a reorganization of the atmosphere, thus sustaining the anomalous atmospheric forcing of the gyre circulation for about 200 years.

The objective of this paper is to identify processes and regions of atmospheric, oceanic and sea ice interactions that play a key role in the transitions between cold and warm NA phases and to suggest a consistent sequence of events causing these transitions. In Section 2.2 we give a brief overview of CCSM4, the set-up of the control simulation and the different experiments that we carried out. Section 2.3 comprises the results structured as follows. We describe how the first cold event manifest itself in Greenland, the NA and globally (Section 2.3.1), followed by a description of the stochastic atmospheric trigger (Section 2.3.2.1), the dynamics of the ocean response and sea ice changes (Section 2.3.2.2) and the atmospheric feedback (Section 2.3.2.3). The sequence of events leading to the abrupt warming is documented in Section 2.3.3. Finally we assess the dependence of the proposed mechanism on the particular background climate (Section 2.3.4) and test the atmospheric trigger in forced ocean simulations (Section 2.3.5). In Section 2.4 we discuss our main findings and a possible influence of tropical temperature and precipitation anomalies on NA atmosphere circulation changes. The paper concludes with a summary in Section 2.5.

2.2 Model

The numerical experiments are performed using CCSM4, which consists of the fully coupled atmosphere, ocean, land and sea ice models. A detailed description of this version can be found in Gent et al. (2011). The ocean component is POP2 and has a horizontal resolution that is constant at 1.125° in longitude and varies in latitude from 0.27° at the equator to approximately 0.7° in high latitudes. In the vertical there are 60 depth levels; the uppermost layer has a thickness of 10 *m*, the deepest layer has a thickness of 250 *m*. The atmospheric component uses a horizontal resolution of 1.9° × 2.25° (longitude and latitude, respectively) with 26 levels in the vertical. The sea ice model shares the same horizontal grid as the ocean model and the land model is on the same horizontal grid as the atmospheric model. This setup constitutes the released version of CCSM4, and further details can be found in Danabasoglu et al. (2012). The subsequent sections will analyze and compare several different simulations listed in Table 2.1. The simulations are either conducted with the fully coupled version or the ocean-sea ice version with prescribed atmospheric fluxes and river run off. The main focus is on a 1000 year long pre-industrial control simulation (CONT), in which the earth's orbital parameters are set to 1990 values and the atmospheric composition is fixed at its 1850 values (for details of the atmospheric composition see Gent et al. (2011)). For comparison with CONT and as initial condi-

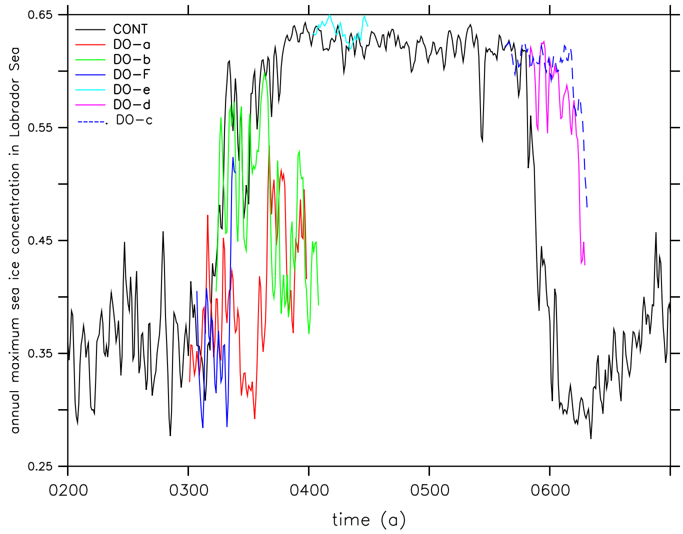

Figure 2.1.: Annual maximum sea ice concentration in the LS (averaged from 65° to 45 ° W and 50° to 70 ° W) for CONT (black). Additionally shown are the sea ice concentrations for the different branch runs (different colors). All curves are smoothed by a 2 year running mean.

tions for some of the experiments described below we make use of an other pre-industrial control simulation (HI). HI differs from CONT only in the horizontal resolution of the atmospheric component which is 0.98° × 1.258°. An overview of differences and similarities between CONT and HI is provided by Shields et al. (2012) and discussed in Section 2.3.4.

Danabasoglu et al. (2012) and Danabasoglu et al. (2014) assess the fidelity of the CCSM ocean module. For CONT in particular we find that the AMOC is well represented at $26.5°N$ with a maximum of 18.4 Sv at 1000 m, compared to the observed maximum of 18.6 Sv, also at 1000 m (Cunningham et al., 2007). The SPG circulation strength (spatial maximum of about 50 Sv) in CONT agrees fairly well with observations by Johns et al. (1995) and Pickart et al. (2002) of 48 and 40 Sv, respectively.

In a 200 year average over a period prior to the transitions CONT features a cold ($\sim 2°C$) and fresh (0.2 psu) bias in the upper 100 m of the western SPG and the LS compared to temperature (Locarnini et al., 2010) and salinity (Antonov et al., 2010) data from the World Ocean Atlas 2009 (WOA09). Below the surface the model is too warm and salty by about 1 $°C$ and about 0.3 psu, respectively. In both, WOA09 and CONT maximum mixed layer depths are during March in the LS with values in excess of 1400 m.

exp	compset	atmosphere		length [years]	starting year	starting from	additional changes
		resolution	forcing				-
CONT	B	2°	-	1000	-	-	-
HI	B	1°	-	1300	-	-	-
LGM	B	1°	-	401	-	-	-
DO_F	B	2°	-	36	305	CONT	-
OI_a	G	-	DO_F year 332/333	11	311	HI	-
OI_b, _c, _d	G	-	DO_F year 312/313	30, 21, 13	299, 311, 321	HI	-
OI_e, _f	G	-	DO_F year 305/306	13	299, 327	HI, OI_b	-
DO_a,_b	B	2°	-	102, 90	299, 321	CONT	-
DO_c,_d	B	2°	-	73, 51	561, 581	CONT	-
DO_e,_f	B	2°	-	51, 51	401, 899	CONT	-
DO_X	B	2°	-	198	1001	CONT	-
DO_CO_2	B	2°	-	96	381	CONT	increased atmospheric CO_2 by 20 ppmv
DO_113k	B	2°	-	201	249	CONT	orbital conditions from 113 kyrs BC
DO_71k	B	2°	-	117	249	CONT	orbital conditions from 71 kyrs BC

Table 2.1.: Simulations analyzed and conducted for this study. The letter G and B in column compset refer to ocean-sea ice simulations and the fully coupled version of CESM, respectively. The setup of the different simulations is described in Section 2.2.

To ensure that the transitions are not caused by any numerical or computational issues several runs branching from CONT were performed to test the reproducibility of the occurring transitions. The branch runs (DO_a-f in Table 2.1) were started using initial conditions from CONT at different points in time. The initial conditions are modified by a random $O(\epsilon)$ perturbation.
The branch runs reproduce the climate transitions (2 warming (DO_c,d) and 3 cooling (DO_a,b and DO_F) transitions) even though the transitions in the branch runs occur at different points in time and not always with the same amplitude as in CONT. The annual maximum sea ice concentration in the LS of the original CONT run (black) and the branch runs (different colors) are depicted in Figure 2.1. The reproducibility of the climate transitions gives us trust in our findings beyond the lack of statistical analysis possibility. A 200-year extension (DO_X) of CONT was conducted without any further transitions occurring, thus the second cold phase last at least 400 years. Possible reasons for the lack of transitions in DO_X are discussed in Section 2.4. This and the occurrence of the branch run transitions at different times suggest that a stochastic process triggers a switch between two climate states. Furthermore the different durations of the cold phases points to the fact that no particular build up time for any kind of reservoir (e.g., warm subsurface water) is involved.
To test the proposed role of the stochastic atmospheric trigger, we conducted several ocean-ice (OI) simulations with different atmospheric forcings (Table 2.1). For this purpose a part of CONT was rerun, saving the atmospheric fluxes at 3 hour intervals (DO_F run). The OI experiments were started from HI initial conditions and were forced with annually repeating atmospheric fluxes from DO_F (July to June). The different starting years and the forcing year from DO_F are listed in Table 2.1. We chose starting years preceding a rapid sea ice increase in DO_F for experiments with transitions from a warm to a cold NA phase (OI_a-d). Year 305/306 in DO_F precedes a rapid sea ice decrease and is utilized to reproduce the warming transition (OI_e and OI_f).

2.3 Results

2.3.1 Sequence of events

The pre-industrial control simulation analyzed here features abrupt surface temperature changes in Greenland and in the whole northern hemisphere. In the entire simulation three transitions between warm and cold NA phases occur (Figure 2.2 (a)). Hereafter we refer to the first warm NA phase (year 50 to 250, as indicated in Figure 2.2) as NA_w1 and to the first cold NA phase (year 350 to 550) as NA_c1. Over the first transition (first red line in Figure 2.2) the annual mean Greenland temperature decreases gradually by approximately 3 $°C$ (averaged over Greenland (55 to 15$°W$ and 65 to 80$°N$)). This is followed by an abrupt warming of about the same amplitude over the second transition (second red line in Figure 2.2). At the south-west coast of Greenland temperature changes are more than three times that value.

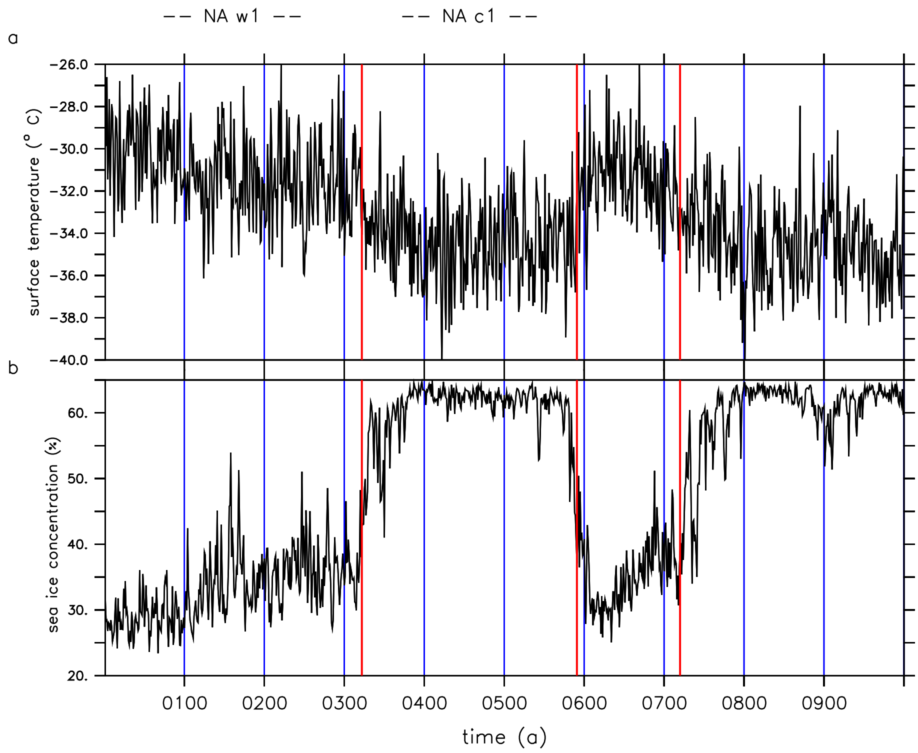

Figure 2.2.: (a) Greenland annual minimum surface temperature [$°C$] averaged from 55 ° to 15$°W$ and 65° to 80$°N$. (b) Annual maximum of sea ice concentration in the LS (as in Fig. 2.1). The different phases of interest are indicated on top, NA_w1 is the period from year 50 to year 250 and NA_c1 from year 350 to 550. The transition between different warm and cold phases, based on Greenland temperature changes, are marked by red horizontal lines.

Cooling and warming are more pronounced during winter months (Figure 2.2 (a)). The global surface temperature signature of NA_c1 is depicted in Figure 2.3. The strong warm anomaly off the coast of New Foundland is due to a contraction of the SPG (described in more detail in Section 2.3.2) and the resulting northward migration of the Gulf Stream. The opposite sign anomalies in the Southern Ocean and parts of Antarctica are small in amplitude (about 0.5 to 1 $°C$) compared to the changes around Greenland. This anti-correlation is suggestive of the “bipolar seesaw“ (Stocker and Johnsen, 2003), but is not analyzed here because of the small signal-to-noise ratio. The tropical temperature difference between NA_c1 and NA_w1 is also small in amplitude compared to the high northern latitude changes, but has the same sign. Tropical Pacific precipitation changes associated with NA_c1 feature a dipole pattern (not shown) that corresponds to a precipitation decrease in the western Pacific warm pool (WPWP) and a simultaneous increase in the eastern tropical Pacific. This is consistent with paleo-reconstructions that connect Greenland stadials with decreased precipitation over the WPWP and dominant El Niño-like conditions (Stott et al. (2002), based on magnesium/calcium composition and $\delta^{18}O$ of planctonic foraminifera).

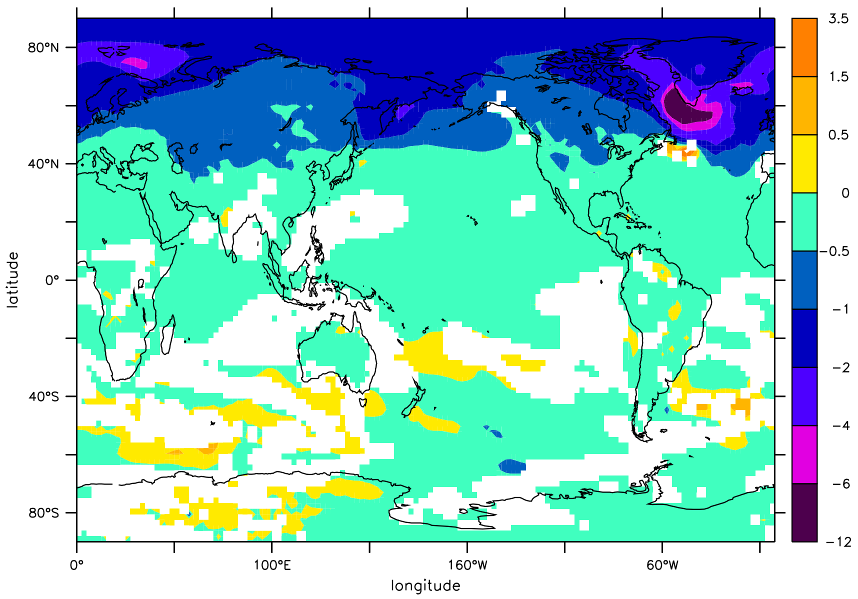

Figure 2.3.: Global temperature signal: Surface temperature difference between years 350 and 550 (NA_c1) and 50 and 250 (NA_w1). Regions are only shaded if correlation with Greenland surface temperature (averaged over the same region as in Fig. 2.2) for the period between year 270 and 470 is significant on a 95 %-level.

The onset of the events based on Greenland temperature are years 326, 591 and 721 (e.g., Figure 2.2, red lines). In the following Section 2.3.2 we focus only on the first cooling event (year 326). The sequence of events leading to the abrupt warming (year 591) is briefly documented in Section 2.3.3. Section 2.3.2 describes the dynamics of the first climate transition based on the following sequence of events. A stochastic atmospheric circulation anomaly, resembling a strong negative North Atlantic Oscillation (NAO) phase

is forcing a circulation anomaly in the SPG (Section 2.3.2.1). The SPG switches to a weak circulation mode due to a salinity driven positive feedback loop, shutting down deep water convection in the LS, and weakening the AMOC. Associated with the weaker circulation mode is a colder surface subpolar ocean (Section 2.3.2.2). As a consequence sea ice concentration increases in the LS, which in turn causes a reorganization of the atmosphere and a drop in Greenland temperature (Section 2.3.2.3).
The atmospheric changes over the NA can thus be separated into two parts: An initial trigger that resembles a negative NAO phase and a positive sea-ice - sea level pressure feedback, namely an anticyclonic anomaly that persists for about 200 years, and sustains the anomalous atmospheric forcing of the ocean.

2.3.2 Dynamical changes

2.3.2.1 Atmospheric trigger - year 310 to year 320

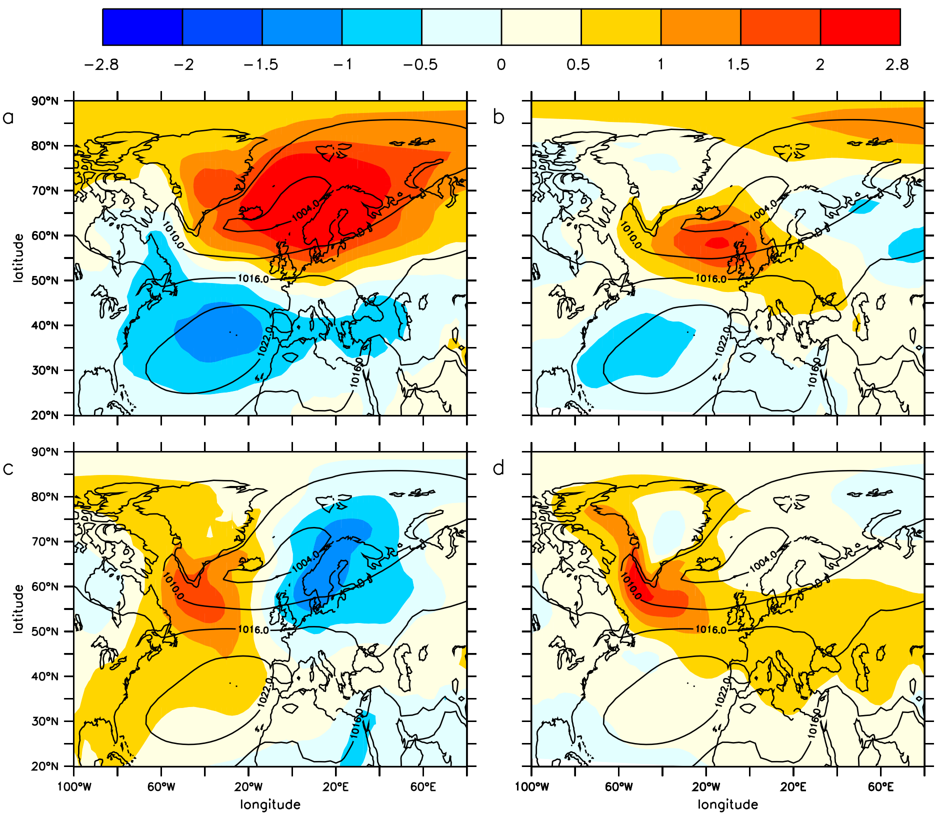

Figure 2.4.: Sea level pressure anomaly [hPa] for year 310 to 315 (a), year 315 to 320 (b), year 320 to 325 (c) and for NA_c1 (year 350 to 550, d). All anomalies are relative to NA_w1 and positive values imply a higher SLP than during Na_w1. Contours show the 1000-year mean of SLP.

In the beginning (year 310 to 315, Figure 2.4 (a)) an anticyclonic SLP anomaly evolves, centered between Greenland and north western Europe and resembling a negative NAO phase. The anticyclonic anomaly moves south westward and decays over the next 5 years (Figure 2.4 (b)). The NAO is known to drive the dominant part of NA - in particular the LS - ocean heat transport variability, through changes in wind stress and buoyancy forcing (e.g., Eden and Willebrand (2001)). The total surface heat flux over the LS weakens at this point by about 14 Wm^{-2} (difference between first (year 270 to 290) and second column (year 310 to 320) in Table 2.2) as expected from a negative NAO phase (i.e., less heat loss of the LS to the atmosphere). The surface heat flux over the entire SPG region decreases as well, though the amplitude is small. At about the same time the wind stress curl north of the zero wind-curl line reduces (Figure 2.5 (a), year 310 to 315 and (b), year 315 to 320). At this point the maximum changes are located above the central and eastern SPG where they account for a 30 to 50 % reduction compared to the long term mean. Furthermore the zero wind-curl line shifts farther north, contributing to a contraction of the SPG.

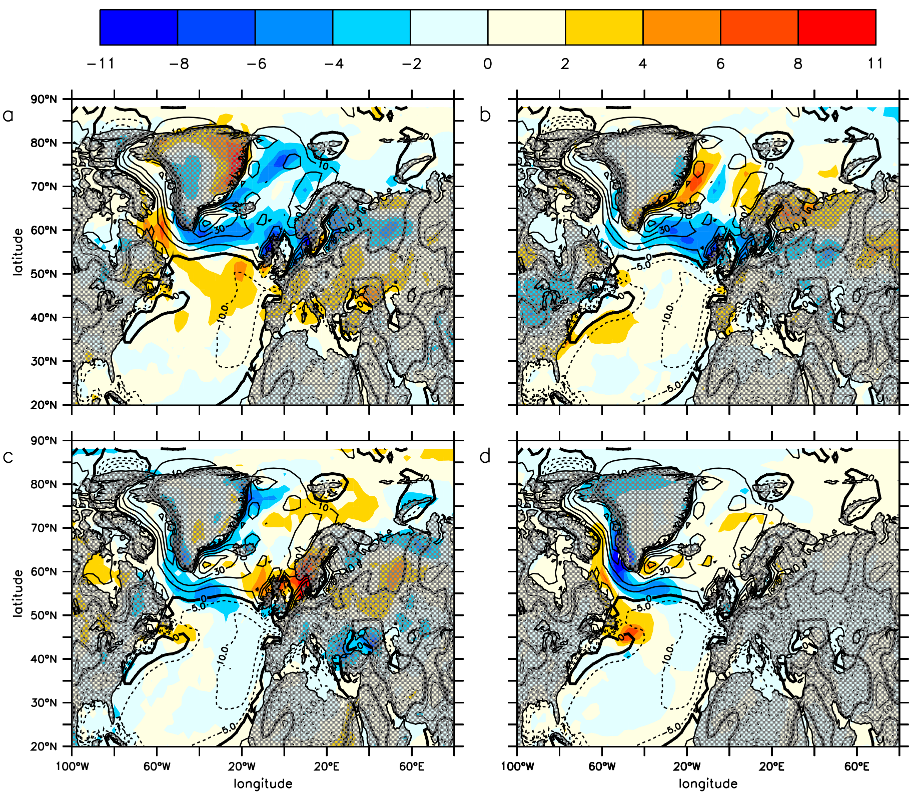

Figure 2.5.: Wind stress curl anomaly [$\cdot 10^{-8}$N m^{-3}] for year 310 to 315 (a), year 315 to 320 (b), year 320 to 325 (c) and for NA_c1 (year 350 to 550, d). All anomalies are relative to NA_w1. Contours show the the 1000-year mean of wind stress curl.

To estimate the importance of the changed wind stress curl in forcing the anomalous SPG circulation the Sverdrup transport was calculated according to Sverdrup theory (e.g., Pedlosky (1996)). The Sverdrup transport in the LS and the north-western NA is compared to the actual circulation changes in this region and the entire SPG (Figure 2.6). The Sverdrup transport reproduces the anomalous SPG circulation well.

2.3.2.2 Ocean and sea ice response - year 315 onward

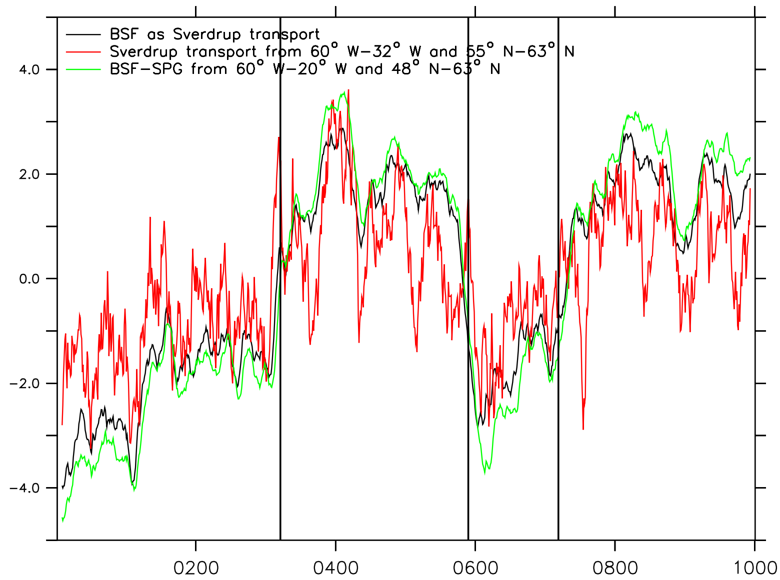

Figure 2.6.: Sverdrup transport anomaly [Sv] (red - averaged from 55° to 63°N and 60° to 32°W), actual circulation anomaly in the SPG [Sv] averaged over the same region as the Sverdrup transport (black) and over the entire SPG (60° to about 20°W and 48° to 63°N, green). All time series are smoothed by a 15-year running mean.

The total NA_w1-NA_c1 difference in the strength of the circulation (represented here by the Barotropic Stream Function (BSF)) in the core region of the SPG accounts for about 10 Sv, a 30 % reduction (Figure 2.7 (contours)). At the southern edge the circulation changes up to 20 Sv due to a northward shift of the Gulf stream path. The temperature of the upper central SPG decreases by up to 8°C in NA_c1 relative to NA_w1 (Figure 2.7 (color)).
At the onset of the first cooling transition the decreased wind stress curl forcing (year 310

onward, Figure 2.5 (a) and (b)) causes a first weakening of the SPG circulation (Figure 2.6) around year 318. This time scale is in excellent agreement with the suggested time lag of 3 years after that the SPG strength reduces in response to wind stress curl changes associated with a negative NAO (Eden and Willebrand, 2001). This weakening initiates a positive feedback loop in the SPG leading to the large ocean temperature (color) and circulation (contours) response depicted in Figure 2.7. Figure 2.8 (a) shows the density-

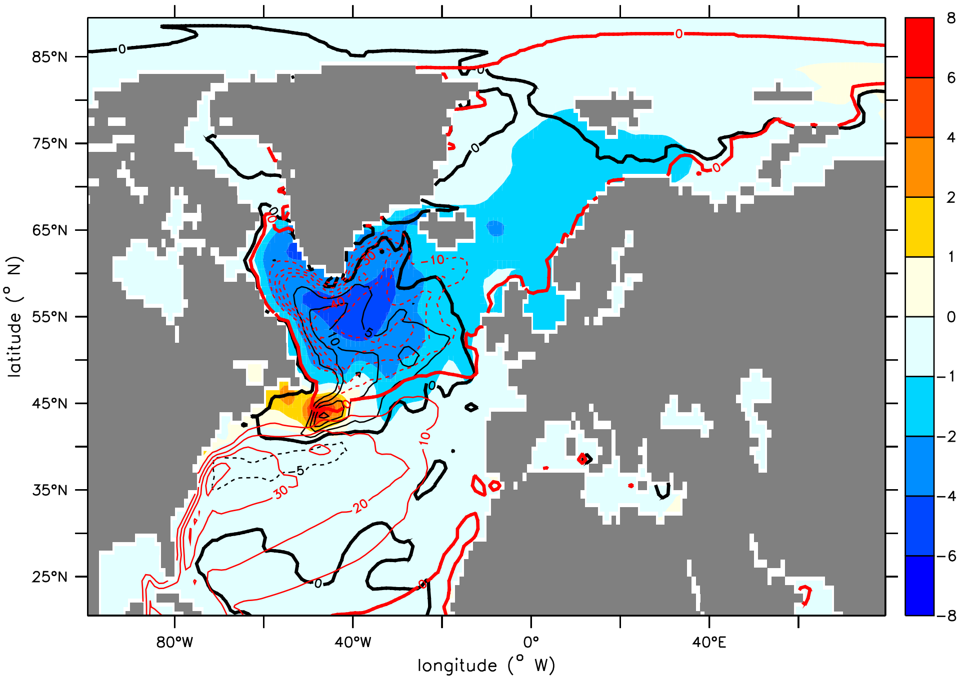

Figure 2.7.: Barotropic stream function anomaly [Sv] (black contours) and temperature anomaly [$°C$] (color) averaged over the upper 100 m in the subpolar gyre, difference between NA_c1 (year 350 to 550) and NA_w1 (year 50 to 250). Contouring interval is 5 Sv, full lines show positive anomalies and dashed lines negative anomalies. The red contours show the 1000 year mean of barotropic stream function [Sv]. The contouring interval is 10 Sv, full contours indicate anticyclonic and dashed contours cyclonic circulation.

depth evolution in the LS. Due to a drop in salinity of 1.6 psu (Figure 2.9 (a), ~ year 319) the density in the upper LS starts to decrease simultaneously (year 319) with the declining gyre circulation. To understand the upper ocean salinity decrease in the LS, salinity budget terms for the upper ~ 300 m of the LS are depicted in Figure 2.10 and

Table 2.2. Salinity advection decreases from year 319 onward (due to advection changes through the southern and eastern face of the box), but this decrease is largely compensated by lower diffusion (including convection) which normally contributes to freshening of the LS. The tendency term becomes negative for a 20-year period from year 315 onward (Table 2.2 and Figure 2.10 (b)), indicating the transition period, due to a negative balance of advection and diffusion. From about year 325 to year 335 the surface fluxes contribute to the negative tendency. Because the surface fluxes do not show a trend over the transition period, this indicates that the decrease of salinity in the LS and the entire SPG is a direct consequence of the slowdown of the SPG circulation. This is consistent with a model study by Born et al. (2013b), who show that salt transport in the Irminger current increases with a stronger circulation of the SPG, independent of salinity in the source region of the Irminger current. They find that enhanced volume transport overcompensates possible low salinity anomalies in the source region by about two orders of magnitude. That implies a decreased salinity transport towards the LS and central parts of the SPG during periods of decreased gyre circulation. A decrease of salinity is seen in the entire water column of the LS (from 65 $^\circ W$ to 55$^\circ W$, Figure 2.9 (a)) but with lower amplitude than at the surface.

budget term		Labrador Sea			
		year 270 -290	year 310-320	year 320-330	year 381-401
advection	temperature $[Wm^{-2}]$	25.23	23.14	14.95	8.47
	salt$\cdot 10^{-8}$[kg $\cdot$ m (kg $\cdot s)^{-1}$]	10.43	10.45	9.21	7.84
diffusion (incl. convection)	temperature $[Wm^{-2}]$	60	48.54	52.7	9.86
	salt $\cdot 10^{-8}$[kg $\cdot$ m (kg $\cdot s)^{-1}$]	-10.29	-10.33	-9.06	-7.69
surface flux	temperature $[Wm^{-2}]$	-86	-72.45	-69.3	-18.87
	salt$\cdot 10^{-8}$[kg $\cdot$ m (kg $\cdot s)^{-1}$]	-0.15	-0.14	-0.16	-0.15
			year 315-335		
tendency	temperature $[Wm^{-2}]$		-2.2		
	salt$\cdot 10^{-8}$[kg $\cdot$ m (kg $\cdot s)^{-1}$]		-0.016		

Table 2.2.: Heat and salinity budget (upper 280 m) of the Labrador Sea (53 $^\circ$ to 65 $^\circ N$ and 60° to 45 $^\circ W$) for the pre-cooling phase during NA_w1 (year 270-290) and a phase after the first transition during NA_c1 (year 381-401). Furthermore two values are given for the transition period (year 310-320 and 320-330). The tendency term is averaged over the transition period. Negative signs imply a cooling and freshening of the box.

As a result of the decreased surface density (Figure 2.8 (a)) the water column in the LS is stably stratified and maximum March Mixed Layer Depth (MLD) reduces from year 319 onward (Figure 2.8 (b)). Eventually, during NA_c1 maximum March MLD is in average below 200 m, indicating no deep water convection. Slightly increased MLD south of Iceland (Figure 2.11) indicate a minor compensation of deep water formation at this location during NA_c1. This is caused by a warm temperature anomaly at a depth of $\sim$ 1300 m (Figure 2.9 (b)). The decrease in deep water convection in the LS causes a slow down of the AMOC from around year 325 (max. AMOC located around a depth of 880 m and between 35° and 40°N, Figure 2.8 (c)).

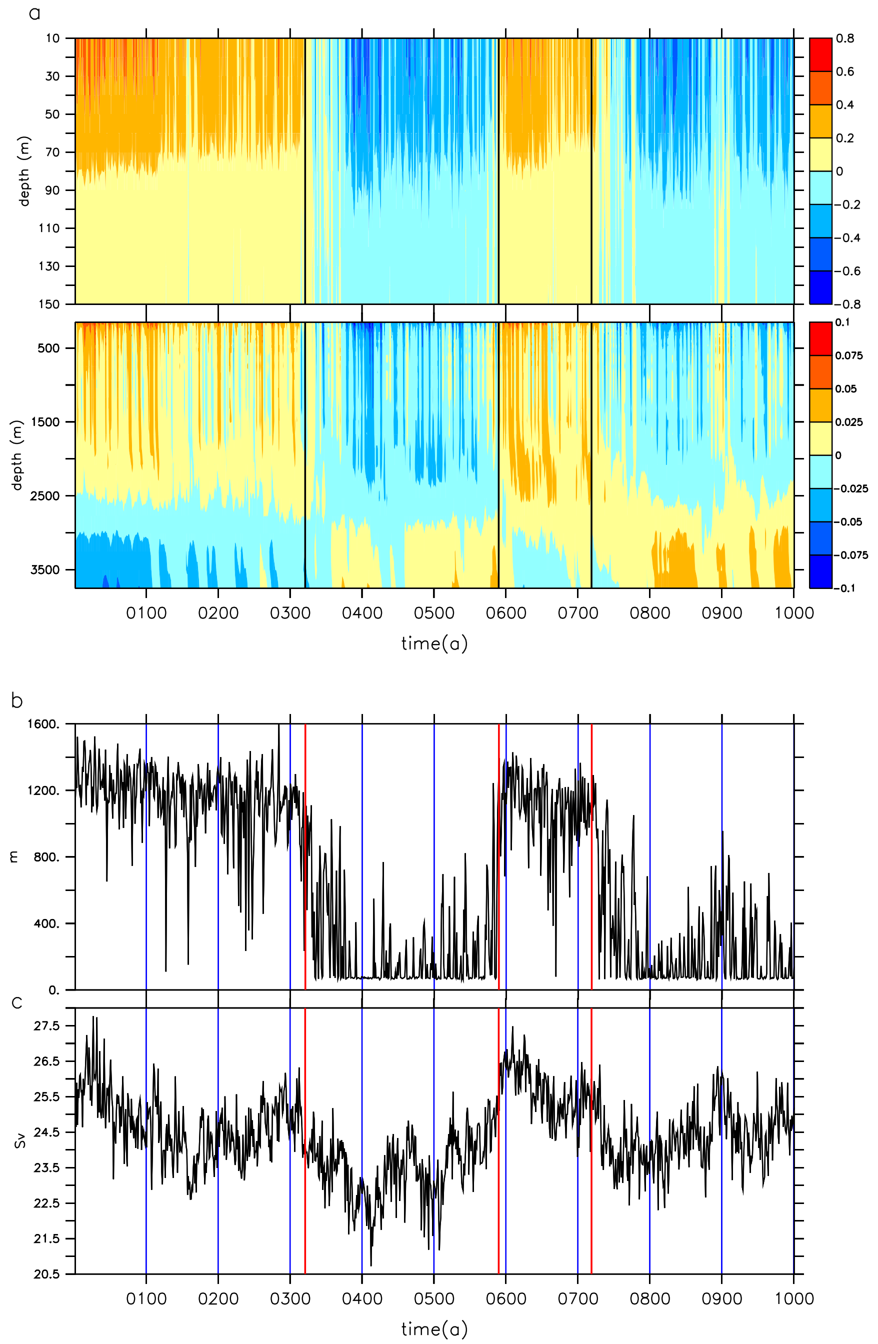

Figure 2.8.: (a) Density anomaly [kgm^{-3}] in the LS (averaged from about 55 ° to 63°N and 60° to 45°W) relative to the 1000-year mean. (b) Maximum march MLD [m] in the LS (same region as in (a)). (c) Maximum AMOC [Sv].

However, the AMOC does not shut down, due to the still active deep water convection in the Nordic Seas and the enhanced deep water convection south of Iceland. The reduced horizontal density gradient between the center and the boundary current (compare to the stronger salt anomalies towards the west in Figure 2.9 (a)) weaken the gyre circulation further, thus closing the positive feedback loop (Born and Stocker (2014) and Born et al. (2013a)).
The cooling of the upper LS is a consequence of reduced convection and advection of temperature (both from year 320 on, Table 2.2 (column 2)). There is a small warm anomaly (0.1 to 0.3 °C, Fig. 2.9 (b)) in the LS in the intermediate and deeper ocean during NA_c1. However, due to the still active deep water convection in the NA the warm anomaly never becomes strong enough to destabilize the water column and thus can not trigger the onset of NA_w1, in contrast to what Dokken et al. (2013) find for the Nordic Seas. The inter-

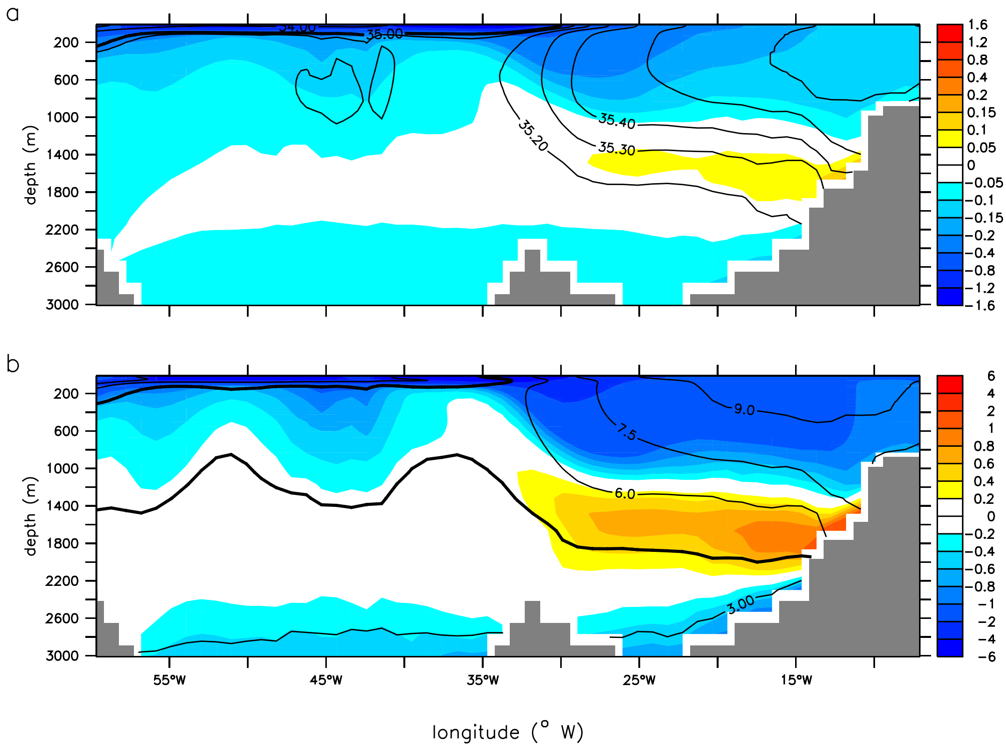

Figure 2.9.: Salinity (a) and temperature (b) anomaly in a cross section through the SPG averaged from about 57° to 61°N. Anomaly is between NA_c1 and NA_w1. Contours show the 1000-year mean and the intervals are 1.5 °C in (a) and 1 psu from 33 to 35 psu and 0.1 psu from 35 to 35.6 psu in (b).

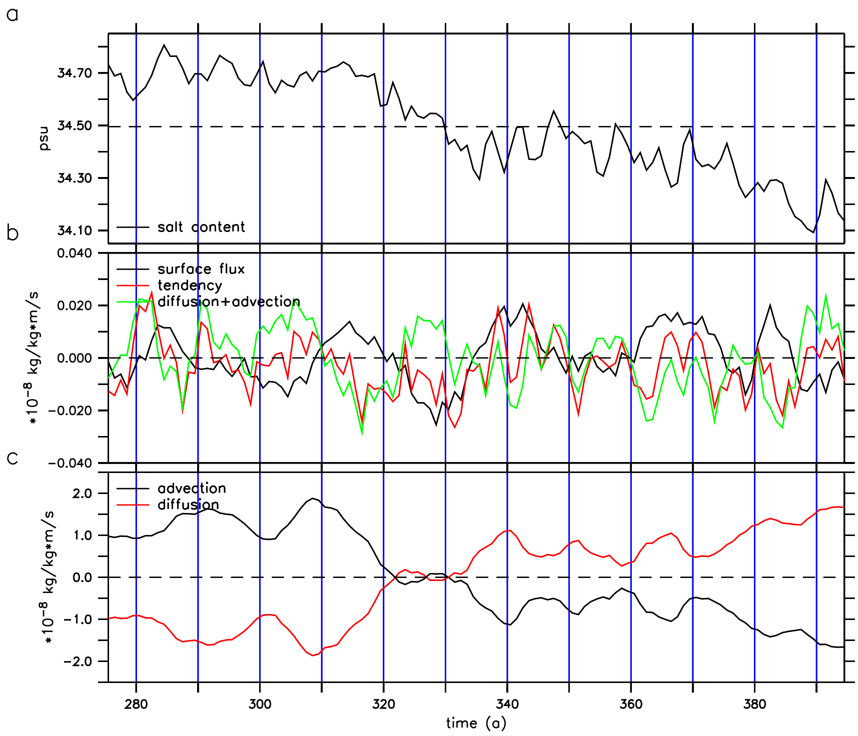

Figure 2.10.: Salinity budget for the upper 280 m of the LS (53 ° to 65 °N and 60° to 45 °W) over the transition between NA_w1 and NA_c1. (a) Salinity content (psu), (b) surface flux anomaly (black), tendency term (red) and combined diffusion and advection anomaly (green) and (c) advection anomaly (black) and diffusion anomaly (red). All budget term time series are smoothed by a 7-year running mean.

mediate depth warming is more pronounced in lower latitudes (up to 45 °N, not shown). In the Nordic Seas the surface layer is fresher and colder during NA_c1. However, the warmer subsurface Atlantic inflow becomes colder and less saline too and a strong halocline is always sustained. This might be due to the enhanced deep water convection south of Iceland. Changes in thermohaline structure around Iceland (the Nordic Seas) occur about 10 (30) years after the decrease in Greenland temperature sets in and reflect thus most likely the changed ocean circulation.
In contrast to the LS the heat budget in the SPG-box (not shown) is dominated by changes in temperature advection, due to a decrease of heat advected into the box through the south and from below, partly balanced by a decrease in heat advected through the north face. Diffusion and surface fluxes counteract the cooling tendency of the decreased advection, but are smaller in magnitude.
As a consequence of the colder ocean temperatures sea ice growth commences (from year

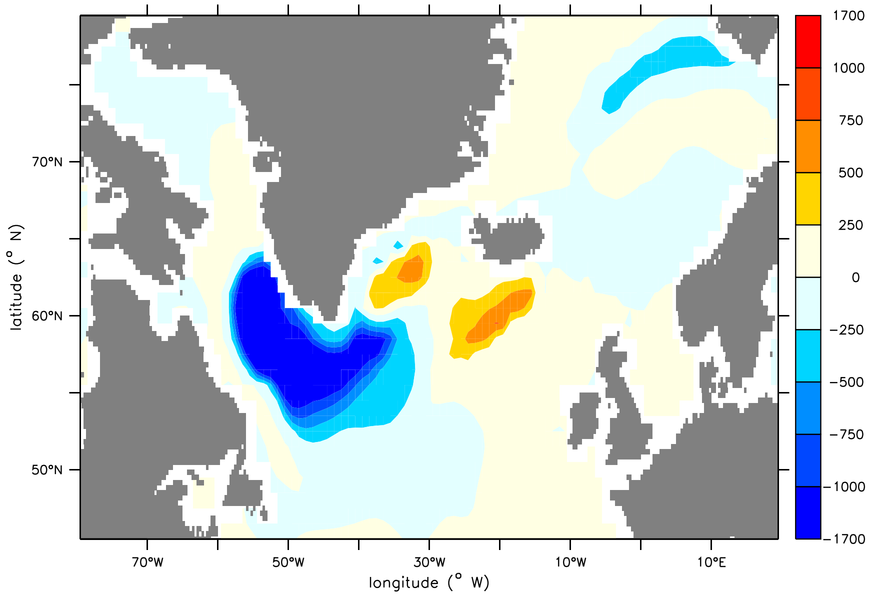

Figure 2.11.: March maximum MLD [*m*] anomaly between NA_c1 and NA_w1

321 onward) in the LS. Annual maximum sea ice concentration, in average, increases here by about 100 % relative to NA_w1, equivalent to about 30 % increased sea ice concentration (Figure 2.2 (b)). The difference in horizontal extent of annual maximum sea ice concentration between NA_c1 and NA_w1 is depicted in Figure 2.12. The changes are largest in the LS (up to a difference of 90 % sea ice coverage) and stretch from there with lower amplitude along the south eastern coast of Greenland, north of Iceland towards Svalbard and until the northern coast of Norway. A similar spatial pattern of sea ice increase is observed at the north-eastern coast of Asia (not shown) though smaller in amplitude. The sea ice edge progresses farther south and east in the Nordic Seas and the LS as indicated by the white and black contours in Figure 2.12. The sea ice increase causes the surface heat fluxes in the LS to decrease dramatically (from year 322 onward). The changed surface heat fluxes partly balance the aforementioned cooling effect of decreased advection and convection. The transition in LS sea ice concentration takes about 80 years from warm to cold (year 326 and 719) and about 20 years from cold to warm (year 591, Figure 2.2 (b)). Both sea ice growth and retreat start in the LS region, before spreading to the other regions. Additionally an increased sea ice cover weakens the SPG circulation through insulating it from wind stress forcing (Jochum et al., 2012).

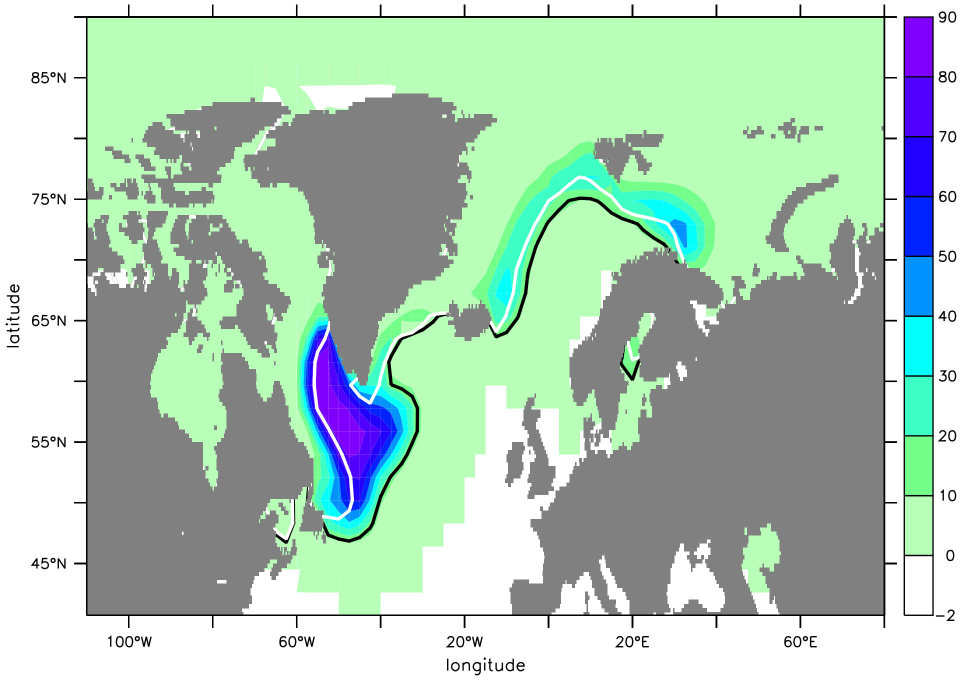

Figure 2.12.: Difference in annual maximum sea ice concentration [%] between NA_c1 and NA_w1. Overlaying contours show the averaged annual maximum sea ice extent (15%) for NA_c1 (black) and NA_w1 (white).

2.3.2.3 Atmosphere response - year 320 onward

The reduced heat fluxes (reduced by about 70 Wm^{-2}, difference between year 270-290 (column 1) and 381-401 (column 4) in Table 2.2) above the LS (i.e., cooling of the atmosphere) are mainly a result of increased sea ice cover in the LS. They force a cold core high pressure anomaly, which sustains the anomalous forcing of the weakened gyre circulation. This atmospheric response starts to become apparent from year 320 to 325 (Figure 2.4 (c)). The anomaly strengthens in amplitude south-west of Greenland above the LS and extends, with reduced amplitude, far across the Asian continent. It persits for about 200 years (Figure 2.4 (d)) with an average spatial maximum of 2.8 hPa above the LS. Associated with this is also a persistent localized decrease in wind stress curl (Figure 2.5 (d)) during NA_c1. The largest changes occur west off Greenland where the wind

stress curl reduces to about 70 % of its original magnitude (NA_w1) and to about 60 % of its original magnitude across central parts of the SPG.
This response of atmospheric circulation to sea ice anomalies was demonstrated by Deser et al. (2007) on shorter timescales, i.e., over one winter/spring season. This is a directly forced baroclinic response and opposite in sign to the equivalent barotropic response to positive (negative) SST anomalies which is invoked to explain the evolution of negative (positive) NAO-phases (e.g., Farneti and Vallis (2011)). The equivalent barotropic response is fully established after 2-2.5 months (Deser et al., 2007) and dominates the overall response. However, in our case the anomalous surface heat fluxes, forcing the anticyclonic anomaly, persist during the entire NA_c1, due to the involved ocean circulation and sea ice changes.
Eventually the sea ice concentration changes cause the drop in Greenland temperature (from year 326 onward) by insulating the atmosphere from the ocean heat reservoir as suggested by Li et al. (2005) and Li et al. (2010).

2.3.3 Warming event

The SLP anomaly decreases for the first time around year 500 but remains then for another ~ 80 years in a slightly lower but stable state. Around year 580 a cyclonic SLP anomaly evolves centered off northern Norway (Figure 2.13 (a), year 578 to 583). From here the cyclonic center moves to the central Arctic Ocean around year 585 (Figure 2.13 (b), year 584 to 589), slowly displacing the remaining anticyclonic SLP anomaly at the southern tip of Greenland (Figure 2.13 (c), year 589 to 594). This SLP anomaly (Figure 2.13 (a) and (b)) resembles closely the anomaly that evolved beside the anticyclone above Greenland in DO_a,b (green and red curve in Figure 2.1) and appeared to hinder the full amplitude of changes to evolve in DO_a,b. Finally SLP drops abruptly to its pre-event value between year 595 and 600 (compare Figure 2.4 (d) and Figure 2.13 (d)). The surface heat fluxes in the LS and SPG change around year 587 and 590 respectively, while the Sverdrup transport features to high interannual variability to determine smaller trends previous to a sudden jump back to the pre-cooling state at around year 595 (Figure 2.6). The SPG gyre circulation changes around year 583 and sea ice concentration (Figure 2.2 (b)) and temperature above the LS follow at year 585 (Figure 2.14). In Figure 2.14 the temperature evolution at different locations across Greenland are compared to changes in temperature above the LS. Compared to the original amplitude above the LS of about $8°C$ the amplitude of annual mean temperature change is reduced to approximately $2°$ to $3°C$ at different points at Greenland. The warming too is more pronounced during winter months (compare to annual minimum temperature in Figure 2.2). It also becomes apparent from Figure 2.14 that the signal transmission from the LS to northern Greenland takes about 5 to 10 years. Thus Greenland temperature increases abruptly from around year 591.

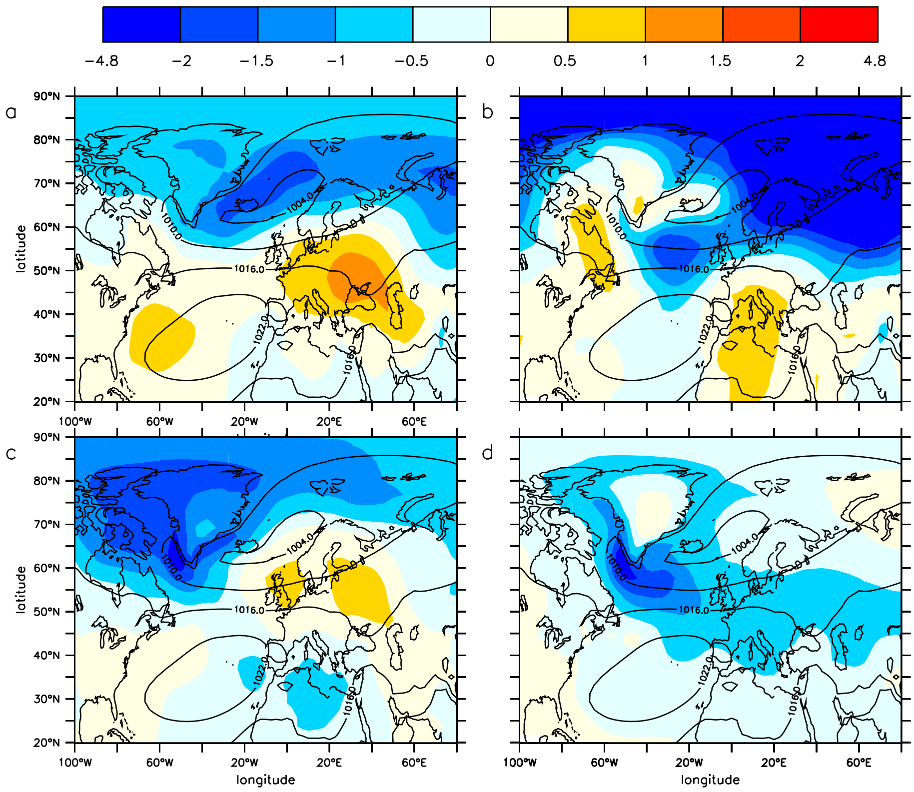

Figure 2.13.: Sea level pressure anomaly [hPa] for year 578 to 583 (a), year 584 to 589 (b), year 589 to 594 (c) and for the second warm phase (year 600 to 700, d). All anomalies are relative to NA_c1 and negative values imply a lower SLP than during Na_c1. Contours show the 1000-year mean of SLP.

In general the warming and the cooling event feature the same sequence of events, that is atmospheric circulation changes (SLP, surface heat flux and wind stress (only determinable for the cooling transition)) followed by SPG circulation changes and eventually a change in sea ice concentration in the LS followed by changes in Greenland temperature. This raises the question why the transitions, at least in Greenland temperature, feature an asymmetric pattern. This question is not addressed in detail but possible causes are discussed in Section 2.4.

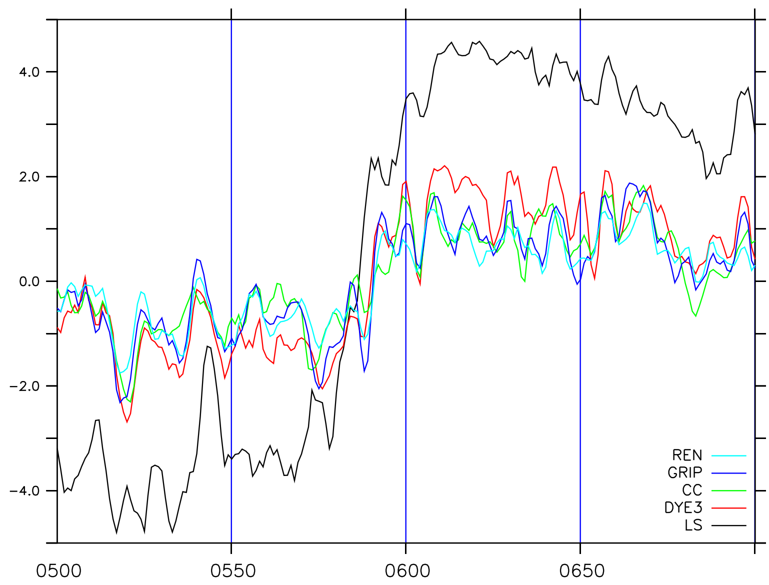

Figure 2.14.: Annual mean temperature anomaly (relative to 1000 year mean) over the warming transition for the LS (55° to 65°N and 50° to 60°W, black) and different gridpoints approximately corresponding to different ice core locations at Greenland: Renland in cyan, GRIP in blue, Camp Century in green and DYE3 in red. All time series are smoothed by a 5 year running mean.

2.3.4 Dependence on the climatic background state - a comparison to the HI pre industrial control simulation

The question arises why such spontaneous climate transitions do not occur in the vast majority of state-of-the-art GCM runs (see Section 1.1.2). In the following section we thus address this question in terms of the dependence of the above described mechanism on the climatic background state -in particular the differences of HI and CONT in the NA are compared. Both runs are set up with the same external boundary conditions and only differ in the resolution of the atmosphere. However, the mean states of ocean and atmosphere are different. The following numbers refer to a comparison between the ocean and atmosphere state in the NA in a 50 year average directly previous to the first transition and the same time period in HI. To begin with HI features a warmer SPG (about 0.5° to 2 °C) and a more saline western SPG (about 0.3 to 0.6 psu) and is slightly less saline in the eastern SPG (about 0.1 psu). These differences alone have some implications for the proposed positive feedback mechanism in the SPG. The effect of salinity anomalies on the density of water is larger for colder temperatures. Thus in HI higher salinity advection anomalies would be necessary to initiate the described positive feedback loop, including the shut-down of deep water formation in the LS. Moreover the western SPG is already less saline in CONT and thus a smaller salinity advection anomaly can already cause the stabilization of the LS water column. Secondly the circulation in the SPG is weaker in CONT and thus also favours a switch to a weak circulation mode. Furthermore the atmospheric mean state over the NA is distinctly different in the two simulations. The Icelandic low is more pronounced in HI, that is a lower mean SLP of about 2 hPa. Figure 2.15 reveals a stronger SLP gradients between Icelandic low and Azores high in HI than in CONT. A smaller SLP anomaly in CONT thus weakens the gradients between the Icelandic low and Azores High sufficiently to trigger the aforementioned changes in wind stress curl and thus eventually the ocean circulation changes. Compared to NCEP reanalysis data (Kalnay et al., 1996) from 1948 until 2014, HI seems to overestimate the gradients, whereas CONT agrees well (HI and CONT are pre-industrial control simulations). The spread of both distributions seems to be realistic. Lastly CONT features stronger ENSO variability than HI and present-day observations (Shields et al. (2012) Fig. 17).

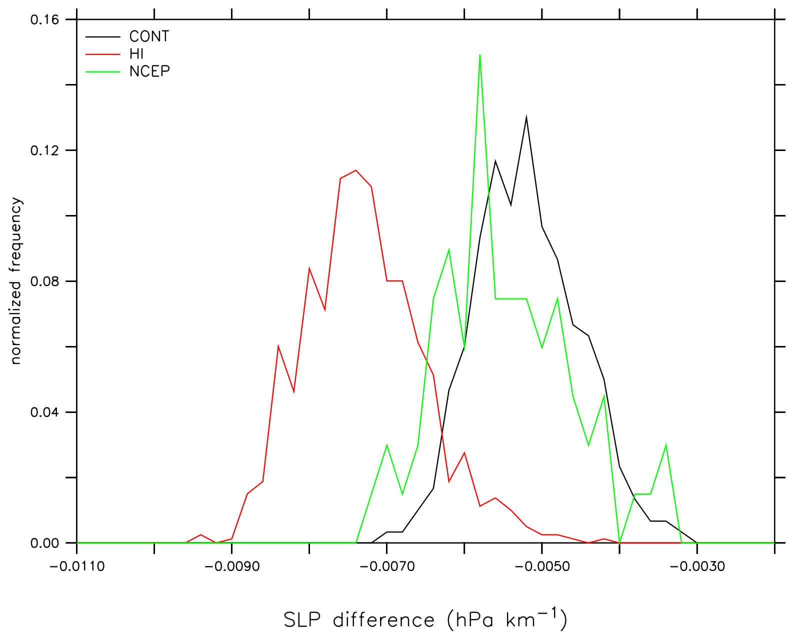

Figure 2.15.: Comparison of normalized annual SLP gradient distribution [$hPa \cdot km^{-1}$]. The SLP gradient is calculated between subtropical high and subpolar low in the Atlantic for NCEP present-day reanalysis (green), CONT (black) and HI (red).

2.3.5 Ocean-sea ice experiments with anomalous atmospheric forcing - testing the trigger

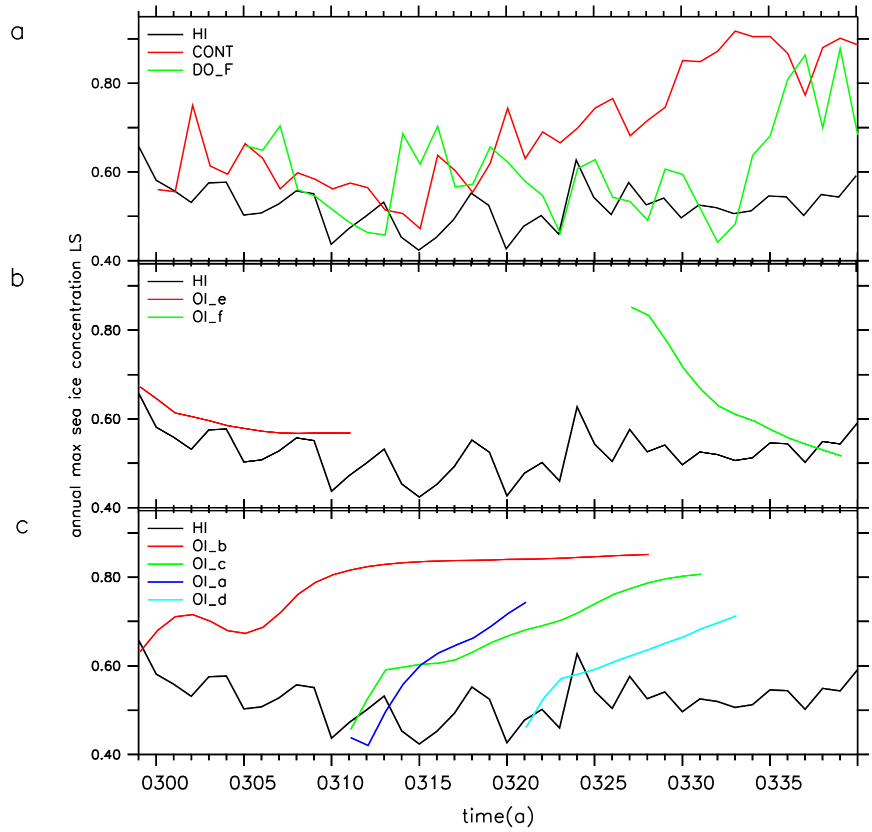

Figure 2.16.: Annual maximum sea ice concentration in the LS (averaged from about 50° to 67°N and 63° to 40°W), in fully coupled simulations HI (black), CONT (red) and DO_F (green) in (a). (b) Same as in (a) but for the declining sea ice concentration (using atmospheric fluxes of year 305/306 from DO_F) OI experiments. (c) Same as in (a) but for increasing sea ice concentration OI runs. For increasing sea ice concentration OI runs different years of atmospheric forcing from DO_F where tested: year 312/313 (OI_b (red), OI_c (green) and OI_d (cyan)) and year 332/333 (OI_a (blue)). As a reference HI is shown as well in panel (b) and (c). See Table 2.1 for experimental setup of simulations.

To test the above proposed mechanism and to infer more details about the atmospheric circulation anomaly and the relative importance of buoyancy and wind stress forcing of the SPG circulation anomaly, several OI simulations are conducted (Section 2.2). In Figure 2.16 the annual maximum sea ice concentration in the LS is depicted as an indicator of the climate transitions. OI_a-d feature rapid increasing sea ice concentration (Figure 2.16 (c)). OI_e,f show a decrease in sea ice concentration (Figure 2.16 (b)) where the later one was started from ocean sea ice conditions of the red curve experiment (i.e., from a high sea ice concentration state).

For the longest experiment (red curve, OI_b) the circulation change of the SPG (not shown) and the MLD in the LS (not shown) between the 5 first and last years of the simulation were compared. The MLD in the LS decreases by about 240 m and the circulation changes in the core region of the SPG account for about 6 Sv - a value similar to the 10 Sv in CONT. Thus the experiments seem not only to reproduce the changes in sea ice concentration, but as well the ocean circulation changes.

2.4 Discussion

Based on the scenario above, three topics deserve further attention:

1. Stochastic forcing
2. Tropical-extratropical atmospheric connections
3. Dependence on background climate state

2.4.1 Stochastic forcing

We tested the proposed mechanism by forcing OI-experiments with atmospheric fluxes extracted from CONT and starting from ocean and sea ice conditions of HI. That these simulations reproduce not only the same changing sea ice concentration but also the same changes in ocean circulation gives us confidence in the aforementioned mechanism. This sensitivity to stochastic forcing raises the question of what forces the SPG in the real world? Unfortunately there is still no consensus on whether buoyancy (e.g., Yeager and Danabasoglu (2014) and Eden and Jung (2001)) or wind forcing (e.g., Eden and Willebrand (2001), Häkkinen et al. (2011)) dominates the strength of the SPG circulation. This depends as well on the considered timescales, with a faster response time to altered wind stress forcing. We showed additionally that the SLP gradients between Icelandic low and Azores high in CONT are weaker than in HI. Thus a smaller stochastic anomaly in CONT can trigger the atmosphere and ocean circulation changes.

Rearrangements in the steady atmospheric circulation pattern and the transient eddy activity above the NA occur during the last glacial period (e.g., Li and Battisti (2008)). The primary cause for these differences in atmospheric circulation is ice sheet topography, in particular the Laurentide ice sheet (e.g., Pausata et al. (2011)). The absence of ice sheet topography driven atmospheric circulation changes could thus also explain why D-O cycles do not occur during the Holocene (see e.g., Wunsch (2006)). There is evidence from observations that atmospheric rearrangements occur prior to Greenland temperature changes. Deuterium excess shows that Greenland precipitation sources change 1-3 years before Greenland air temperature (Steffensen et al., 2008). Change of moisture source region implies an abrupt change of the local atmospheric circulation or the opening of a new source (by e.g., changing from sea ice covered to open ocean). Both changes are seen in CONT: we find atmospheric rearrangements over the NA prior to the abrupt temperature change. In addition the sea ice cover and temperature changes in the LS lead the temperature signal in Greenland (Figure 2.14) and thus establish/remove a possible Greenland precipitation source.

Additionally the $^{231}Pa/^{230}Th$ reconstructions by Böhm et al. (2015) suggest that a strong AMOC prevailed during most parts of the last glacial period and shut down of the AMOC occurred only during Heinrich events close to LGM. This view is supported by our findings, which provide a mechanism for abrupt Greenland climate shifts without strong AMOC variations.

An interesting aspect of the atmospheric response is that it might contribute to the sawtooth-shape of the Greenland temperature signal. Deser et al. (2004) and Deser et al. (2007) find that decreased sea ice concentration (or warmer SST) causes a cyclonic anomaly stronger in amplitude than the anticyclonic anomaly forced by increased sea ice concentration (colder SSTs). Thus larger changes in sea ice cover and temperature are necessary to build up the anticyclonic anomaly than decreasing it again.

However, Deser et al. (2004) and Deser et al. (2007) are based on atmosphere model simulations with prescribed SST and sea ice extent anomalies from observed trends. Feedbacks on the SST and sea ice anomalies can thus only be estimated by a comparison of the observed atmospheric trends and the atmospheric response in their simulations; they estimate the feedback to be negative but weak.

2.4.2 Tropical- extratropical connections

The initial change in SLP is in the range of natural variability, thus no further trigger is needed to explain the occurrence of the stochastic atmospheric anomaly over the NA.

In the extratropics El Niño Southern Oscillation (ENSO) variability is known to alter in particular the likelihood of extreme pressure events to occur (e.g., Sardeshmukh et al. (2000) and Palmer (1993)). Therefore in the following section we discuss changes in temperature and precipitation in the tropical Pacific and possible connections with the anomalous NA atmospheric circulation.

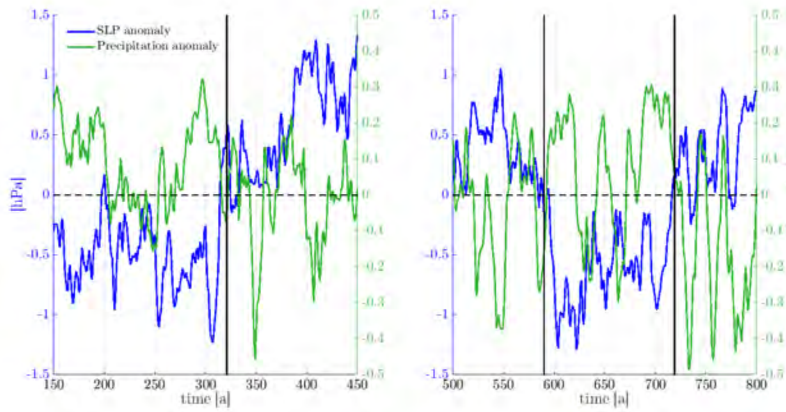

Figure 2.17.: Precipitation anomaly [$mm \cdot day^{-1}$] in the western tropical Pacific, averaged from 100° to 180 °E and 8°S to 8°N in green and sea level pressure anomaly [hPa] over the NA, averaged from 50° to 20 °W and 50° to 65 °N in blue. Both time series are smoothed with a running mean over 10 years. For the first cooling event around year 326 on the left and for the abrupt warming and the second cooling event around year 591 and 721, respectively on the right.

For all three transitions (warm to cold: year 326 and 719; cold to warm: first changes at year 550, finally back to initial state around year 590) changes in tropical precipitation occur simultaneously or previous to the changes in SLP over the NA (Figure 2.17). Teleconnections from tropics to extratropics work virtually instantaneous, whereas a signal transferred inversely takes about two to three years (Chiang and Bitz, 2005). Two other strong increases in precipitation at around year 350 and 890 are both followed by a weakening of the anticyclone and a temporary drop in sea ice concentration (compare to Figure 2.2). Furthermore temperatures in the WPWP are anomalously warm for about 20 to 30 years previously to the two cooling events. The shifts in tropical atmospheric deep convection associated with SST changes generate planetary waves that modify global patterns of SLP (e.g., Sardeshmukh and Hoskins (1988)). It is difficult to associate unambiguously particular sea level pressure changes with particular convection changes (Ting and Sardeshmukh, 1993), but the present SLP differences between NA_c1 and NA_w1 are quite similar to pressure differences induced by El Niño teleconnections (e.g., Trenberth et al. (1998)): in particular a weakening of the pressure difference between the Azores

and Iceland. A modeling study by Merkel et al. (2010) shows altered ENSO teleconnections during past glacial climates. They demonstrate that teleconnections into the NA were strong during pre-industrial times (not shown, but also true for CONT) and Greenland interstadials, while there were weak or no teleconnections during LGM, Heinrich stadial 1 and Greenland stadials (Figure 11 in Merkel et al. (2010)). Furthermore different ENSO variability is expected with different orbital forcing as also demonstrated by a modeling study of Timmermann et al. (2007). Paleo-reconstructions showed that ENSO was at work over past glacial climates (e.g., Tudhope and Coauthors (2001)). Whether the strength was weaker, stronger or not altered at all during past glacial climates is still debated. Whether the suggested tropical changes are a plausible scenario for D-O cycles depends thus upon better paleo-reconstructions of altered ENSO strength and variability and its relative timing to Greenland ice cores.
As described in Section 1.1.1, there is also evidence for abrupt climate shifts in the NA under Holocene conditions (e.g., Bond et al. (1997)). The modeling study by Liu et al. (2014), consistent with most paleo-ENSO reconstructions, describe an orbitally induced strengthening of ENSO during the Holocene epoch relative to the deglaciation. Moy et al. (2002), based on a Laguna sediment record in southern Ecuador, reconstruct millennial-scale variability of ENSO during the Holocene.

2.4.3 Dependence on background climate state

As mentioned previously, no further transitions between NA cold and warm phases occur in a 200 year extension of this simulation, implying that the last cold state lasts for at least 400 years. This points towards a strong dependence on the climatic background state for the full chain of aforementioned processes to evolve. The analyzed simulation has a warm bias in global average, but a cold bias in the NA and drifts towards a colder state. The ocean loses heat at -0.09 Wm^{-2} over the last 600 years (Shields et al., 2012). Furthermore the NA (20° -70°N) becomes more saline at intermediate depth while the upper NA ($\leq$ 500 m) becomes less saline, which has a stabilizing effect for the cold phase as stronger salinity anomalies are necessary for deep water convection to resume. We discussed in Section 2.3 2.3.4 the differences between HI and CONT and how these differences promote the positive feedback loop in SPG circulation, salinity advection and deep water convection intensity as well as the probability of the triggering SLP anomaly to occur. CONT represents in several aspects a climate that is biased towards a glacial climate (e.g., temperature of the SPG).
The reproducibility of the transitions together with their occurrence at different points in time compared to the original simulation indicate that no long term memory effects are

necessary for the abrupt transitions to occur. Hence it supports our hypothesis that rather quasi-stochastic atmospheric forcing triggers a switch in a per se unstable ocean circulation regime, the strong and weak SPG circulation modes. It would be thus very interesting to analyze a parameter space (mainly of temperature and salinity) for which the SPG can flip. Born and Stocker (2014) show that a simple 4-box model of the SPG is bistable. However, in reality and in a fully coupled climate model the parameter space would be more complex (i.e., ocean-atmosphere and ocean-sea ice feedbacks). How representative this simple model is for the real SPG remains unclear, but for our argumentation it is sufficient that the SPG is sensitive to small perturbations.

The dependence of the oscillations on the mean state of the SPG is an obvious drawback. The present mechanism should thus be evaluated under MIS3 conditions.

2.5 Summary

D-O-like transitions in Greenland temperature are found in a free CCSM4 integration and analyzed. It is notoriously difficult to establish cause and consequence in fully coupled simulations. With this caveat in mind we suggest that the climate transitions are triggered by a stochastic change in SLP pattern over the NA. This state is associated with a weakened wind stress curl over the SPG. Consequently the gyre circulation slows down and advects less warm and saline subtropical waters to high latitudes, initiating a positive feedback loop towards a persistent weaker state of the SPG circulation and deep water convection in the LS. Sea ice growth commences in the LS due to locally reduced warm water transport and decreased ocean-atmosphere heat flux. The sea ice anomaly here allows for a cold core high to develop at the south-western tip of Greenland and sustains the anomalous SLP pattern for about 200 years, the entire cold NA phase. The decreased deep water convection leads furthermore to a reduced AMOC of about 3 to 4 Sv and thus a further reduction in northward heat transport. The onset of the warming is initiated by a stronger Icelandic low and thus by removing the anomalous atmospheric forcing the SPG circulation recovers, deep water convection resumes, sea ice cover retreats and Greenland temperature rises abruptly. The possible influence of tropical precipitation anomalies on the NA atmospheric trigger is discussed.
The present coupling between SPG, sea-ice and Icelandic low has already been hypothesized by Seager and Battisti (2007). The central role of the sea ice has already been discussed by Li et al. (2005), though the mechanism causing a sudden sea ice retreat remains unclear. We have now identified a possible cause for sea ice changes: stochastic

atmospheric forcing. The initial trigger of the transitions occurring herein and in Drijfhout et al. (2013) are in both cases stochastic atmospheric circulation anomalies. Additionally, the persistent anticyclonic anomalies above the NA during the cold event are alike. However the mechanisms sustaining this persistent anomaly are different. While Drijfhout et al. (2013) attributes the persistent anomaly to sea ice-atmosphere interactions later on amplified by ocean circulation feedbacks (mostly AMOC), we find that the changed oceanic gyre circulation plays a key role. Even though we see changes in thermohaline properties in the Nordic Seas and the LS we find no evidence for the mechanism suggested by Dokken et al. (2013). Note, though, that the climate state of CONT is likely to be far from MIS3.

The present results are a promising starting point into the dynamics behind D-O cycles. To us it appears that their most critical and uncertain component is their sensitivity to the NA background state and the structure of atmospheric noise that is needed to trigger a switch in the SPG state. Thus, we plan to continue our work with three complementary approaches: Firstly, constrain the mean state of the SPG as well as timing and nature of atmospheric circulation changes during MIS3 with paleo-proxies; secondly, perform more idealized GCM studies in which we can control background state and atmospheric noise; and thirdly, set up a full MIS3 simulation with CESM.

Acknowledgments

We are grateful to Matthew Long and Keith Lindsay for helping setup the ocean-ice simulations. Further we thank Andreas Born and Gokhan Danabasoglu for their insightful comments. We would like to thank Sybren Drijfhout and two anonymous reviewers for the constructive comments that helped to significantly improve this study. NCEP Reanalysis data are provided by the NOAA/OAR/ESRL PSD, Boulder, Colorado, USA, from their Web site at http://www.esrl.noaa.gov/psd/. Computing resources were provided by the Climate Simulation Laboratory at NCAR's Computational and Information Systems Laboratory, sponsored by the National Science Foundation and other agencies. The research leading to these results has received funding from the European Research Council under the European Community's Seventh Framework Programme (FP7/2007-2013) / ERC grant agreement number 610055 as part of the ice2ice project.

Bibliography

Antonov, J., and Coauthors, 2010: World Ocean Atlas 2009, Volume 2: Salinity. S. Levitus, Ed. *NOAA Atlas NESDIS*, **69**.

Böhm, E., and Coauthors, 2015: Strong and deep Atlantic meridional overturning circulation during the last glacial cycle. *Nature*, **517 (7532)**, 73–76.

Bond, G., and Coauthors, 1997: A pervasive millennial-scale cycle in North Atlantic Holocene and glacial climates. *Science*, **278 (5341)**, 1257–1266.

Born, A., and T. F. Stocker, 2014: Two stable equilibria of the Atlantic subpolar gyre. *J. Phys. Oceanogr.*, **44 (1)**, 246–264.

Born, A., T. F. Stocker, C. C. Raible, and A. Levermann, 2013a: Is the Atlantic subpolar gyre bistable in comprehensive coupled climate models? *Clim. Dynam.*, **40**, 2993–3007, doi:10.1007/s00382-012-1525-7.

Born, A., T. F. Stocker, and A. B. Sandø, 2013b: Coupling of eastern and western subpolar North Atlantic: Salt transport in the Irminger Current. *Ocean Science Discussions*, **10 (2)**, 555–579, doi:10.5194/osd-10-555-2013, [http://www.ocean-sci-discuss.net/10/555/2013/].

Chiang, J. C. H., and C. M. Bitz, 2005: Influence of high latitude ice cover on the marine Intertropical Convergence Zone. *Clim. Dynam.*, **25 (5)**, 477–496, doi: 10.1007/s00382-005-0040-5.

Cunningham, S. A., and Coauthors, 2007: Temporal variability of the Atlantic meridional overturning circulation at 26.5 N. *Science*, **317 (5840)**, 935–938.

Danabasoglu, G., S. C. Bates, B. P. Briegleb, S. R. Jayne, M. Jochum, W. G. Large, S. Peacock, and S. G. Yeager, 2012: The CCSM4 ocean component. *J. Climate*, **25 (5)**, 1361–1389, doi:10.1175/JCLI-D-11-00091.1.

Danabasoglu, G., and Coauthors, 2014: North Atlantic simulations in coordinated ocean-ice reference experiments phase ii (CORE-II). Part I: Mean states. *Ocean Modelling*, **73**, 76–107.

Deser, C., G. Magnusdottir, R. Saravanan, and A. Phillips, 2004: The effects of North Atlantic SST and sea ice anomalies on the winter circulation in CCM3. Part II: Direct and indirect components of the response. *J. Climate*, **17 (5)**, 877–889.

Deser, C., R. A. Tomas, and S. Peng, 2007: The transient atmospheric circulation response to North Atlantic SST and sea ice anomalies. *J. Climate*, **20 (18)**, 4751–4767, doi: 10.1175/JCLI4278.1.

Dokken, T. M., K. H. Nisancioglu, C. Li, D. S. Battisti, and C. Kissel, 2013: Dansgaard-Oeschger cycles: Interactions between ocean and sea ice intrinsic to the Nordic seas. *Paleoceanography*, **28 (3)**, 491–502, doi:10.1002/palo.20042.

Drijfhout, S., E. Gleeson, H. A. Dijkstra, and V. Livina, 2013: Spontaneous abrupt climate change due to an atmospheric blocking–sea-ice–ocean feedback in an unforced climate model simulation. *Proc. Nat. Acad. Sci. USA*, **110 (49)**, 19 713–19 718, doi:10.1073/pnas.1304912110.

Eden, C., and T. Jung, 2001: North Atlantic interdecadal variability: oceanic response to the North Atlantic Oscillation (1865-1997). *J. Climate*, **14 (5)**, 676–691.

Eden, C., and J. Willebrand, 2001: Mechanism of interannual to decadal variability of the North Atlantic circulation. *J. Climate*, **14 (10)**, 2266–2280.

Farneti, R., and G. K. Vallis, 2011: Mechanisms of interdecadal climate variability and the role of ocean–atmosphere coupling. *Clim. Dynam.*, **36 (1-2)**, 289–308, doi:10.1007/s00382-009-0674-9.

Gent, P. R., and Coauthors, 2011: The Community Climate System Model version 4. *J. Climate*, **24 (19)**, 4973–4991, doi:10.1175/2011JCLI4083.1.

Häkkinen, S., P. B. Rhines, and D. L. Worthen, 2011: Atmospheric blocking and Atlantic multidecadal ocean variability. *Science*, **334 (6056)**, 655–659, doi:10.1126/science.1205683.

Jochum, M., A. Jahn, S. Peacock, D. A. Bailey, J. T. Fasullo, J. Kay, S. Levis, and B. Otto-Bliesner, 2012: True to Milankovitch: Glacial Inception in the new Community Climate System Model. *J. Climate*, **25 (7)**, 2226–2239, doi:10.1175/JCLI-D-11-000.44.1.

Johns, W., T. Shay, J. Bane, and D. Watts, 1995: Gulf Stream structure, transport, and recirculation near 68 W. *Journal of Geophysical Research: Oceans (1978–2012)*, **100 (C1)**, 817–838.

Kalnay, E., and Coauthors, 1996: The NCEP/NCAR 40-year reanalysis project. *Bull. Amer. Meteorol. Soc.*, **77 (3)**, 437–471, doi:10.1175/1520-0477.

Li, C., and D. S. Battisti, 2008: Reduced Atlantic storminess during Last Glacial Maximum: Evidence from a coupled climate model. *J. Climate*, **21 (14)**, 3561–3579.

Li, C., D. S. Battisti, and C. M. Bitz, 2010: Can North Atlantic Sea Ice Anomalies Account for Dansgaard-Oeschger Climate Signals? *J. Climate*, **23 (20)**, 5457–5475.

Li, C., D. S. Battisti, D. P. Schrag, and E. Tziperman, 2005: Abrupt climate shifts in Greenland due to displacements of the sea ice edge. *Geophys. Res. Lett.*, **32 (19)**, L19 702, doi:10.1029/2005GL023492.

Liu, Z., Z. Lu, X. Wen, B. Otto-Bliesner, A. Timmermann, and K. Cobb, 2014: Evolution and forcing mechanisms of El Nino over the past 21,000 years. *Nature*, **515 (7528)**, 550–553.

Locarnini, R., A. Mishonov, J. Antonov, T. Boyer, H. Garcia, O. Baranova, M. Zweng, and D. Johnson, 2010: World Ocean Atlas 2009, Volume 1: Temperature. S. Levitus, Ed. *NOAA Atlas NESDIS*, **68**.

Merkel, U., M. Prange, and M. Schulz, 2010: ENSO variability and teleconnections during glacial climates. *Quaternary Science Reviews*, **29 (1)**, 86–100, doi:10.1016/j.quascirev.2009.11.006.

Moy, C. M., G. O. Seltzer, D. T. Rodbell, and D. M. Anderson, 2002: Variability of El Niño/Southern Oscillation activity at millennial timescales during the Holocene epoch. *Nature*, **420 (6912)**, 162–165.

Palmer, T. N., 1993: Extended-range atmospheric prediction and the Lorenz model. *Bull. Amer. Meteorol. Soc.*, **74 (1)**, 49–65.

Pausata, F., C. Li, J. Wettstein, M. Kageyama, and K. Nisancioglu, 2011: The key role of topography in altering North Atlantic atmospheric circulation during the last glacial period. *Climate of the Past*, **7 (4)**, 1089–1101.

Pedlosky, J., 1996: *Ocean circulation theory*. Springer, 453 pp.

Pickart, R. S., D. J. Torres, and R. A. Clarke, 2002: Hydrography of the Labrador Sea during active convection. *Journal of Physical Oceanography*, **32 (2)**, 428–457.

Sardeshmukh, P. D., G. P. Compo, and C. Penland, 2000: Changes of probability associated with El Niño. *J. Climate*, **13 (24)**, 4268–4286.

Sardeshmukh, P. D., and B. J. Hoskins, 1988: The generation of global rotational flow by steady idealized tropical divergence. *J. Atmos. Sci.*, **45 (7)**, 1228–1251.

Seager, R., and D. S. Battisti, 2007: Challenges to our understanding of the general circulation: abrupt climate change. *Global Circulation of the Atmosphere*, Princeton Univ. Press, Princeton, N. J., 331–371.

Shields, C. A., D. A. Bailey, G. Danabasoglu, M. Jochum, J. T. Kiehl, S. Levis, and S. Park, 2012: The Low-Resolution CCSM4. *J. Climate*, **25 (12)**, 3993–4014, doi:10.1175/JCLI-D-11-00260.1, [http://journals.ametsoc.org/doi/abs/10.1175/JCLI-D-11-00260.1].

Steffensen, J. P., and Coauthors, 2008: High-resolution Greenland ice core data show abrupt climate change happens in few years. *Science*, **321 (5889)**, 680–684, doi:10.1126/science.1156393.

Stocker, T. F., and S. J. Johnsen, 2003: A minimum thermodynamic model for the bipolar seesaw. *Paleoceanography*, **18 (4)**, 11–1–11–9, doi:10.1029/2003PA000920, [http://www.agu.org/pubs/crossref/2003/2003PA000920.shtml].

Stott, L., C. Poulsen, S. Lund, and R. Thunell, 2002: Super ENSO and global climate oscillations at millennial time scales. *Science*, **297 (5579)**, 222–226, doi:10.1126/science.1071627.

Timmermann, A., S. J. Lorenz, S.-I. An, A. Clement, and S.-P. Xie, 2007: The effect of orbital forcing on the mean climate and variability of the tropical Pacific. *J. Climate*, **20 (16)**, 4147–4159, doi:10.1175/JCLI4240.1.

Ting, M., and P. D. Sardeshmukh, 1993: Factors determining the extratropical response to equatorial diabatic heating anomalies. *J. Atmos. Sci.*, **50 (6)**, 907–918.

Trenberth, K. E., G. W. Branstator, D. Karoly, A. Kumar, N.-C. Lau, and C. Ropelewski, 1998: Progress during TOGA in understanding and modeling global teleconnections associated with tropical sea surface temperatures. *J. Geophys. Res.: Oceans (1978–2012)*, **103 (C7)**, 14 291–14 324.

Tudhope, A. W., and Coauthors, 2001: Variability in the El Niño-Southern Oscillation through a glacial-interglacial cycle. *Science*, **291 (5508)**, 1511–1517, doi:10.1126/science.1057969.

Wunsch, C., 2006: Abrupt climate change: An alternative view. *Quat. Res.*, **65 (2)**, 191–203, doi:10.1016/j.yqres.2005.10.006.

Yeager, S., and G. Danabasoglu, 2014: The origins of late-twentieth-century variations in the large-scale North Atlantic circulation. *J. Climate*, **27 (9)**, 3222–3247, doi:10.1175/JCLI-D-13-00125.1.

3 The tropical trigger

3.1 Introduction

Here, we will argue that a centennial scale ENSO-like mode of variability is the origin of the NA cold an warm phases described in the previous chapter. This mode is correlated with SLP anomalies in the NA. We support our hypothesis of a tropical origin of the NA phases with evidence for centennial scale ENSO-like variability in a second pre-industrial control simulation (HI, see Table 2.1 and corresponding text for details of this simulation). The ENSO-like variability in HI features the same characteristics as in CONT, but no warm and cold NA phases occur in HI, suggesting that it cannot be the NA phases in CONT triggering the centennial ENSO-like variability.
SSTs in the tropical Pacific vary on seasonal, interannual (ENSO, Bjerknes (1969)), decadal to centennial (e.g., Wittenberg (2009)) and even on millennial time scales (e.g., modelling: Clement et al. (2001); Timmermann et al. (2007), Sadekov et al. (2013) and Stott et al. (2002)). Mean climate background changes often interact with these different modes of variability in a nonlinear way (e.g., Timmermann (2003)), making it impossible to determine cause and effect.
A detailed description of physical modes of variability associated with tropical Pacific SST variability on different timescales and hypotheses on how the tropics could play an active (rather than passive) role in abrupt millennial scale climate variability during the last glacial can be found in the general Introduction (Sec. 1.2) and can be summarized as follows. Firstly there is clear evidence for tropical ENSO-like variability on centennial to millennial timescales during the past (e.g., Sadekov et al. (2013) and Stott et al. (2002)). Furthermore miscellaneous modelling studies demonstrate that such changes have the potential to alter the atmospheric circulation on a global scale (e.g., Vavrus et al. (2006) with a focus on NH Pacific). Ding et al. (2014) and Yin and Battisti (2001) show how anomalies in tropical Pacific SST pattern alter through a Rossby wave-train in particular SLP and the geopotential height field in western Canada and Greenland.
The cold NA phases are correlated with more El Niño-like conditions (Sec.3.2.2) and increased variance of ENSO (Sec.3.2.3). Modulation of ENSO amplitude (and period) can

be the consequence of either changes in the mean background climate or changes in the seasonal cycle (e.g., Wang and An (2002) and Tziperman et al. (1997)) or due to nonlinear interaction of the former with ENSO's intrinsic timescale (e.g. Timmermann (2003)). In CONT no structural differences in the seasonal cycle occur between the NA cold and warm phases (Sec. 3.2.1). However, there exist distinct differences in the mean background climate (Sec.3.2.2). In Sec.3.3 we suggest that the aforementioned changes are the expression of decadal ENSO amplitude modulations (DEAMs, Timmermann (2003)). In this context the shift to more El Niño-like conditions can be interpreted as an east-west displacement of ENSO's center of action (Timmermann, 2003). NA warm phases are associated with El Niños (La Niñas) occurring farther to the west (east). Thermocline anomalies, the change in ENSO variance and the east-west displacement associated with DEAMs in CONT are in accordance with the findings of Timmermann (2003), who suggests that DEAMs are generated within the tropics, through nonlinear interaction between ENSO's intrinsic time scale and changes in the mean background climate. We thus hypothesise that ENSO modulation on decadal to centennial scales in CONT - associated with the NA warm and cold phases- are generated in the tropics. The changes in the tropical Pacific are thus clearly linked to the NA warm and cold phases. Lead/Lag correlation between several variables in the Pacific and the NA conform with both - the Pacific or the NA - leading by a couple of years. We document several indications that the tropical mode is generated internally in the tropics (Sec. 3.4 and Sec. 3.3).
To disentangle ENSO and ENSO-like variability EOFs and corresponding Principal Components (PCs) of high (HP) and low pass (LP) filtered tropical Pacific SST anomalies are calculated. A linear regression between global SLP fields and the ENSO and ENSO-like modes of variability is performed to show the different NA atmospheric circulation pattern associated with them (Sec. 3.3). This is followed by a discussion of different possible linkages of the tropical Pacific and the NA. For this purpose we look for evidence (or the non-existence of such evidence) in CONT for different already proposed linkages between NA and the tropical Pacific (Sec. 3.4). This section finishes with a discussion of changes in the mean ENSO period between NA warm and cold phases and associated phase lock of ENSO and through this we show a possible linkage to millennial scale climate variability during the last glacial (Sec. 3.5.1.1).

3.2 Tropical Pacific inter- and intra- annual variability in CONT

In this section we briefly assess the realism of ENSO variability in CONT. ENSO's dominant period and amplitude is determined by both, the mean background climate (e.g., Wang and An (2002)) and the seasonal cycle (e.g., Tziperman et al. (1997)). Thus, we

a

TABLE 1. Niño-3-mean SST (°C) and standard deviation of the seasonal cycle and the interannual variability.

Source	Mean	Seasonal cycle	Interannual variability
HadSST	25.7	0.95	0.79
T31x3_1850	24.0	1.08	0.65
T31x3_20C	24.1	1.03	0.69
FV2x1_1850	25.4	0.59	1.37
FV1x1_1850	25.4	0.72	1.02

b

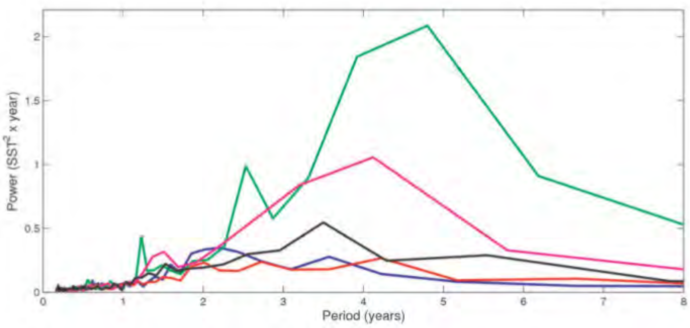

Figure 3.1.: From Shields et al. (2012): (a) Comparison of seasonal cycle strength, interannual variability (ENSO strength) and mean SST in the tropical Pacific for different versions of CCSM and the HadSST reanalysis product. CONT corresponds to $FV2x\_1\_1850$ and HI to $FV1x\_1\_1850$. (b) Original caption from Shields et al. (2012): Power spectrum for Nino-3 SST anomalies for HadSST (black), $T31x3\_1850$ (blue), $T31x3\_20C$ (red), $FV2x1\_1850$ (green), $FV1x1\_1850$ (purple). The area under a line, when integrated across all periods, yields the total variance

assess in the following first the differences between the NA phases in the seasonal cycle (Sec. 3.2.1) and secondly in mean background climate of the tropical Pacific (Sec. 3.2.2). This is followed by a description of how these changes effect ENSO's amplitude and dominant period (Sec. 3.2.3). Lastly the effects of ENSO modulation on decadal to centennial scales on the NH atmospheric circulation are presented (Sec. 3.3).
The spatial pattern of ENSO variability and the timing of the seasonal cycle are simulated

with sufficient realism in CONT (Deser et al., 2012). Niño 3.4 SSTs feature a double spectral peak at periods of ~ 2.5 and ~ 5 years (Fig. 3.1 (b)) in good agreement with HadISST (see Fig. 4 in Deser et al. (2012)). However, CONT overestimates the maximum power by about a factor of 4. A detailed description of ENSO and its global teleconnections and ENSO modulation on decadal to centennial scales in CCSM4 and in CONT and HI in particular is provided by Deser et al. (2012). CONT features very high interannual variability in tropical Pacific SST anomalies. In Table 3.1 (a) (adapted from Shields et al. (2012)) the strength of the seasonal cycle and of ENSO variability is compared between different versions of CCSM and the HadSST reanalysis product (CONT is $FV2x$_1_1850 in Table 3.1 and HI is $FV1x$_1_1850). CONT features a very weak seasonal cycle and associated with this strong interannual variability. The interannual variability in CONT exceeds the one of HadSST by about a factor of two. The anti-correlation between a weak seasonal cycle and strong ENSO variability seems generally to hold for all the CCSM simulation and the HadSST data-set and is in good agreement with the findings of Guilyardi (2006). However, there are few observations to constrain ENSO variability before about a century ago. Thus, even though variability associated with ENSO in CONT is double that of the one inferred from HadSST this ENSO variability might not be unrealistic. Furthermore, there is considerable modulation of ENSO on decadal to centennial timescales present in CONT (Sec. 3.3). Thus, there are as well decades (not shown) that agree better with HadSST (see Wittenberg (2009) for a discussion on whether historical records of ENSO suffice to constrain ENSO simulations).

3.2.1 The seasonal cycle and its importance for ENSO's period

ENSO events have the tendency to peak during the end of the year, which is a consequence of ENSO's phase lock to the annual cycle. Most important for this phase lock behaviour is the seasonality of SSTs (Tziperman et al., 1997).
Fig. 3.2 (a) depicts the monthly standard deviation (*std*) of Niño 3.4 SST for NA_c1 (dark blue), NA_c2 (light blue), NA_w1 (red) and NA_w2 (yellow).

In CONT the time of maximum variability (the time when most ENSO-events peak) is shifted by about 2 months compared to observations (Deser et al., 2012). The *std* peaks in February during NA_c1 and NA_c2 and in January-February during the NA_w1 and NA_w2 phases. In general the variance seem to decrease over the entire simulation (cf. NA_c2 with NA_c1 and NA_w2 with NA_w1). But the variance changes as well together with the NA warm and cold phases. In all months the *std* is clearly decreased by about $0.2 - 0.4\ ^{\circ}C$ during both warm phases and increased during the cold phases. The *std* of

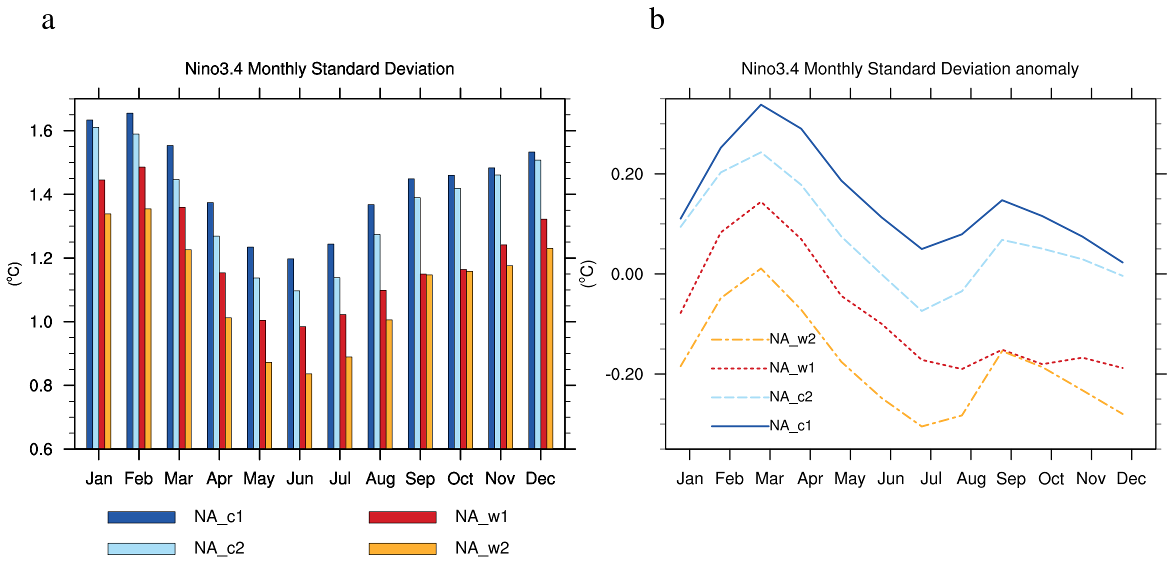

Figure 3.2.: (a) The seasonal cycle in terms of monthly Niño 3.4 SST standard deviation (σ) for NA_w1 (red), NA_c1 (light blue), NA_c2 (dark blue) and NA_w2 (yellow). (b) Difference between the two cold and warm phases relative to the 1000 year climatology.

annual Niño 3.4 SST anomalies is σ = 1.0 for NA_w1 and σ = 1.3 for NA_c1. However, no structural changes in the seasonal cycle are seen between the cold NA warm and cold phases, i.e., no change in the strength of the seasonal cycle or a shift of ENSO's peak time (Fig. 3.2 (b)).

3.2.2 Differences in the tropical Pacific between warm and cold NA phases

The mean tropical surface temperature change in the tropics (global) amounts only to about 0.3°C. However, there are distinct changes in the spatial pattern of tropical Pacific SST variability (Fig. 3.3). Yin and Battisti (2001) find that the spatial pattern of tropical SSTs is more relevant for global atmospheric circulation changes than the amplitude of SST changes. Thus even the small amplitude changes seen in CONT are potentially relevant for the aforementioned NA atmospheric circulation changes (Chapter 2) and are explored in the following. Cold NA phases are linked to more dominant El Niño-like conditions and warm NA phases with more dominant La Niña-like conditions. Relevant changes occur in SST anomalies (Fig.3.3), zonal wind anomalies over the central equatorial Pacific (Fig. 3.5), the temperature of the WPWP (Fig. 3.7), the thermocline depth (Fig. 3.4) in the tropical east and west Pacific and consequently the thermocline slope.

Precipitation and SLP changes (Fig. 3.6 and Fig. 3.8, respectively) - indicative of

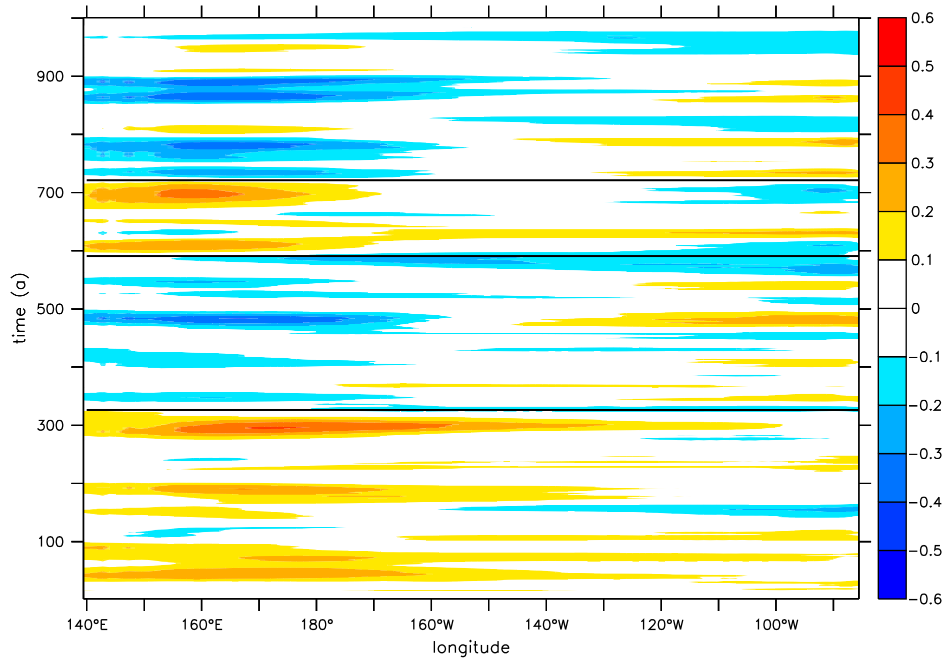

Figure 3.3.: Sea surface temperature anomaly [$°C$] in the tropical Pacific (averaged from $10\ °S$ to $10\ °N$. A 30-year running mean is applied. The black lines indicate the onset of the transitions in Greenland temperature.

changes in deep atmospheric convection are important for global teleconnections and thus for a possible linkage to the NA. The potential effects of aforementioned mean climate changes for the dominant ENSO period are briefly discussed at the end of this Section.

Tropical Pacific SSTs shift towards more dominant El Niño-like conditions during NA cold phases and to La Niña-like conditions during NA warm phases (Fig. 3.3). The signal is strongest in the Niño 5 and 6 regions (above the western and far western Pacific). The absence of a clear temperature signal in the Niño 3 and 4 regions is related to the dominant mode of variability on decadal to centennial scales and the associated east-west displacement (see Sec. 3.3).

For the dynamics of ENSO it is really the gradient in SST that matter. These are strengthened during warm NA phases and weakened during the cold phases (not shown, but also evident in Fig.3.3) between about $160\ °E$ and $120\ °W$, indicating as well a shift to more dominant El Niño-like conditions during the cold NA phases. The cold NA phases are furthermore associated with enhanced ENSO variability (see previous Sec. 3.2.1). The linkage between SST gradients and ENSO variance is in good agreement with paleo-

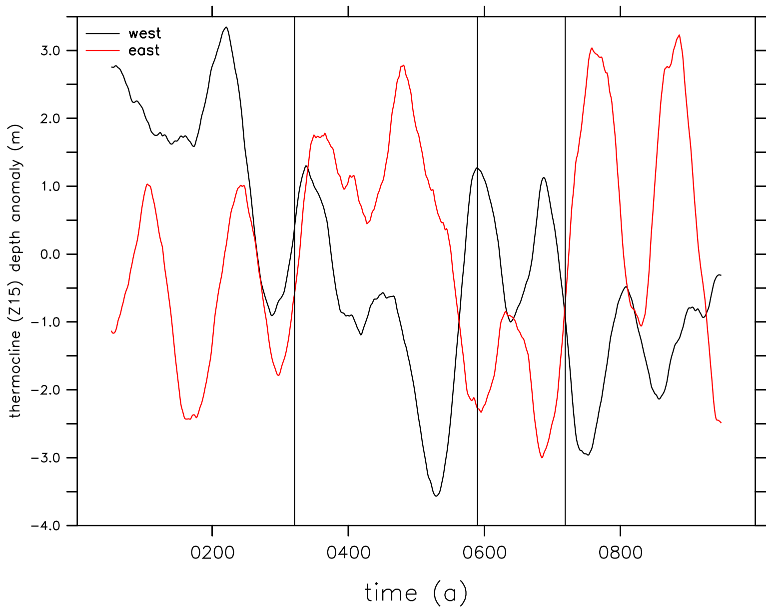

Figure 3.4.: Long term changes (50-year triangle smoothed) in thermocline depth [m] anomalies (depth of the 15°C-isotherm) in the equatorial east (red, averaged from about 4.5°S − 8.5°N and 101°W − 84.5°W) and off-equatorial west (black, averaged from about 8.5°N − 11.5°N and 129.5°E − 141°E) Pacific.

reconstructions. Sadekov et al. (2013) finds that increased zonal gradients during the (warm) early Holocene are associated with decreased ENSO variability, while the opposite is true for the (cold) deglaciation. However, their analysis only spans the time until 20 *kyr* BC and thus covers only GS-1 and GS-2. The anti-correlation between the strength of zonal SST gradients and ENSO variability is opposite to the relationship linear ENSO models would predict (Sadekov et al., 2013; Timmermann, 2003). In CONT this anti-correlation is a result of nonlinear ENSO amplitude modulations (further detail in Sec.3.3). Closely linked to changes in SST gradients are those of the thermocline depth and its slope. The mean thermocline depth (the thermocline is taken here as the annual mean 15°C-isotherm) in the tropical Pacific shallows by about 4 m over the first 500 years and increases slightly during NA_w2 (not shown). Fig. 3.4 depicts the thermocline depth anomaly for the western (black) and eastern (red) tropical Pacific. The thermocline depth anomalies between east and west Pacific are anti-correlated and covary with the Atlantic warm and cold phases. A shallower thermocline in the east Pacific (as during NA_w1 and NA_w2) allows colder water to be pumped up and thus increasing eastward propagation of SST anomalies, corresponding to more La Niña-like conditions. At the same time a deeper thermocline in the western Pacific during the NA warm phases (Fig. 3.4) can lead to less upwelling and thus less cooling in the WPWP, also favouring more La

Niña-like conditions. The weaker zonal winds (Fig. 3.5) during the NA cold phases over

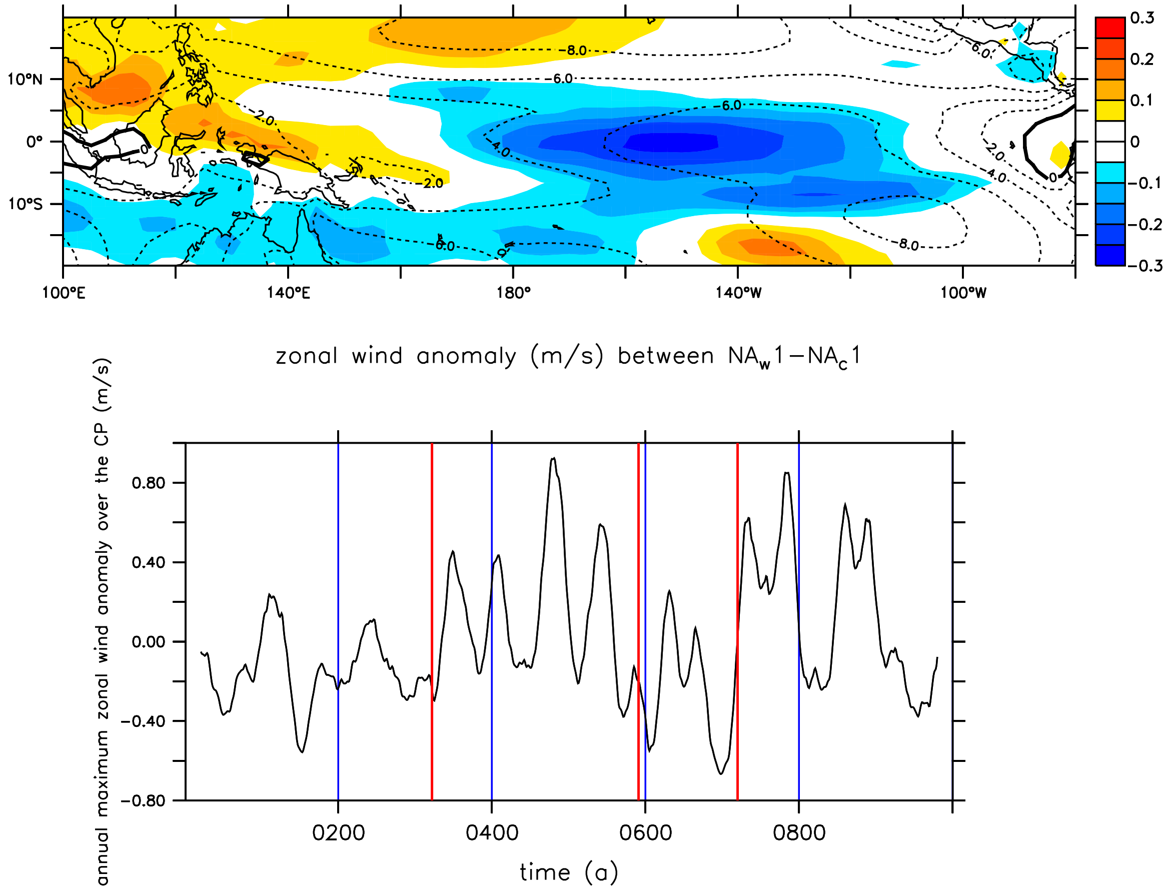

Figure 3.5.: Upper panel: Zonal wind anomaly $[m/s]$ between NA_w1 and NA_c1. Overlaying contours show the 1000 year mean of the zonal wind component. The contour interval is 2 m/s and negative contours represent easterly winds. Lower panel: Annual maximum zonal wind anomaly averaged over the region of strongest changes (from 180 $°W$ to 120$°W$ and 5$°S$ and 5$°N$) in the upper panel. The time series is smoothed by a triangular 30 year LP filter. The vertical red lines indicate the onset of NA phase transitions, in terms of Greenland temperature.

the CP - the region of strongest SST gradients- can either be cause or consequence of the weakened SST gradients. Weaker zonal winds over the region of strongest SST gradients support weaker westward propagation of SST anomalies and simultaneously allowing for less cold water being upwelled in the east (Fedorov and Philander, 2000) during the NA cold phases, in accordance with more El Niño-like conditions. On the other hand weaker SST gradients result in a weaker Walker circulation and hence causing weaker trade winds (Gill, 1980).

The average surface temperature of the WPWP (Fig. 3.7, here defined as the Pacific part of the Indo-Pacific warm pool (annual mean SST being above 29°C)) covary as well in tandem with the NA phases. Warmer temperatures (by about 0.2°C) are associated with the warm NA phases. During the height of NA_c1 (around year 500, when a first weakening of the SLP anomaly in the NA occurs (cf. to Fig. 2.17)), no annual mean SSTs above 29.5 °C exist (this is the only time in the 1000-year CONT run). This can effect westerly wind bursts, which are believed to play a role in triggering ENSO events. McPhaden (1999) report that during the 1997-98 El Niño the strongest westerly surface winds and atmospheric deep convection occurred only over areas with SST greater than 29°C and migrated eastward together with the 29°C-SST isotherm.

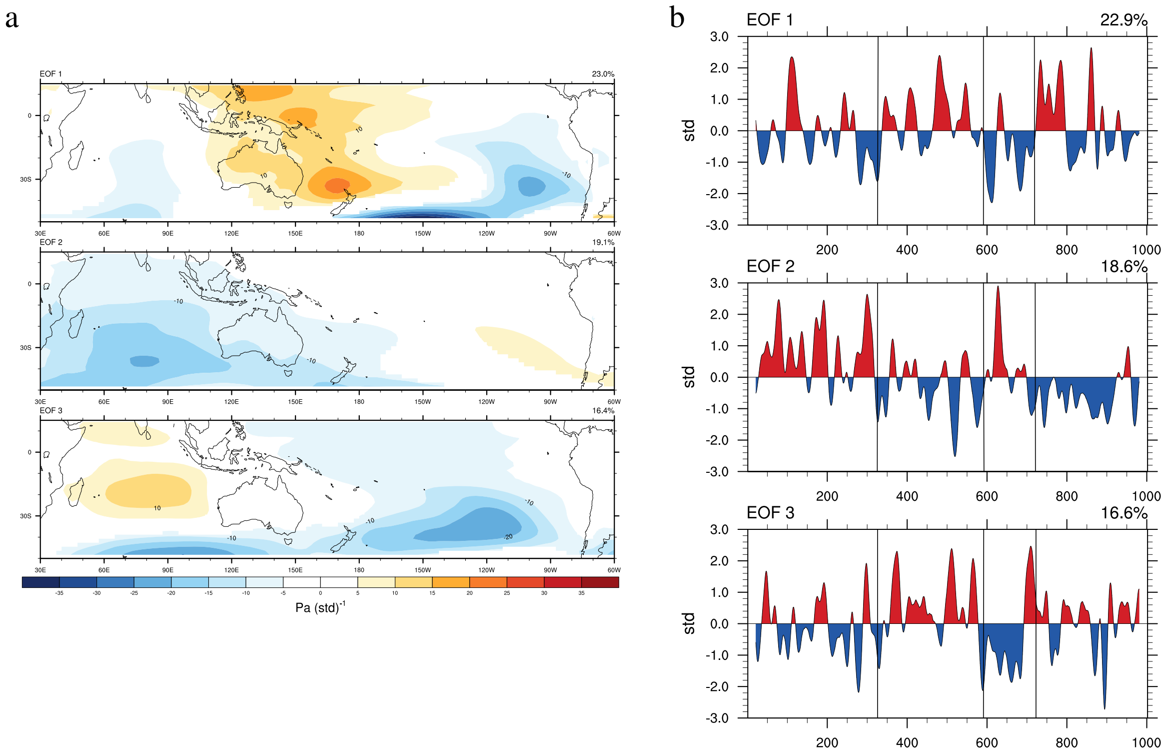

Figure 3.6.: (a) Tropical and southern hemisphere subtropical Pacific EOF 1 to 3 of LP filtered SLP anomalies in units of $Pa(std)^{-1}$. The corresponding PCs are shown in (b). The black vertical lines indicate the onset of NA phase transitions, based on Greenland temperature.

For atmospheric deep convection and global teleconnections the Indo-Pacific warm pool region is particular important (e.g., Branstator (1985)). Observations show that large scale rising motion require SSTs that exceed a threshold of about 27.5 °C (Graham and

Barnett, 1987).

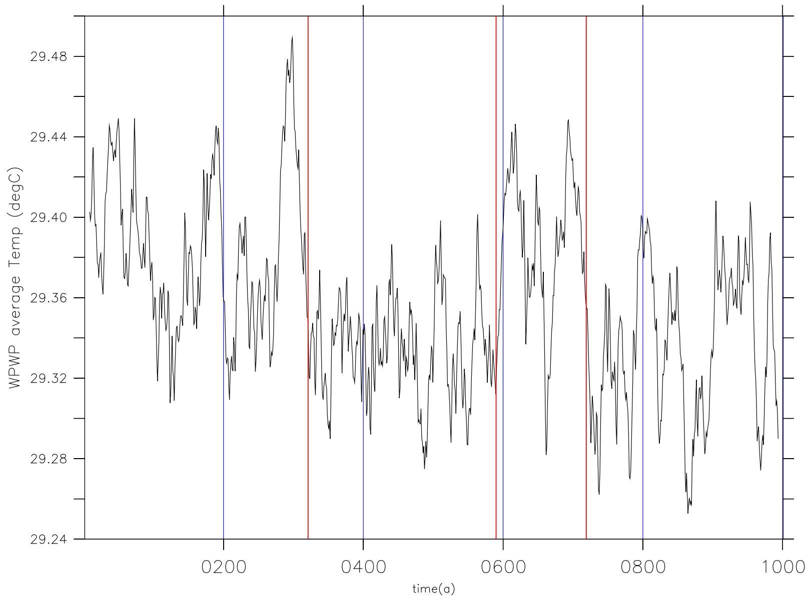

Figure 3.7.: Average temperature of the WPWP (the area with annual mean SST ≥ 29 $°C$, from about 128 $°E$ on, i.e., without the Indian ocean part). A 15-year running mean is applied to the time series. The red horizontal lines indicate the onset of the transitions in Greenland temperature.

Accordingly, reduced WPWP temperature are accompanied by reduced atmospheric convection during NA cold phases as indicated by precipitation anomalies (Fig.3.8). The dipole pattern between the eastern and western tropical Pacific closely resembles precipitation anomalies resulting from changes in tropical atmospheric deep convection induced by ENSO variability and are indicative of a weakening of the Walker circulation during the NA cold phases (in accordance with the weaker easterlies). This dipole pattern in precipitation is consistent with paleo-reconstructions that connect Greenland stadials with decreased precipitation over the WPWP and dominant El Niño-like conditions (Stott et al. (2002), based on magnesium/calcium composition and $\delta^{18}O$ of planctonic foraminifera). The maximum annual mean precipitation change occurs over the WPWP and accounts for about 0.5 $mm \cdot day^{-1}$ (annual maximum change at the same location accounts for about 1 $mm \cdot day^{-1}$, not shown) , a decrease of about 10 % compared to the 1000 year mean (contours in Fig. 3.8). The pattern of precipitation changes associated with the

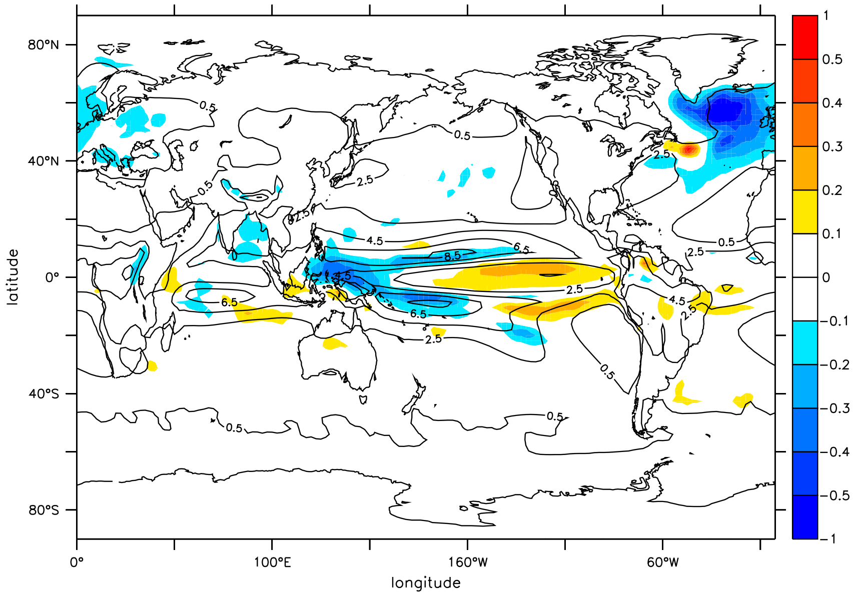

Figure 3.8.: Precipitation anomaly [$mm \cdot day^{-1}$] between NA_c1 and NA_w1. Overlaying contours show the 1000 year mean. The spacing between contours is 2 $mm \cdot day^{-1}$.

NA phases corresponds to the second EOF of precipitation variability (not shown) in the tropical Pacific (and the first EOF of LP filtered variability (Fig. A 3)) and is thus again closely linked to the dominant decadal mode of variability and the associated east-west displacement.

To assess the atmospheric circulation changes associated with the aforementioned mean state changes, relevant for the connection to the NA phases, the EOFs and corresponding PCs of 30-year LP filtered SLP anomalies in the tropical Pacific domain are presented. The first EOF of HP filtered SLP (not shown) corresponds to the Southern Oscillation pattern, with opposite sign anomalies of SLP to the east and west of Australia. The first EOF of LP filtered variability is again linked to the east-west displacement of SST anomalies with the same sign anomalies occurring over the Indian Ocean and off the coast of South America and an opposite sign anomaly over Australia and Indonesia (Fig 3.6 (a), upper panel). Increased SLP over Australia and Indonesia is associated with the NA cold phases, again in accordance with more El Niño-like conditions and the aforementioned changes in zonal winds. All three LP filtered PCs (Fig. 3.6 (b)) covary with the NA phases and have 10-times smaller amplitudes ($Pa(std)^{-1}$) than the HP filtered SLP variability. The third LP filtered EOF shows increased SLP during NA cold phases over the region of the subtropical Pacific jet stream and is potentially relevant for southern Hemisphere changes (further detail in Chapter 4).

3.2.2.1 Implications of mean background climate change for ENSO period

Changes in mean background have the potential to alter ENSO propagation structure and through this amplitude and the dominant period. In the following we discuss the potential effect of the above described changes in mean background for ENSO period.
The effect of decreasing mean thermocline depth is a shift to longer ENSO periods (Wang and An, 2002; Fedorov and Philander, 2000), also present in CONT in association with NA cold phase (see next Sec. 3.2.3). Fedorov and Philander (2000) describe that an increase in the dominant ENSO period occurred (even though with low significance due to short record of ENSO observations) between the late 1970s and early 1980s, together with a weakening of the easterlies and an increase in thermocline depth in the eastern Pacific. This switch in ENSO period is further accompanied by more dominant El Niño-like conditions during the 80s and 90s. Fedorov and Philander (2000) describe two idealized modes of ENSO variability to explain the difference in pre- and post-shift ENSO behaviour. Associated with their mode A (corresponding to the delayed oscillator (Suarez and Schopf, 1988; Battisti and Hirst, 1989)) are intense winds in the CP, elevating the thermocline in the eastern and deepening it in the western Pacific. This mode is associated with eastward phase propagation. Their mode B has westward phase propagation and is associated with a shallower mean thermocline. The effect on SST in this mode is not through vertical movement of the thermocline but through entrainment of cold waters across the thermocline. The second mode (B) is associated with warm anomalies that are shifted towards the CP compared to mode A (cf. to their Fig. 3). Wang and An (2002) further show that this switch in ENSO behaviour is associated with an east-west displacement of SST gradients and zonal equatorial winds. The competition between zonal and vertical advection results in either prevailing eastward or westward propagation of SST anomalies (Wang and An, 2002). In the delayed oscillator paradigm (Suarez and Schopf (1988) and Battisti and Hirst (1989)) the mechanism behind changes in the dominant ENSO period in response to east-west displacements of SST anomalies, and associated with this the equatorial zonal wind anomalies, is the increased/decreased distance the oceanic Rossby waves have to travel before being reflected (Wang and An, 2002).

3.2.3 Shifts in amplitude and dominant period of ENSO variability

We discussed in the previous sections evidences for changes in the tropical Pacific mean climate and according changes in Niño 3.4 SST variance, associated with the NA phases. If the mean background climate changes one would expect changes in ENSO structure and propagation and thus in the dominant oscillation period and amplitude (e.g., Timmermann (2003), Wang and An (2002)). Here we present evidence for ENSO amplitude modulation and changes of the dominant oscillation period in tandem with the NA phases.

In order to assess the different periods of variability and possible changes between the two different phases we present in the following results from a wavenumber 6 Morlet wavelet analysis (Fig. 3.9). The analysis follows the methodology of Torrence and Compo (1998)). ENSO variability of CONT has higher amplitudes than observations by about a factor of 2 (see Sec. 3.2). From Fig. 3.9 it becomes further clear that the period of ENSO in CONT is in the upper end of observed ENSO variability. In CONT the peaks that are significantly (95%) different from the red noise null hypothesis are located between 3 and 12 years (black contours in Fig. 3.9), whereas the observed ENSO variability has a period between 2-8 years. Wavelet analysis of the second PC of unfiltered tropical Pacific SST anomalies (not shown), which is associated with the dominant decadal mode (Sec. 3.3), reveals significant peaks with periods from 30 to 130 years (Fig.3.9 (b)). Furthermore, there are three time intervals (around year 300, 600 and 700) with no significant variability in any frequency band (dark blue regions in Fig.3.9 (a)). We will focus on these three periods in the next section. Lastly we see that during the first 300 years (corresponding to NA_w1) there is less variability and on shorter timescales than during the rest of the simulation. This becomes even more evident from Fig. 3.10, depicting the scale averaged wavelet power from Fig. 3.9 over the 4 to 8 year ENSO band. In the first 300 years (NA_w1) there is only one peak (around year 250) that crosses the 95%-confidence level (red horizontal line) and is thus significantly different from the red noise hypothesis. This indicates that during NA_w1 there is no ENSO variability in the 4 to 8 year band (however, in the period band from 2 to 4 years there is, not shown). For NA_w2 the picture is less clear. The variance is relatively low, however there are still two peaks above the 95%-confidence level, despite the short duration ($O(100\ yr)$) of NA_w2. During both NA_c1 and NA_c2 there are plenty of phases where ENSO variability in the 4 to 8 year band is present. So clearly there is higher ENSO variability during the cold NA phases. That there is no significant ENSO variability in the 4 to 8 year band during NA_w1, but it is commonly present in NA_c1 and NA_c2 indicates a shift of the dominant ENSO period towards longer timescales during the cold NA phases. This shift towards longer timescales of ENSO period agrees well with findings by Wang and An

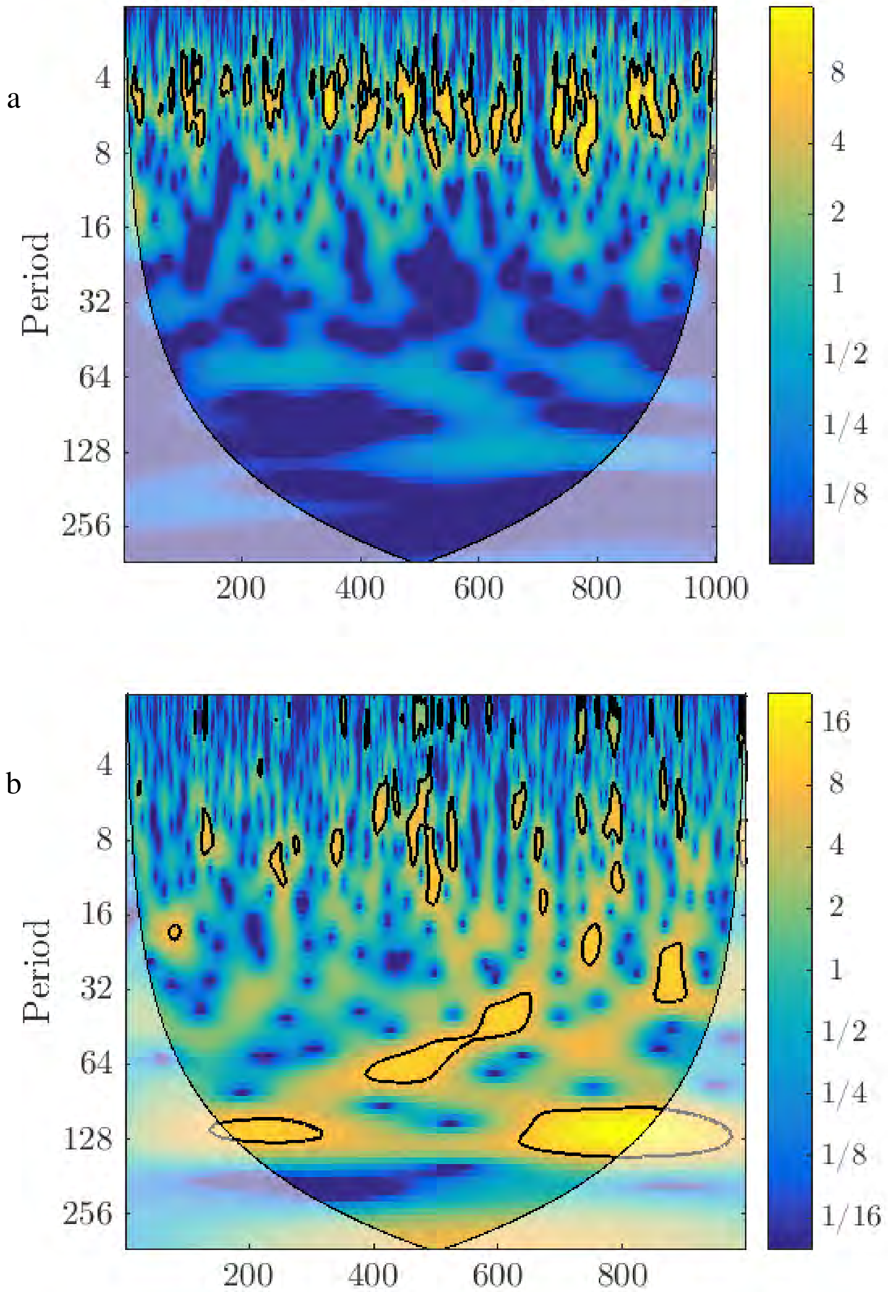

Figure 3.9.: Wavenumber 6 Morlet Wavelet analysis of (a) annual Niño 3.4 SST anomalies in units of normalized variance (σ^2). The black contours represent the 95%- confidence level assuming red noise. The transparent regions on the sides of the figure represent the Cone of Influence, where edge effects become important. (b) the same as in (a), but for the PC 2 of tropical SST (Fig. A 1). The Figure was produced with the matlab toolbox of Grinsted et al. (2004)

(2002) for similar changes in the mean background climate of the tropical Pacific.

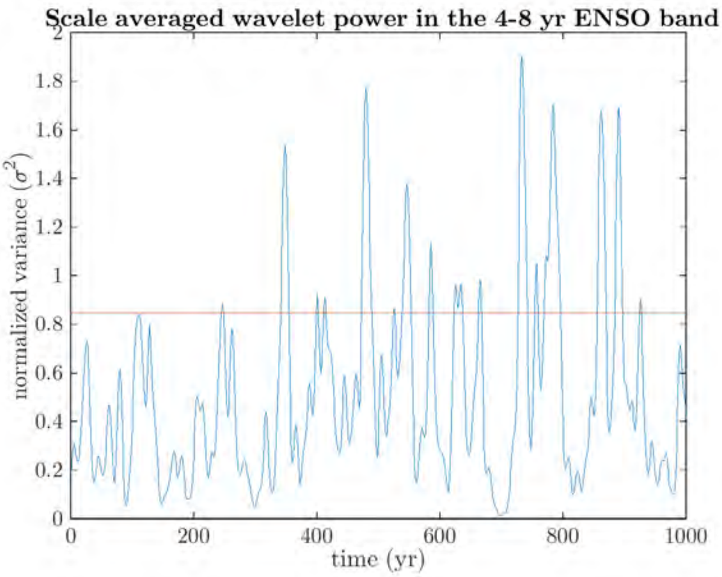

Figure 3.10.: Scale averaged (4 to 8 year ENSO band) wavelet power from a wavenumber 6 Morlet Wavelet analysis in units of normalized variance. The red line indicates the 95% confidence level, assuming red noise (order 1 auto-regressive process with lag-1 auto-correlation of α = 0.72).

Figure 3.11 depicts time averaged and normalized variance from the wavelet analysis. The mean over all 20 year periods from NA_c1 and NA_c2 (solid) and from both warm periods (dashed) are shown together with their standard deviation (blue-cold and red-warm). Beside the fact that there is considerable variability between the single 20 year periods (high *std*), there is a significant difference in variance between the warm and cold phases, in particular for periods between 4 to 6 years (mean for the cold periods is above the upper standard deviation of the warm phases for periods between $\sim$ 4 to 6 years).

To conclude, changes in dominant period of ENSO between the NA warm and cold phases occur and accord well with changes in the mean background climate of the tropical Pacific that can effect, through changes in propagation and structure, the dominant ENSO period. The link between increased ENSO variability and dominant El Niño-like conditions (i.e., weakened zonal gradients) during NA cold phases is counterintuitive. The distribution of ENSO variability is distinctly skewed, thus any changes in variance of ENSO, as identified above, will cause directly changes in the mean climate of the tropical Pacific (Timmermann, 2003). The differences in the mean tropical Pacific climate (Sec. 3.2.2) could thus very well be the consequence rather than the cause of increased ENSO variability. We shall see though in the following Sec. 3.3 that the aforementioned changes in ENSO variance and mean state are in accordance with a mode of DEAMs identified by Timmermann (2003).

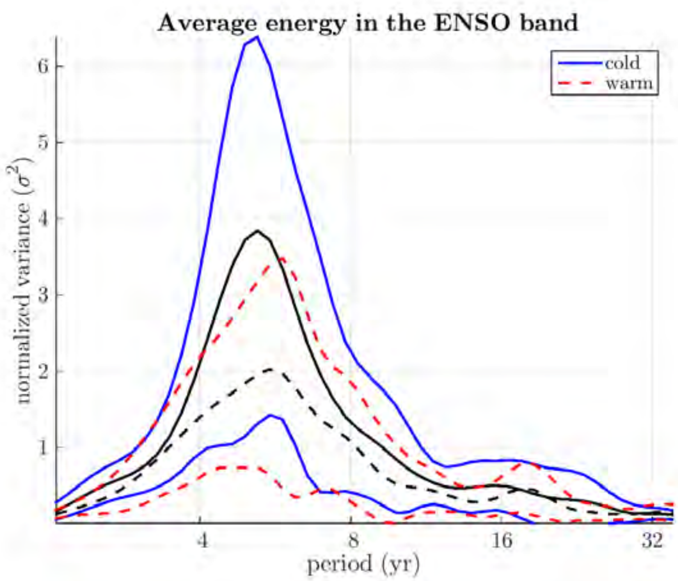

Figure 3.11.: Time averaged wavelet power from a wavenumber 6 Morlet Wavelet analysis in units of normalized variance. The black lines show the mean over all 20-year periods from the cold (solid) and warm (dashed) NA phases. The blue (red) lines show the *std* of this 20-year averages for the cold (warm) phase.

3.3 From decadal to centennial scale tropical variability in CONT

In the previous section we described the differences in the tropical Pacific between NA_c1 and NA_w1 and highlighted the similarity of these anomalies to ENSO induced changes and their relevance for ENSO variability. Decadal modes of tropical Pacific variability have very similar spatial signatures, for example through modulating ENSO's amplitude. In this section we provide evidence that DEAMs can account for much of the aforementioned mean changes. NA warm phases correspond to dominantly positive phases of this mode of variability, with El Niños (La Niñas) occurring further to the west (east) (Fig. 3.12 (c), upper panel). The opposite is true for NA cold phases. The findings in this section are in good agreement with the characteristics of DEAMs in Timmermann (2003)'s study. Furthermore global atmospheric circulation pattern associated with the decadal mode are presented and found to be clearly linked to the NA atmospheric feedback.
The first EOF (Fig. A 1, upper panel) of tropical Pacific SST anomalies is the "classical" ENSO signal, with an equatorial confined cold tongue to the east and a broader opposite sign anomaly to the west. The first EOF of 20yr LP filtered SST anomalies (Fig. 3.12 (b), upper panel; and the second EOF Fig. A 1, lower panel) resemble a pattern that is known under many different names. Ashok et al. (2007) termed it El Niño Modoki (also as the second EOF, while the first EOF is the "classical ENSO" or east Pacific (EP) El Niño).

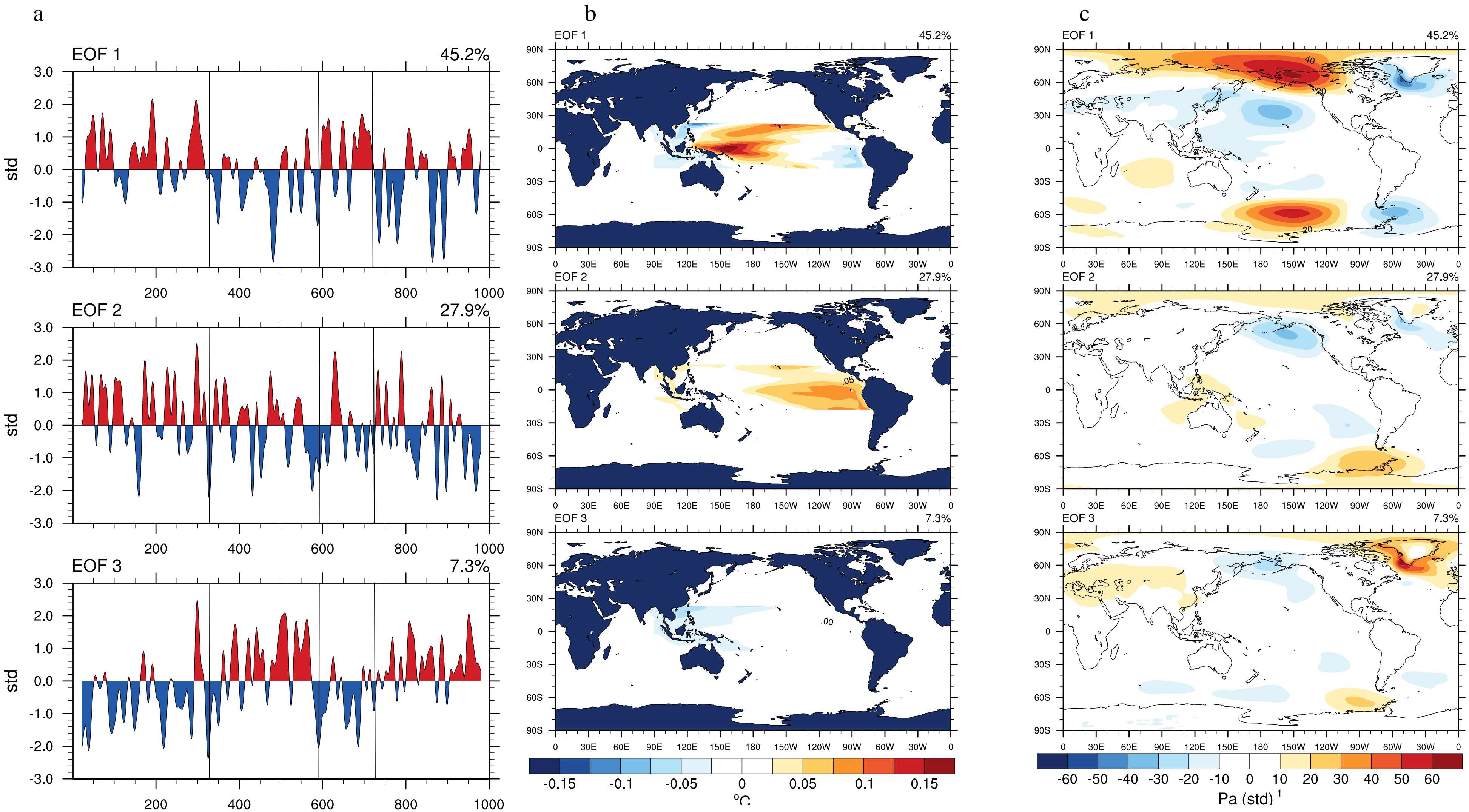

Figure 3.12.: Regression between PC 1 to 3 (a) of 20 year LP filtered tropical Pacific SST anomalies (b) and global SLP anomalies (c). SLP anomalies are only shaded if the regression coefficient is different from 0 with 95% confidence, based on a two sided student's t-test. Note that the spatial pattern of SST and SLP anomalies is not sensitive to the choice of LP filtering them by 12-50 years. The black vertical lines indicate the onset of the NA phases, based on Greenland temperature.

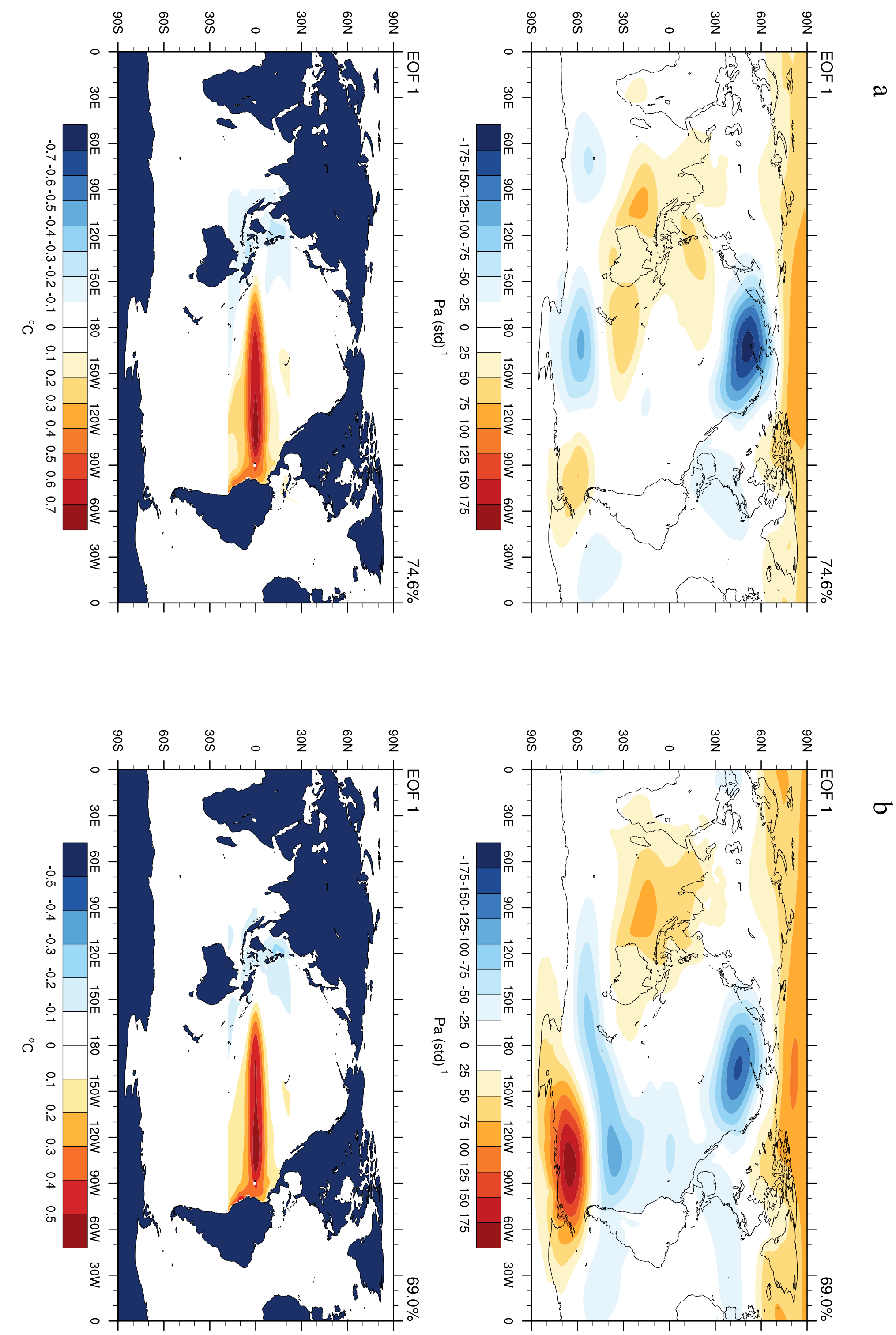

Figure 3.13.: Same as Fig. 3.12 but for HP filtered tropical Pacific SST anomalies for CONT in (a) and HI in (b). Only the first EOF and SLP regression are shown.

Other names of the Modoki mode are for example central Pacific (CP) El Niño (Kao and Yu, 2009) or Date Line El Niño (Larkin and Harrison, 2005). We refer to it in the following as Modoki mode or pattern.
The Modoki pattern (EOF2 of unfiltered SST anomalies or EOF 1 of LP filtered SST anomalies) is clearly less equatorial confined than the classical cold tongue El Niño pattern (EOF1 in Fig.3.13 (a)) The Modoki mode is the dominant pattern of variability on decadal timescales, as inferred from the first EOF (explaining $\sim$ 45% of variability) of the 20-year LP filtered tropical Pacific SST anomalies. It is clearly associated with the NA phases (Fig.3.12 (c), upper panel), with El Niños (La Niñas) occurring further to the west (east) during the warm phases and in accordance with the findings of Timmermann (2003). The Modoki mode can be interpreted as an east-west displacement of the main center of action of ENSO variability (Fig. 3.12 (b), upper panel). The phases are most pronounced in the third EOF and the transitions tend to occur after the transition in the first EOF (Fig. 3.12 (c), lower panel), but explains only 7 % of the total LP filtered SST anomaly variability.

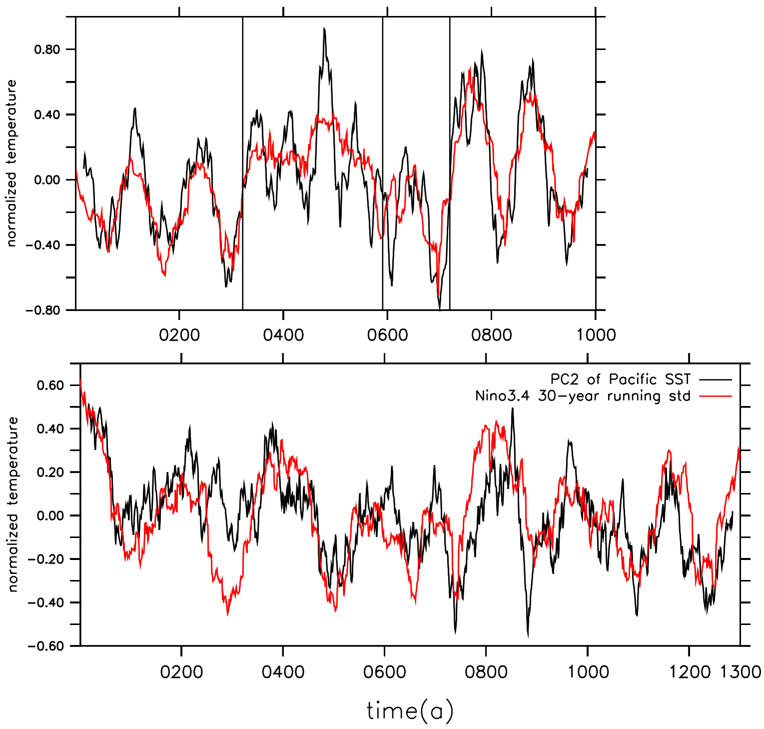

Figure 3.14.: Niño 3.4 30-year running *std* in red and PC2 of tropical Pacific SST anomalies smoothed by a 30-year running mean in black. (a) for CONT, black vertical lines indicate the onset of NA phases based on Greenland temperature. (b) for HI.

The Modoki mode in CONT has a timescale of $\sim$ 20 to 130 years (Sec. 3.2.3, Fig.3.9 (b) and e.g., Fig.3.12 (c), upper panel) and dominantly positive phases - with El Niños (La Niñas) occurring farther to the west (east) - correspond to warm and dominantly negative phases of this mode to cold NA phases (Fig. 3.12 (b) and (a), upper panel). Associated with this mode of variability are besides SST changes, variations in the Pacific thermocline depth (Fig. 3.16). The cold phases are associated with warming (cooling) in subsurface temperature to the east (west) of about 0.5 $°C$. and hence a deepening of the thermocline in the east and accordingly a reduction of the thermocline slope.
A comparison of the 30-year running mean Modoki mode and 30-year Niño 3.4 SST *std* yields a correlation of 0.77 (Fig.3.14 (a)). Furthermore we see that enhanced Niño 3.4 SST *std* is linked to cold NA phases. The Modoki mode - the east-west displacement of ENSO's center of action, the ENSO amplitude modulations and the thermocline depth anomalies - has the same characteristics as the DEAM mode identified by (Timmermann, 2003), who suggests that this mode originates from within the tropics. The author shows that the DEAMs are not a forced response to decadal mean state changes (the east-west displacement) and do not behave in a simple linear cause-consequence relation. Instead it is suggested that DEAMs and the east-west displacement are the expression of coupled nonlinear dynamics. The author illustrates that a homoclinic bifurcation scenario can account for ENSO amplitude modulation on longer timescales than predicted by linear theory.
Differences between the findings of Timmermann (2003) and CONT exist in the amplitude of changes and in the timescales. In Timmermann (2003)'s study the subsurface temperature anomalies reach values in excess of 2 $°C$ whereas in CONT the amplitude has maximum values of 0.5 $°C$. However, the 0.5 $°C$ anomaly in CONT corresponds to the difference between NA warm and cold phases that are linked to dominant positive and dominant negative phases of the Modoki mode, respectively. The 2 $°C$ in Timmermann (2003)'s study are associated with the 16 year timescale of a 'single' DEAM. The timescale of DEAMs is longer and less regular in CONT ($\sim 20 - 100$ years, see Fig. 3.9 (b) and Fig.3.14, upper) than the 16 year timescale found by Timmermann (2003). A possible explanation could be the different ENSO periods in CONT (a dominant period of 6 years) and in Timmermann (2003)'s study (dominant period of 2-3 years).
Evidence for ENSO modulation on decadal timescales comes furthermore from observations. Zhang et al. (1997) identified two major shifts of ENSO-like variability by analysing different reanalysis products. Their identified ENSO-like variability pattern is less equatorial confined (as in CONT) and has a stronger SLP signature in the extrat-

ropical northern Hemisphere than ENSO variability.

3.3.1 Atmospheric circulation pattern associated with the Modoki mode

In particular for global atmospheric circulation changes the east-west displacement of ENSO is relevant. Yin and Battisti (2001) point out, that it is the pattern of tropical Pacific SST anomalies that determine the atmospheric circulation changes on a global scale rather than the amplitude. It is thus expected that the global teleconnections of the Modoki mode are different from the spatial teleconnection pattern of the "classical ENSO" mode. Indeed Ashok et al. (2007) finds that the teleconnections of El Niño Modoki resemble in many regards rather the one of a La Niña.
To assess global atmospheric circulation changes associated with the identified mode of ENSO-like variability we show global regression pattern between SLP and PCs of ENSO-like (LP filtered) and ENSO (HP filtered) variability (Fig. 3.12 (c) and (d), respectively). The global SLP field associated with EOF1 of LP filtered tropical Pacific SST variability (Fig. 3.12 (a), upper) is characterized by distinct SLP anomalies in the high latitudes of both Hemispheres. Negative phases of this mode (linked with the cold NA phases and enhanced convection over the WPWP) are correlated with a weakened Aleutian Low, strengthened SLP over the Weddell Sea and decreased SLP over the Ross Sea. The latter is potentially relevant for a southern Hemisphere response to the NA phases and is discussed in further detail in Chapter 4. The most prominent feature is the increased SLP over the LS region and can be clearly linked to the atmospheric feedback to sea ice increase during NA_c1 in the LS (cf. Fig. 2.4 and Fig. 2.12 and corresponding text). The teleconnection pattern of HP filtered tropical Pacific SST anomalies are in principal similar to the LP filtered ones, but reveal a distinctly different SLP pattern in the NA (cf. Fig. 3.12 (c), upper panel to Fig. 3.13 (a), upper panel). Although the SLP anomalies of the HP filtered SSTs have in general a higher amplitude (by a factor of ~ 2, note the different color scales), this is not true for the NA, where the SLP anomalies resemble the NAO (in accordance with typical ENSO teleconnections) and have an amplitude of ~ 25 $Pa(std)^{-1}$. The maximum NA SLP anomaly associated with the LP filtered SSTs has an amplitude of 70 $Pa(std)^{-1}$. A possible explanation for the relation between the SLP in the NH (in the North Atlantic, but in particular the Aleutian Low) and the tropical Pacific SST mode of variability is Rossby wave propagation. Enhanced (decreased) convection over the WPWP - as seen for NA_c1 (NA_w1) - cause vortex stretching (squeezing), required

for Rossby wave propagation (Hoskins and Karoly, 1981).
The correlation between the 30-year running *std* of Niño 3.4 SST anomalies and 30-year running mean NA SLP anomalies is ~ 0.6 and has maximum correlation around 0-lag, consistent with both, the tropical Pacific or the NA leading by a couple of years (Fig.3.15).

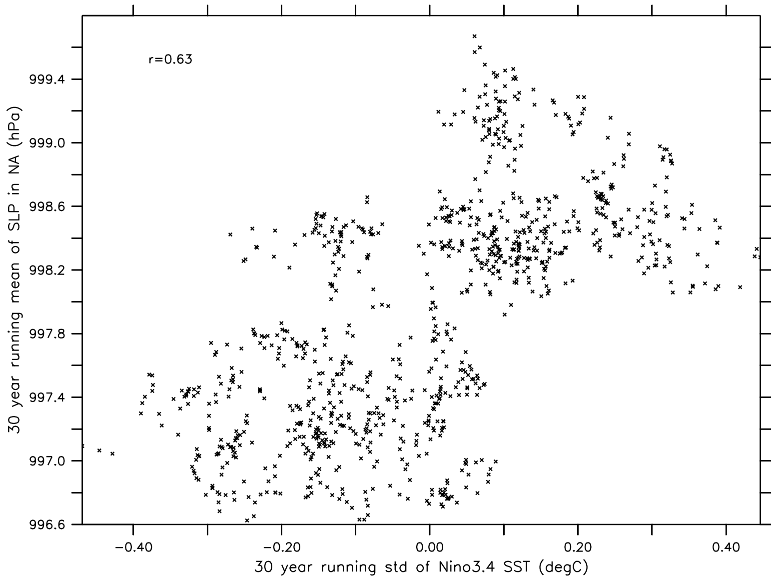

Figure 3.15.: Scatter plot of 30-year running *std* of Niño 3.4 SST anomalies (red curve in Fig. 3.14 (a)) and annual minimum SLP in the NA (averaged from $65°W - 10°E$ and $50°N - 75°N$) smoothed by a 30-year running mean at 0-lag.

So clearly there is evidence for two different states in the tropical Pacific - in terms of mean climate as well as in ENSO variance - that covary with the changes between warm and cold NA phases. This section suggests that the Modoki mode accounts for much of the tropical Pacific differences between NA warm and cold phases. Furthermore Timmermann (2003) shows that this mode can be generated by nonlinear dynamics in the tropics. This supports our earlier speculations (Sec.2.4.2) that tropical variability could trigger the NA cold and warm phases. However, there exist several conceivable ways of how the tropical Pacific and the NA are linked. Therefore in the next section we will discuss these different possible linkages and their evidence in CONT.

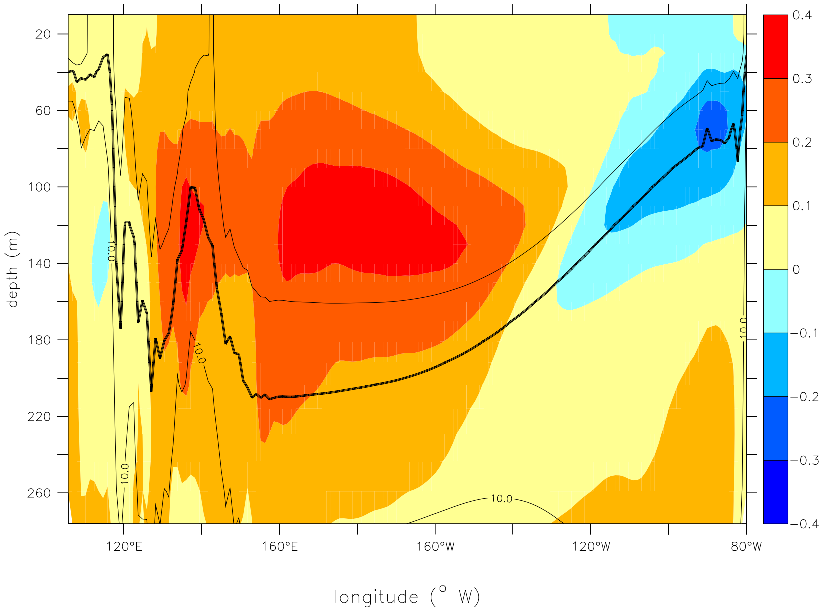

Figure 3.16.: Temperature anomaly [$°C$] between NA_w1 and NA_c1 (warm - cold) for a meridional average from $10°S$ to $10°N$ across the Pacific. Contours show the position of the long term mean of the 10°-, 15°- and 20 °-Isotherm. The 15$°C$-Isotherm is thick.

3.4 Discussion of possible relations between the NA and the tropics

It is not possible to establish cause and effect of the tropical- extra-tropical connection in CONT in terms of a lead/lag correlation. Both, a lead or a lag, by a couple of years of the tropical Pacific relative to the NA phases would be consistent with the time span of maximal correlation. There are four conceivable possibilities of how the NA phases and the associated changes in the tropical Pacific could be linked.

- the phases in the NA and the tropical Pacific could be unrelated and occur only coincidentally at the same time. However, we consider the chance that 3 climate transitions with different climate conditions lasting over several centuries occur in a 1000 year long simulation at the same time independently in the NA and the tropical Pacific as unlikely and do not discuss it further.
- something third causes the transitions in both the tropical Pacific and the NA (e.g., southern Hemisphere changes). However, we find no indications for significant

changes outside of the tropical Pacific and the NA in CONT (Chapter 2) and this possibility finds thus also no further consideration.

- tropical variability is caused by NA warm and cold phases (e.g., as in Zhang and Delworth (2005) and Dong and Sutton (2002))

- the tropical phases are intrinsic to the tropics (e.g., the aforementioned Modoki mode) and trigger the NA phases through e.g., Rossby wave propagation

In Sec. 3.4.1 the third hypothesis is explored and it is demonstrated that essential parts of the pathway, connecting the NA and the tropical Pacific, suggested by Zhang and Delworth (2005) are absent in CONT. Thus if the NA phases were causing the tropical Pacific phases, a mechanism different from the one suggested by Zhang and Delworth (2005) has to be responsible.
In the previous section we hypothesised that the Modoki mode does not depend on extratropical dynamics and causes the NA phases. We support this idea in Sec. 3.4.2 by presenting evidence for similar centennial scale tropical Pacific variability in HI, where no NA warm and cold phases occur.

3.4.1 Comparison to Zhang and Delworth (2005)

The spatial pattern of precipitation anomalies (Fig. 3.8) - indicative of atmospheric convection differences - in the equatorial Pacific between NA warm and cold phases in CONT (weakening and eastward shift of the Walker circulation during NA_c1) are very similar to the response of the tropical Pacific to freshwater hosing in the NA performed by Zhang and Delworth (2005) and Dong and Sutton (2002). The physical mechanism of altered atmospheric tropical Pacific convection suggested by Zhang and Delworth (2005) and Dong and Sutton (2002) is summarized schematically by Clement and Peterson (2008) in Fig. 3.17. In the following this mechanism is briefly summarized and compared to changes in CONT.
Dong and Sutton (2002) show that the southward migration of the Atlantic ITCZ, associated with freshwater induced cooling (warming) of the NA (South Atlantic), trigger a single El Niño event after 7 to 8 years, suggesting that coupled ocean-atmosphere adjustments to NH cooling can connect the Atlantic and tropical Pacific way faster than ocean processes alone. The timescale of about 8 years would be still fast enough to be relevant for linking the NA and tropical Pacific in CONT (cf. Fig. 3.15 and corresponding text). However, essential parts of the suggested pathway are not present in CONT, indicating

that an other mechanism must exist for the linkage of NA phases and the tropical Pacific.

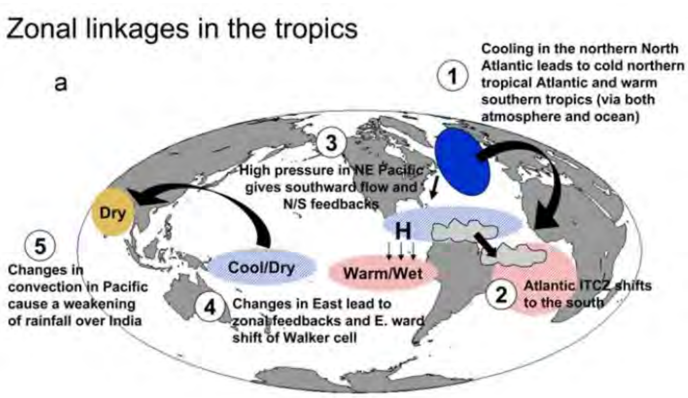

Figure 3.17.: Schematic of tropical zonal linkages in response to NA cooling, taken from Clement and Peterson (2008) and based on the mechanism suggested by Zhang and Delworth (2005) and Dong and Sutton (2002). Process 2 (the southward migration of the ITCZ in the Atlantic is present in CONT, too. However, the amplitude of the tropical Atlantic changes is negligible compared to Zhang and Delworth (2005)'s study. See text for further detail.

The numbers in the following paragraph refer to the study by Zhang and Delworth (2005), but are representative for both studies. The fresh water hosing in the NA causes an abrupt weakening ($O(14\ Sv)$) of the maximum AMOC to $\sim 5\ Sv$. The reduced heat transport associated with the reduced AMOC causes large scale cooling of the surface Atlantic Ocean by up to 10 $°C$ locally and still up to 4 $°C$ in the tropical NA, as well as a distinct warming (up to $\sim 2.5°C$) in the southern Atlantic. The large scale cooling causes a pronounced southward displacement of the tropical Atlantic ITCZ which is a robust model response to a weakening of the AMOC strength (e.g., Chiang et al. (2008); Kageyama et al. (2013)). The southward migration of the ITCZ weakens the SH Hadley cell and causes a reduction of the SH subtropical jet. A southward shift of precipitation occurs as a result of the displacement of maximum vertical velocities. The changes in tropical Atlantic precipitation, due to the southward displacement of the ITCZ, amount to 4.3 $mm \cdot day^{-1}$. The zonal connection from the NA to the eastern Pacific arises from the strong cooling in the NA off the central American coast (with reduced precipitation) that increases SLP here and over the northeastern tropical Pacific. As a result the Hadley circulation in the eastern Pacific weakens and causes an equatorial asymmetric pattern. The anomalous southward winds associated with the weaker Hadley circulation result in enhanced upwelling and cooling north of the equator and anomalous downwelling and

warming south of the equator. The cross-equatorial SST anomalies reinforce the anomalous Hadley circulation. The increased SST in the southeastern tropical Pacific eventually decrease the Walker circulation (Zhang and Delworth, 2005).
The Atlantic ITCZ migrates as well southward in CONT during NA_c1 (Fig. 3.18). There is a small intensification of the northeasterly trade winds, which seems to be a general feature of tropical Atlantic response to the southward shift of the Atlantic ITCZ, inferred from GCM simulations (Chiang et al., 2008; Lee et al., 2011). However, the maximum difference in precipitation in the tropical Atlantic amounts only to 0.1 $mm \cdot day^{-1}$. The changes in tropical Atlantic precipitation due to ITCZ shifts are thus by a factor of 40 smaller than in the findings of Zhang and Delworth (2005).

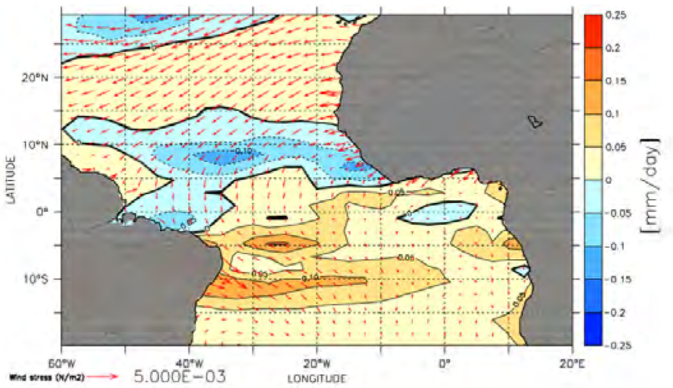

Figure 3.18.: From Rheinlaender (2015): Difference in precipitation (shading, $mm\ day^{-1}$) and wind-stress (vectors, $N\ m^{-2}$) between the cold (year 400-550) and the warm phase (year 50-250) over the tropical Atlantic region. Vectors correspond to the zonal and meridional components of the anomalous wind-stress and a reference vector of length (0.005 $N\ m^{-2}$) is plotted in the lower left corner for comparison. Contour interval is 0.05 $mm\ day^{-1}$. The precipitation anomalies are indicative of a minor southward shift of the Atlantic ITCZ.

The hampered atmospheric response in CONT is the result of two key differences between the NA phases in CONT and the fresh water induced cooling situation in Zhang and Delworth (2005). Firstly, the AMOC changes in association with the NA phases in CONT are minor compared to the fresh water hosing experiments (in CONT $O(4\ Sv)$, amounting to a maximum AMOC during the cold phase of $\sim 20\ Sv$). Secondly and closely linked to the former, the strong cooling in CONT is confined to the LS and Greenland. In a zonal average the areas north of $40°N$ still cool by about $1°C$, the remainder of the NA cools only by 0 to 0.5 $°C$. However, the tropical Pacific precipitation and circulation changes are of the same order of magnitude as in Zhang and Delworth (2005)'s study (the precipitation difference in annual maximum precipitation between NA_c1 and NA_w1 is 1 $mm \cdot day^{-1}$ and in annual average 0.5 $mm \cdot day^{-1}$). Furthermore SLP anomalies associated

with the NA warm and cold phases in CONT are confined to the western Pacific (Fig. 3.6 and 3.12). The lack of increased SLP in the eastern Pacific can be explained by the weak cooling in the NA off the central American coast in CONT. No signature - an equatorial asymmetric pattern in SST and precipitation anomalies - of a weakened Hadley circulation is found in CONT. This implies that the second essential part of Zhang and Delworth (2005)'s pathway - the weakening of the Hadley circulation in the eastern Pacific - is also not present in CONT.
The mechanism connecting the tropical Pacific and the NA cooling, suggested by Zhang and Delworth (2005) and Dong and Sutton (2002) cannot account for the big share of tropical Pacific changes in CONT. This is most likely a consequence of a minor decrease of AMOC strength and the associated marginal ITCZ shift in the tropical Atlantic in CONT. This indicates further that a different physical mechanism connecting the tropical Pacific and the NA must be present in CONT. However, the NA cooling might reinforce the original precipitation anomalies in the tropical Pacific.

3.4.2 Tropical variability causing the NA phases

In the following we focus on the presence of similar decadal to centennial scale modes of ENSO variability in HI, where no NA cold and warm phases occur. This suggests that the tropical mode of centennial scale ENSO modulation originates in the tropical Pacific, further supporting our conclusions drawn in the previous section (Sec.3.3).

Figure 3.19 shows EOF 1 to 3 pattern of tropical Pacific SST anomalies and the regression between the corresponding PCs and global SLP anomalies for HI. The analysis is split into the HP and LP filtered components of SST anomalies (same as in Fig. 3.12 for CONT). The spatial pattern of the LP filtered EOF 1 is identical to the LP filtered EOF 1 in CONT, but explains about 10% less of the low frequency variability (31.9% in HI versus 44.9% in CONT, cf. Fig.3.12 (b), upper panel and Fig.3.19 (b), upper panel). Furthermore the amplitude of SST variations with this mode in HI is smaller by about a factor of 2, compared to CONT. In most areas the SLP anomalies associated with this mode accord with the spatial pattern of SLP anomalies in CONT (cf. Fig. 3.19 (a), upper panel and Fig. 3.12 (a), upper panel). Minor differences in the pattern of the Aleutian low exist. However, the most prominent SLP anomaly over the Baffin Bay area and the LS - present in CONT - is lacking in HI. In CONT we find the clear signature of the atmospheric feedback to sea ice anomalies in the LS during the cold and warm NA phases (cf. Fig.2.4 (d) and Fig.2.12) with a maximum SLP response of 0.7 $hPa(std)^{-1}$ of SST anomalies. In HI we find only a weak relationship of 0.1 $hPa(std)^{-1}$ between the SLP in

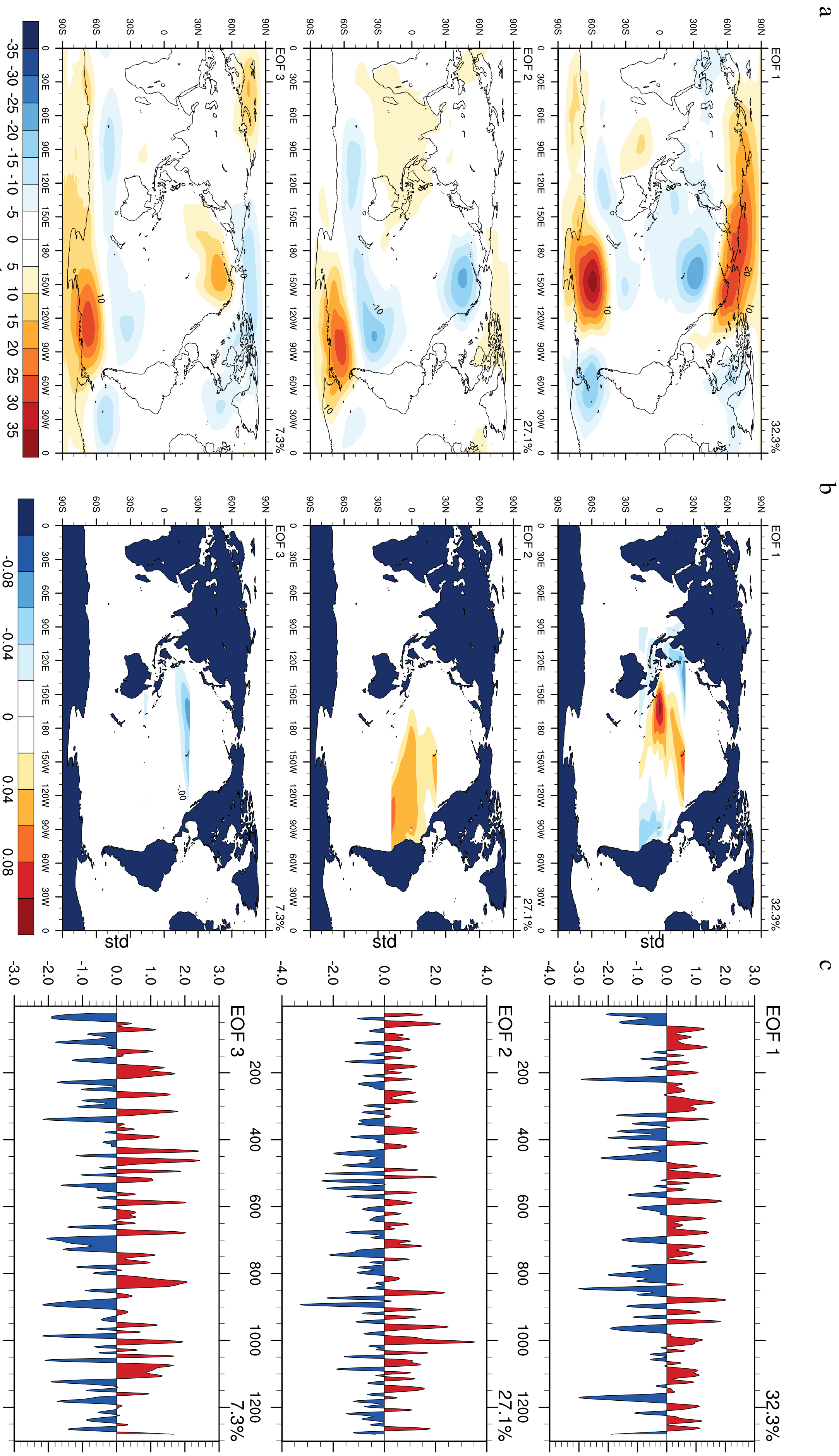

Figure 3.19.: As in Fig. 3.12 but for HI

the Baffin Bay area and the Modoki mode of SST anomalies. The Modoki mode in HI has in general weaker teleconnections than in CONT with a maximum amplitude of about 0.4 $hPa(std)^{-1}$ of SST anomalies (e.g., above the Bellinghausen Sea, the Aleutian Arc and the subtropical Pacific).
ENSO (HP filtered) variability in HI has stronger teleconnections in the southern Hemisphere than CONT. The EOF 1 of HP filtered SST anomalies in HI reveals a "classical ENSO" cold-tongue pattern that is slightly more equatorial confined than in CONT (cf. Fig.3.13 (a), middle panel and Fig.3.13 (b), middle panel). The spatial pattern of the Southern Oscillation (SO) is clearly stronger pronounced in HI.
When considering the PC (Fig. 3.19 (c), upper panel) of the Modoki mode it becomes clear that phases of dominant positive and negative conditions alternate on centennial timescales. For example the periods between year 300-450 and 750-850 are dominated by negative phases of the Modoki mode - with El Niños (La Niñas) occurring farther to the east (west) - while for example years 250 to 350 are dominated by positive phases. The timescale of $\mathcal{O}(100yr)$ appears as well in a wavelet analysis of the second PC of unfiltered SST anomalies (Fig. A.2) and can also be seen in Fig.3.14 (b).
The different phases of the Modoki mode do not only appear in the EOF analysis, but also in precipitation anomalies between these phases (Fig. 3.20 (a)), in SST and thermocline depth anomalies between east and west Pacific (not shown). Furthermore the increased ENSO variance associated with the Modoki mode is also present (cf. 30-year running mean of PC2 of unfiltered SST anomalies (black) and 30-year running *std* of Niño 3.4 SST anomalies (red) in Fig.3.14, lower panel). The main difference between CONT and HI in this regard is the overall smaller amplitude of SST variability in HI and the reduced teleconnection pattern of ENSO-like variability (in terms of SLP anomalies per *std* of SST anomalies) compared to CONT. In particular in the LS and the NA region the differences are pronounced. The presence of this centennial scale variability in both HI and CONT together with the fact that no NA warm and cold phases occur in HI suggests that it is not the NA phases that cause the centennial scale tropical Pacific variability. However, the tropical Pacific phases might very well be amplified by the NA phases. An indication for this could be the higher amplitudes of SST anomalies associated with the Modoki mode in CONT.

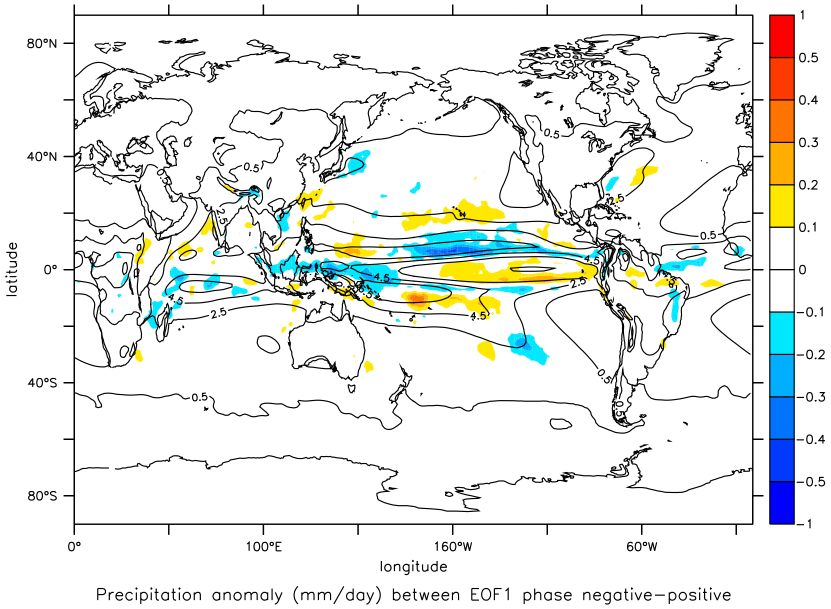

Figure 3.20.: Precipitation anomaly [$mm \cdot day^{-1}$] between simulation year 330 to 450 and 230 to 320 in HI. Overlaying contours show the 1300 year mean. The spacing between contours is 2 $mm \cdot day^{-1}$.

3.5 Discussion & Summary

3.5.1 Discussion

Changes in CONT in the tropical Pacific are relative small (at least compared to the NA) and thus it might seem unlikely that these changes are responsible for the large scale changes in the NA. However, Yin and Battisti (2001) have demonstrated that it is rather the spatial pattern of SST anomalies in the tropical Pacific that matter for the large scale atmospheric circulation and teleconnections to high latitudes. In fact they find that a scenario with different spatial SST pattern in the tropical Pacific and a mean SST change of about 1 $°C$ has stronger effects than a uniform cooling of about 3 $°C$, applied over the entire tropical Pacific.

The Modoki mode manifests itself as an east-west displacement of ENSO's center of activity. Support for such mode switches on decadal scales comes from observations of ENSO-like variability (e.g., Zhang et al. (1997); Giese and Ray (2011); Fedorov and Philander (2000) and Wang and An (2002)). A shift of ENSO's center of action in association with NA cooling has further implications. In a recent study Karamperidou et al. (2015) suggest a shift between dominance of EP and CP El Niños during the Holocene. They suggest that a shift between CP and EP ENSO flavours can potentially help to disentangle conflicting information about past ENSO variability from different paleo-proxies. Various proxies record ENSO's teleconnections, rather than ENSO variability itself. Teleconnections of EP and CP ENSO types differ substantially (Wang et al., 2012; Karamperidou et al., 2015) In particular the influence on Indian and east Asian monsoon appears to be stronger for CP type ENSO variability (e.g., Kumar et al. (2006) and Zhang et al. (2011)). We argued in this chapter that the Modoki mode does not depend on extra-tropical dynamics and supported this hypothesis with evidence for the presence of centennial scale ENSO-like variability in HI. However, the possibility that something third triggers both the NA phases and the tropical Pacific changes in CONT, but fails to trigger changes in the NA in HI cannot be discarded. Targeted experiments with modified tropical Pacific SST anomalies could give further insight in the cause and effect relationship between the tropical Pacific and the NA.

3.5.1.1 ENSO phase lock

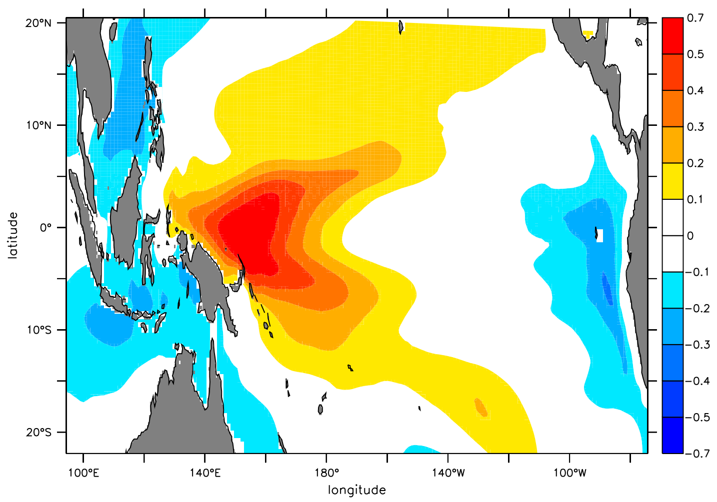

Figure 3.21.: SST anomaly (°C) averaged over all phase lock years (annual Niño 3.4 SST anomaly does not exceed ±0.5 °C for a minimum of 5 years), relative to 1000 year long term mean in CONT.

Clement et al. (2001) identify a mechanism by which slowly varying orbital forcing can alter ENSO behaviour and through this can give rise to abrupt millennial scale climate variability on a global scale. Due to non-linear interaction of ENSOs intrinsic timescale with the seasonal cycle the dominant period of ENSO changes. Under certain orbital conditions - and when the ENSO system transitions from one dominant period regime to the other - ENSO variability can lock completely to the annual cycle. The reason for this being that when ENSO transitions from one period regime to another it is not able to prefer one and thus locks to the forcing (i.e., the seasonal cycle). This complete phase lock of ENSO (Niño 3.4 SST anomalies do not exceed 0.5 $^{\circ}C$ for a minimum of 5 years) lasts, depending on eccentricity, for a decade up to several centuries. Clement et al. (2001) identified a La Niña like pattern in SST in association with the phase lock events.
We have identified changes in ENSO period in association with dominant positive and negative phases of the Modoki mode. Motivated by Clement et al. (2001)'s study we identify 11 phase lock events in CONT (i.e., annual mean Niño 3.4 SST anomalies do not exceed 0.5 $^{\circ}C$ for a minimum of 5 years). Two of these events last 6 and 7 years occurring shortly before the transition between NA_w1 to NA_c1 (year 294-299 and 309-313) and the transition between NA_w2 and NA_c1 (year 688-693 and 695-702). This phase lock is also visible in the wavelet spectrum, with almost zero variance in all period bands (dark blue colors in Fig. 3.9 (a) and (b)). All other phase lock events appear to occur as well in association with a phase switch of the Modoki mode. The SST pattern in CONT associated with all phase lock events is depicted in Fig. 3.21 and is almost identical over all these events. The SST anomalies of the phase lock events are similar to the spatial pattern of SST anomalies associated with the Modoki mode. An alternative hypothesis to test in the future is thus, that the switch - and the associated muted ENSO variability - between dominant positive and negative phases trigger the NA climate transitions.

3.5.2 Summary

The tropical Pacific mean climate fluctuates between more dominant El Niño-like and La Niña-like conditions, in tandem with the NA cold and NA warm phases. These mean climate changes are in accordance with a tendency towards longer periods of ENSO during NA cold phases. At the same time the variance of Niño 3.4 SST anomalies increases, which can cause - as a direct consequence of the skewed ENSO distribution, with warm events tending to attain higher amplitudes - El Niño-like conditions.
The increased variance is associated with a mode of ENSO-like variability (Modoki mode) that manifests as an east-west displacement of ENSO's center of action. El Niños

are displaced farther to the east and La Niñas to the west during NA cold phases. The characteristics of the Modoki mode are in accordance with the findings of Timmermann (2003), though DEAMs in Timmermann (2003)'s study feature a decadal time scale. The author suggests that mean changes and ENSO amplitude modulation are both the expression of coupled nonlinear dynamics, without requiring extratropical dynamics.
The Modoki mode is correlated with SLP anomalies over the NA and feature the characteristic signature of the NA atmospheric feedback to sea ice anomalies in the LS. A mode of centennial scale ENSO-like variability with the same characteristics as in CONT is identified in HI. No NA warm and cold phases occur in HI, supporting further our hypothesis that the ENSO-like changes in CONT are not a consequence of the NA phases. Lastly, it is shown that a mechanism - suggested by Zhang and Delworth (2005) and Dong and Sutton (2002) - by which NA cold phases could induce similar tropical Pacific precipitation anomalies as seen in CONT, cannot account for the big share of these anomalies in CONT. This is most likely a consequence of a minor decrease in AMOC in association with the NA cold phases in CONT and consequently a negligible southward migration of the Atlantic ITCZ.
Motivated by the findings of Clement et al. (2001), we discussed an alternative hypothesis - related to muted ENSO variability in association with switches between positive and negative phases of the Modoki mode.

Bibliography

Ashok, K., S. K. Behera, S. A. Rao, H. Weng, and T. Yamagata, 2007: El Niño Modoki and its possible teleconnection. *Journal of Geophysical Research: Oceans (1978–2012)*, **112 (C11)**.

Battisti, D. S., and A. C. Hirst, 1989: Interannual variability in a tropical atmosphere-ocean model: Influence of the basic state, ocean geometry and nonlinearity. *Journal of the Atmospheric Sciences*, **46 (12)**, 1687–1712.

Bjerknes, J., 1969: Atmospheric teleconnections from the equatorial Pacific 1. *Monthly Weather Review*, **97 (3)**, 163–172.

Branstator, G., 1985: Analysis of general circulation model sea-surface temperature anomaly simulations using a linear model. Part I: Forced solutions. *Journal of the atmospheric sciences*, **42 (21)**, 2225–2241.

Chiang, J. C., W. Cheng, and C. M. Bitz, 2008: Fast teleconnections to the tropical Atlantic sector from Atlantic thermohaline adjustment. *Geophysical Research Letters*, **35 (7)**.

Clement, A. C., M. A. Cane, and R. Seager, 2001: An Orbitally Driven Tropical Source for Abrupt Climate Change. *Journal of Climate*, **14 (11)**, 2369–2375.

Clement, A. C., and L. C. Peterson, 2008: Mechanisms of abrupt climate change of the last glacial period. *Reviews of Geophysics*, **46 (4)**.

Deser, C., and Coauthors, 2012: ENSO and Pacific decadal variability in the Community Climate System Model version 4. *Journal of Climate*, **25 (8)**, 2622–2651.

Ding, Q., J. M. Wallace, D. S. Battisti, E. J. Steig, A. J. Gallant, H.-J. Kim, and L. Geng, 2014: Tropical forcing of the recent rapid Arctic warming in northeastern Canada and Greenland. *Nature*, **509 (7499)**, 209–212.

Dong, B.-W., and R. Sutton, 2002: Adjustment of the coupled ocean–atmosphere system to a sudden change in the thermohaline circulation. *Geophysical Research Letters*, **29 (15)**, 18–1.

Fedorov, A. V., and S. G. Philander, 2000: Is El Niño changing? *Science*, **288 (5473)**, 1997–2002.

Giese, B. S., and S. Ray, 2011: El Niño variability in simple ocean data assimilation (SODA), 1871–2008. *Journal of Geophysical Research: Oceans (1978–2012)*, **116 (C2)**.

Gill, A., 1980: Some simple solutions for heat-induced tropical circulation. *Royal Meteorological Society, Quarterly Journal*, **106**, 447–462.

Graham, N., and T. Barnett, 1987: Sea surface temperature, surface wind divergence, and convection over tropical oceans. *Science*, **238 (4827)**, 657–659.

Grinsted, A., J. C. Moore, and S. Jevrejeva, 2004: Application of the cross wavelet transform and wavelet coherence to geophysical time series. *Nonlinear processes in geophysics*, **11 (5/6)**, 561–566.

Guilyardi, E., 2006: El Niño–mean state–seasonal cycle interactions in a multi-model ensemble. *Climate Dynamics*, **26 (4)**, 329–348.

Hoskins, B. J., and D. J. Karoly, 1981: The steady linear response of a spherical atmosphere to thermal and orographic forcing. *Journal of the Atmospheric Sciences*, **38 (6)**, 1179–1196.

Kageyama, M., and Coauthors, 2013: Climatic impacts of fresh water hosing under Last Glacial Maximum conditions: a multi-model study. *Climate of the Past*, **9 (2)**, 935–953, doi:10.5194/cp-9-935-2013.

Kao, H.-Y., and J.-Y. Yu, 2009: Contrasting eastern-Pacific and central-Pacific types of ENSO. *Journal of Climate*, **22 (3)**, 615–632.

Karamperidou, C., P. N. Di Nezio, A. Timmermann, F.-F. Jin, and K. M. Cobb, 2015: The response of ENSO flavors to mid-Holocene climate: Implications for proxy interpretation. *Paleoceanography*.

Kumar, K. K., B. Rajagopalan, M. Hoerling, G. Bates, and M. Cane, 2006: Unraveling the mystery of Indian monsoon failure during El Nino. *Science*, **314 (5796)**, 115–119.

Larkin, N. K., and D. Harrison, 2005: Global seasonal temperature and precipitation anomalies during El Niño autumn and winter. *Geophysical Research Letters*, **32 (16)**.

Lee, S.-Y., J. C. Chiang, K. Matsumoto, and K. S. Tokos, 2011: Southern Ocean wind response to North Atlantic cooling and the rise in atmospheric CO2: Modeling perspective and paleoceanographic implications. *Paleoceanography*, **26 (1)**.

McPhaden, M. J., 1999: Genesis and evolution of the 1997-98 El Niño. *Science*, **283 (5404)**, 950–954.

Rheinlaender, J., 2015: Interhemispheric climate variability in a pre-industrial control simulation of CCSM4. M.S. thesis, University of Copenhagen, Niels Bohr Institute, Danmark.

Sadekov, A. Y., R. Ganeshram, L. Pichevin, R. Berdin, E. McClymont, H. Elderfield, and A. W. Tudhope, 2013: Palaeoclimate reconstructions reveal a strong link between El Nino-Southern Oscillation and Tropical Pacific mean state. *Nature communications*, **4**.

Shields, C. A., D. A. Bailey, G. Danabasoglu, M. Jochum, J. T. Kiehl, S. Levis, and S. Park, 2012: The Low-Resolution CCSM4. *J. Climate*, **25 (12)**, 3993–4014, doi:10.1175/JCLI-D-11-00260.1, [http://journals.ametsoc.org/doi/abs/10.1175/JCLI-D-11-00260.1].

Stott, L., C. Poulsen, S. Lund, and R. Thunell, 2002: Super ENSO and global climate oscillations at millennial time scales. *Science*, **297 (5579)**, 222–226, doi:10.1126/science.1071627.

Suarez, M. J., and P. S. Schopf, 1988: A delayed action oscillator for ENSO. *Journal of the atmospheric Sciences*, **45 (21)**, 3283–3287.

Timmermann, A., 2003: Decadal ENSO amplitude modulations: A nonlinear paradigm. *Global and Planetary Change*, **37 (1)**, 135–156.

Timmermann, A., S. J. Lorenz, S.-I. An, A. Clement, and S.-P. Xie, 2007: The effect of orbital forcing on the mean climate and variability of the tropical Pacific. *J. Climate*, **20 (16)**, 4147–4159, doi:10.1175/JCLI4240.1.

Torrence, C., and G. P. Compo, 1998: A practical guide to wavelet analysis. *Bulletin of the American Meteorological society*, **79 (1)**, 61–78.

Tziperman, E., S. E. Zebiak, and M. A. Cane, 1997: Mechanisms of seasonal-ENSO interaction. *Journal of the atmospheric sciences*, **54 (1)**, 61–71.

Vavrus, S., M. Notaro, and Z. Liu, 2006: A Mechanism for Abrupt Climate Change Associated with Tropical Pacific SSTs. *Journal of climate*, **19 (2)**, 242–256.

Wang, B., and S. An, 2002: A mechanism for decadal changes of ENSO behavior: Roles of background wind changes. *Climate Dynamics*, **18 (6)**, 475–486.

Wang, C., C. Deser, J.-Y. Yu, P. DiNezio, and A. Clement, 2012: El Nino and southern oscillation (ENSO): a review. *Coral Reefs of the Eastern Pacific*, 3–19.

Wittenberg, A. T., 2009: Are historical records sufficient to constrain ENSO simulations? *Geophysical Research Letters*, **36 (12)**.

Yin, J. H., and D. S. Battisti, 2001: The importance of tropical sea surface temperature patterns in simulations of Last Glacial Maximum climate. *Journal of Climate*, **14 (4)**, 565–581.

Zhang, R., and T. L. Delworth, 2005: Simulated tropical response to a substantial weakening of the Atlantic thermohaline circulation. *Journal of Climate*, **18 (12)**, 1853–1860.

Zhang, W., F.-F. JIN, J. LI, and H.-L. REN, 2011: Contrasting Impacts of Two-Type El Niño over the Western North Pacific during Boreal Autumn. *Journal of the Meteorological Society of Japan. Ser. II*, **89 (5)**, 563–569, doi:10.2151/jmsj.2011-510.

Zhang, Y., J. M. Wallace, and D. S. Battisti, 1997: ENSO-like interdecadal variability: 1900-93. *Journal of climate*, **10 (5)**, 1004–1020.

4 Southern Hemisphere response

Each D-O event is associated with an Antarctic Isotope Maximum (AIM) event with temperature changes between $1°C$ to $3°C$ (e.g., Blunier and Brook (2001)). The inferred Antarctic temperature changes are gradual and in anti-phase with Greenland temperature over a D-O cycle (Barbante et al., 2006).

In CONT temperature anomalies associated with NA cold phases around Antarctica and in the Southern Ocean are spatially variable, small in amplitude and are in general not significantly correlated with Greenland temperature over the transitions (Fig. 2.3). One exception to this exist, a band of warm anomalies ($\sim 0.5°C$) along the latitudes of $\sim 20°S$ (Pacific sector), $\sim 40°S$ (Atlantic sector) and $\sim 60°S$ (Indian Ocean sector). In this Chapter we explore why there is no strong interhemispheric coupling associated with the NA warm and cold phases.

The classical bipolar ocean seesaw model (Stocker and Johnsen, 2003; Crowley, 1992) and the atmosphere-surface ocean mechanism proposed by Lee et al. (2011) both rely on a strong AMOC reduction. A major AMOC reduction is absent in CONT, which is likely the cause for the weak interhemispheric coupling.

However, there is still considerable debate about major AMOC reductions in association with every D-O events (Böhm et al., 2015; Lynch-Stieglitz et al., 2014; Kissel et al., 2008; Gottschalk et al., 2015). Furthermore, Wunsch (2006) argued that any reduction in ocean heat transport would be compensated by a corresponding increase in atmospheric heat transport. It is also possible that the simple seesaw model is ruled out in the real world due to the ACC, acting as a dynamical barrier for signal transmission across it (e.g., Ferrari and Nikurashin (2010); Marshall et al. (2006). Lastly, the Antarctic response to fresh water hosing experiments differs distinctly between climate models (Kageyama et al., 2013). With this caveats about interhemispheric coupling concepts in mind, we analyse the SH response to NA warm and cold phases in terms of:

(a) ocean circulation adjustments in the NA and the Southern Atlantic in response to the NA cooling

(b) atmospheric rearrangements associated with the NA cooling

(c) atmospheric teleconnections of the tropical mode of variability in the SH

In the last part of this chapter we show that an increase of atmospheric CO_2 concentration by 20 *ppmv*, as observed for some D-O events (e.g. Bereiter et al. (2012); Ahn and Brook (2014)), adds to a more pronounced SH warming signal.

4.1 Advection of subsurface warm anomaly in the Atlantic Ocean

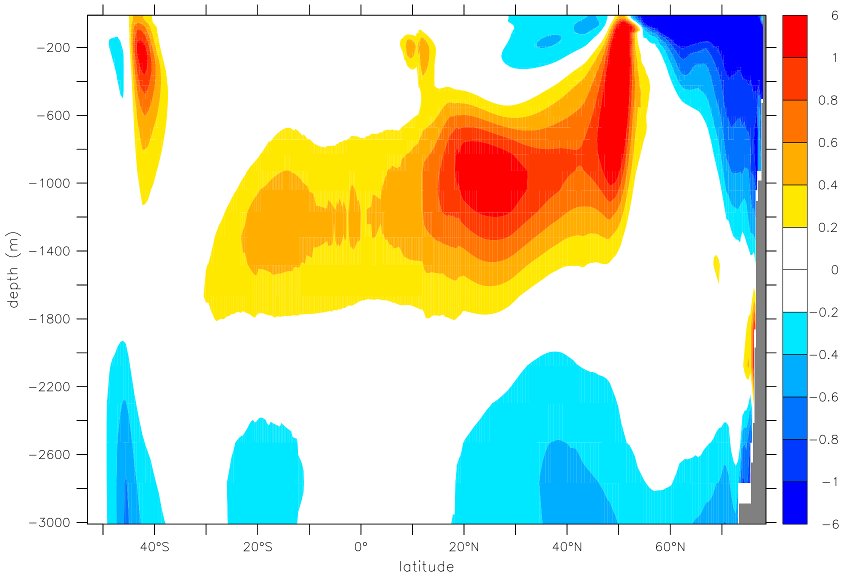

Figure 4.1.: Zonal average of Atlantic temperature anomalies [$°C$] between NA_c1 and NA_w1.

In Chapter 2 we showed that a decreased SPG circulation is essential to the cold NA phases in CCSM4. The deep convection cessation during NA cold phases eventually reduces the maximum AMOC strength by $\sim 4\ Sv$. Associated with this decrease is a reduced northward heat transport. We note though that this is a small reduction compared to fresh water hosing experiments. Following the interhemispheric coupling ideas of Crowley (1992) and Stocker and Johnsen (2003) the reduced AMOC should warm the South Atlantic. However, in CONT the AMOC strength in the southern Atlantic ($20°S$) is only reduced by $\sim 2\ Sv$ with a lag of approximately 16 years with respect to $40°N$ (Rheinlaender, 2015). SSTs in the South Atlantic do not show a clear warming trend during NA cold phases, with the exception of a localized warm anomaly of $\sim 0.5°C$ around $40°S$ (Fig. 2.3). Furthermore, there is a pronounced warm anomaly at the SPG- subtropical gyre (STG) boundary in the NA around $45°N$. The two warm anomalies are connected by

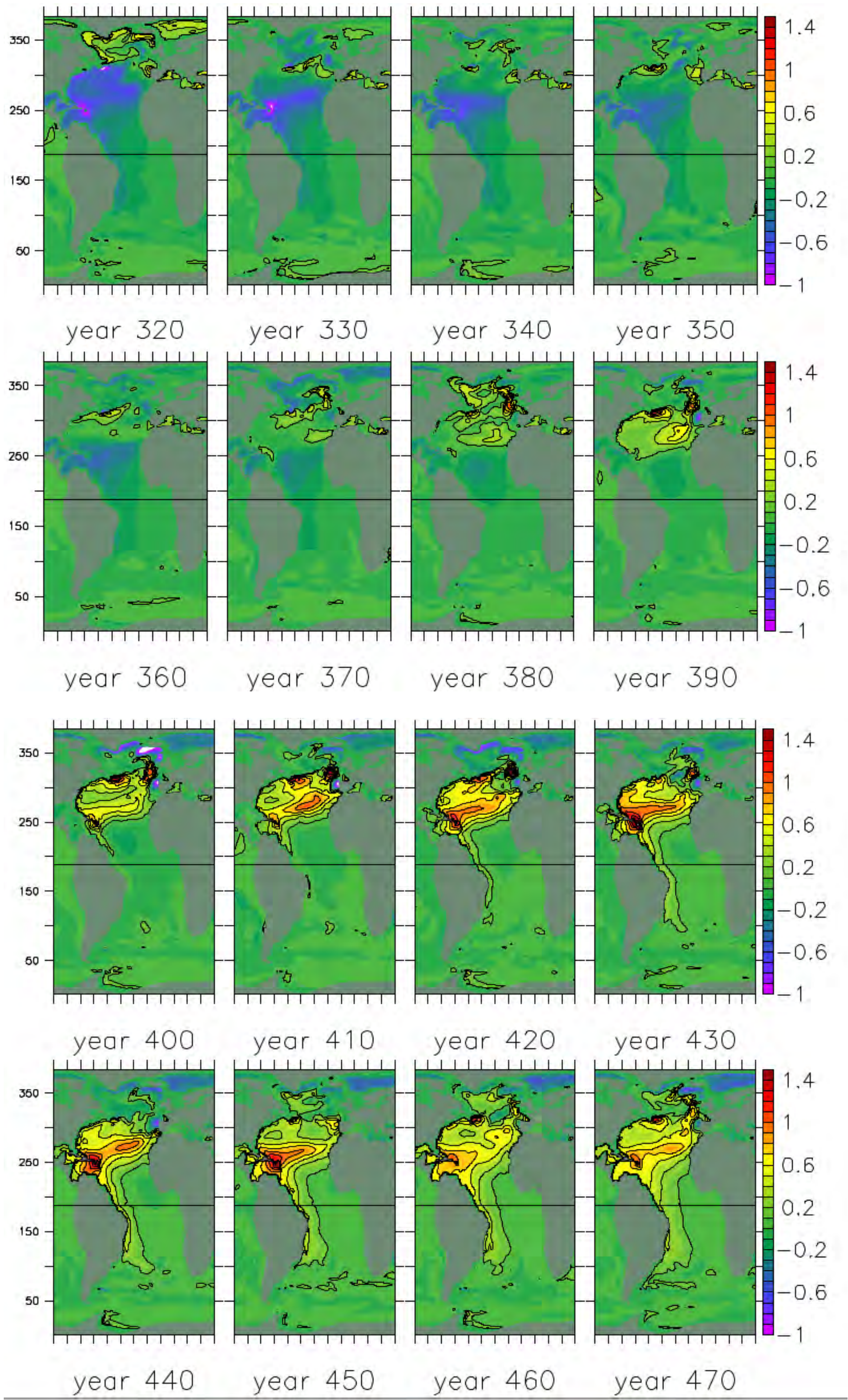

Figure 4.2.: From Rheinlaender (2015): Evolution and propagation of the subsurface temperature anomaly [$°C$]. The contour interval is $0.2°C$ and starts from anomalies of $0.1°C$. The panels correspond to anomalies of 10 year intervals of the potential temperature at 1000 m depth. The anomalies are relative to the long-term mean.

propagation of subsurface warm anomalies:
The strong warming at the intergyre boundary is the consequence of the northward shift of the Gulf Stream path during NA cold phases, due to the contraction of the SPG (see Sec. 2). A weak reduction of the STG circulation (max. $\sim$ 5 Sv) adds further to the warming. A heat budget of the upper $\sim$ 300 m of the STG (from 32°N-42°N and 70°W-30°W, not shown) reveals that a slight decrease in temperature occurs due to decreased advection ($\sim$ 4 Wm^{-2}) for the cooling transition. This is a result of decreased heat advection from the south ($\mathcal{O}$(30 Wm^{-2})) almost countered by decreased heat advection across the northern face. No significant changes in surface fluxes or diffusion occur. In the SPG (from 50°N-60°N and 50°W-10°W, not shown) the heat advection from the south changes by more than 50 Wm^{-2}. This suggest an anomalous heat convergence during the NA cold phase between 42°N and 50°N, corresponding exactly to the aforementioned warm anomaly at the intergyre boundary. The intergyre boundary is associated with the zero-wind-stress curl line, the change from westerlies at the latitudes of the SPG, driving southward Ekman transport, to easterlies at the latitudes of the STG, driving northward Ekman transport. The intergyre boundary is, as a result of the Ekman convergence, associated with downwelling. The warm anomaly that builds up at the intergyre boundary is consequently brought to mid-depth (Fig. 4.1, about 700 to 1500 m).
From here the subsurface warm anomaly propagates first with the gyre circulation and later along the western boundary (Fig. 4.2, taken from Rheinlaender (2015)):
Around year 350, approximately 40 years after the onset of NA_c1, the first indication of subsurface warming becomes visible at around 40°N (Fig. 4.2). In the following decades the subsurface (1000 m) warm anomaly spreads with the anticyclonic circulation of the STG. The anomaly propagates first to the east, where a part of the warm anomaly spreads northward, following the eastern boundary current of the SPG with consequences for the increased deep water convection south of Iceland (cf. Fig. 2.11 and corresponding text). The remaining part propagates first southward, then eastward, reaching the western boundary at around year 400. During this period the subsurface warm anomaly continuously strengthens and reaches its maximum ($\sim$ 2°C) at the western boundary in the NA mid-latitudes ($\sim$ 20°N). The lag correlation between subsurface temperatures at 40°N and 20°N is maximal for a 20°N-lag of approximately 20 years, consistent with gyre recirculation time scales (Rheinlaender, 2015).
From here the subsurface anomaly propagates in a confined band along the western boundary (Fig. 4.2). The propagation from here progresses distinctly faster and the subsurface warm anomaly reaches the equator around year 420 and the subtropical South Atlantic (20°S) around year 430. Within one further decade it propagates until 40°S,

the southern boundary of the South Atlantic STG, from where the subsurface anomaly upwells, resulting in surface warming here (Fig. 2.3 and 4.1). Farther southward propagation is inhibited by the ACC. This is likely a consequence of the ACC acting as a dynamical barrier against meridional flow, owed to its strong baroclinicity (e.g., Ferrari and Nikurashin (2010); Marshall et al. (2006)). However, the amplitude of the subsurface warm anomaly has also reduced by about 70 % with respect to the $2°C$ anomaly in the mid-latitude NA (Rheinlaender, 2015). We thus cannot exclude the possibility that the absence of farther temperature propagation is simply due to the small amplitude.

These findings are different from Schmittner et al. (2003)'s results, who analyse interhemispheric coupling in response to fresh water hosing and resulting AMOC changes. Schmittner et al. (2003) suggests a fast propagation of the subsurface warm anomalies in the southern and northern Atlantic by coastal and equatorial Kelvin waves and propagation into the interior by Rossby waves, following the ideas of Kawase (1987) and Johnson and Marshall (2002). The long time lag of approximately 500 years between Antarctic temperature and Greenland temperature in Schmittner et al. (2003)'s study is a consequence of the slow propagation southward of $40°S$, across the latitudes of the ACC. The absence of meridional boundaries along these latitudes rules out a fast propagation by coastal waves. The warm subsurface anomaly at $40°S$ in Schmittner et al. (2003)'s study has an amplitude of $\sim 5°C$ and is by a factor of 10 stronger than the warm anomaly at $40°S$ in CONT. Furthermore, the authors note that a weakening of the ACC due to diminished meridional density gradients occurs when the NA cools, which facilitates the temperature propagation across the ACC. In contrast in CONT a relative long time lag is already introduced by the propagation in the NA. The differences in CONT and Schmittner et al. (2003)'s study could be linked to the different mechanisms involved. In CONT the major contribution to temperature anomalies is attributed to horizontal circulation adjustments (i.e., the gyre circulation), with heat convergence at the SPG-STG intergyre boundary.

4.2 Atmospheric pathways

In the introduction we summarized a recently proposed atmosphere-surface ocean interhemispheric coupling process, resulting in enhanced Southern Ocean upwelling, when Greenland cools (Chiang et al., 2014; Lee et al., 2011). Similar to the arguments presented in the previous Chapter (Sec. 3.4.1), this mechanism is hampered in CONT due to a negligible southward migration of the Atlantic ITCZ. We briefly summarize the differences between CONT and Lee et al. (2011)'s study.

Following the idea of a tropical trigger for the NA climate transitions we explore in the second part a connection between the tropical Modoki mode and SH atmospheric circulation anomalies.

4.2.1 Atlantic ITCZ shifts - an atmospheric pathway

Lee et al. (2011); Chiang et al. (2014) show that NA cooling results in strengthened westerlies in the SH. This is the result of a southward migration of the Atlantic ITCZ, resulting in a weakened subtropical jet in the Pacific that causes in turn an intensification of the eddy-driven SH mid-latitude westerlies. The strengthened westerlies lead to enhanced northward Ekman transport, which is compensated by enhanced upwelling from depth (Toggweiler and Samuels, 1998). Lee et al. (2011) further applied the wind stress anomalies to an EMIC, including an interactive marine biogeochemistry component. The enhanced upwelling results in a significant increase of atmospheric CO_2 of 20 and 60 ppmv, including and excluding the marine biological response, respectively.

A minor southward shift in the tropical Atlantic precipitation occurs during NA cold phases in CONT (see previous Chapter Fig. 3.18). However, the changes are significantly smaller compared to the changes in Lee et al. (2011)'s study. Lee et al. (2011) find an increase of the westerlies of 25 % and positive (negative) precipitation anomalies of up to 16 $mm\ day^{-1}$ southward (northward) of the initial location of the Atlantic ITCZ. The Atlantic precipitation anomalies in CONT in association with the minor southward migration of the ITCZ are of the order of 0.1 $mm\ day^{-1}$ and associated wind-stress changes are also weak. The slight increase in westerlies (see next section Fig. 4.4, lower) might however contribute to enhanced upwelling at the southern boundary of the South Atlantic STG, and add to the upwelling of the aforementioned subsurface warm anomaly. The minor changes in the location of the Atlantic ITCZ are likely a result of regionally confined cooling in CONT, compared to Lee et al. (2011)'s and Chiang et al. (2014)'s study.

4.2.2 A tropical connection

The Modoki mode is associated with a distinct dipole pattern of SLP anomalies above the Southern Ocean (Fig. 4.3). Phases with a predominant displacement of El Niños to the eastern Pacific (NA cold phases) are associated with increased SLP above the Drake Passage and parts of the Weddell Sea and decreased SLP over the Ross Sea. The correlation between 10 year low pass filtered SLP anomalies over the Weddell Sea and precipitation anomalies in the WPWP (associated with the Modoki mode) is -0.68 (Rheinlaender,

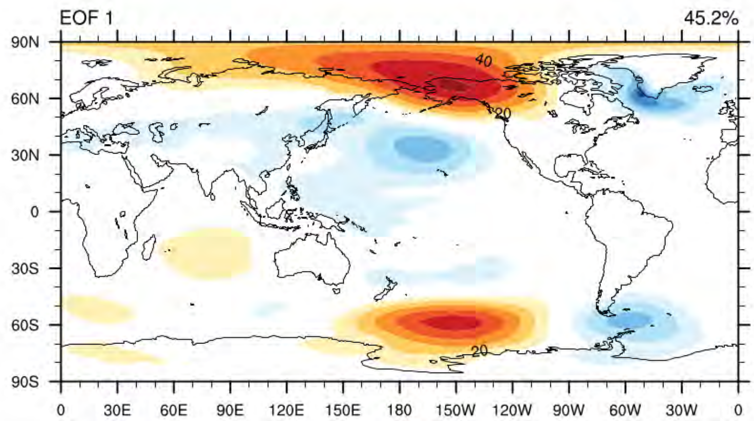

Figure 4.3.: SLP anomalies $[Pa \cdot std^{-1}]$ associated with SST anomalies of the Modoki mode (see Chapter 3). The sign of the SLP anomalies corresponds to NA warm phases.

2015). This pattern of SLP anomalies resembles the Antarctic Dipole pattern (ADP), which describes an out-of-phase relationship of SLP, temperature and sea ice anomalies between the Bellinghausen Sea and the Ross Sea (Pacific sector) and the Weddell Sea (Atlantic sector) (e.g., Yuan (2004)). Liu et al. (2002) suggest that the ADP represents the strongest extra-tropical anomalies varying in association with ENSO. Warm ENSO events cause an out-of-phase behaviour of the Atlantic and Pacific Hadley Cells, resulting in weakening of the former and strengthening of the latter (Rind et al., 2001). This in turn reduces the strength of the Pacific Ferrel Cell and a weakens the Atlantic Ferrel Cell. The resulting poleward heat transport anomalies cause decreased temperatures in the Atlantic and increased temperatures in the Pacific (Liu et al., 2002). Additionally, a warm ENSO event can trigger a stationary Rossby wave train, resulting in SLP anomalies in phase with the ones resulting from the meridional mean flow changes and thus amplify the ADP anomalies (Yuan, 2004). The ADP pattern in SLP anomalies is consistent with temperature anomalies, minor changes in zonal wind stress (Fig. 4.4) and minor changes in sea ice concentration (not shown).

During NA warm phases the wind-stress shows an anomalous cyclonic circulation centered over the Weddell Sea. The resulting onshore winds in the Weddell Sea cause negative temperature anomalies in response to advection of cold air from the Antarctic continent. The strongest increase in zonal wind-stress occurs in the eastern Pacific and the Drake passage ($\sim$ 10 % relative to the cold state, Rheinlaender (2015)). In the remaining Southern Ocean the wind stress changes are negligible.

In the NA the changes in SLP initiated a positive feedback loop, resulting in persistent and high amplitude changes. Previous studies showed that a cyclonic wind field helps to intensify and maintain open ocean polynyas (Timmermann et al., 1999). Timmermann

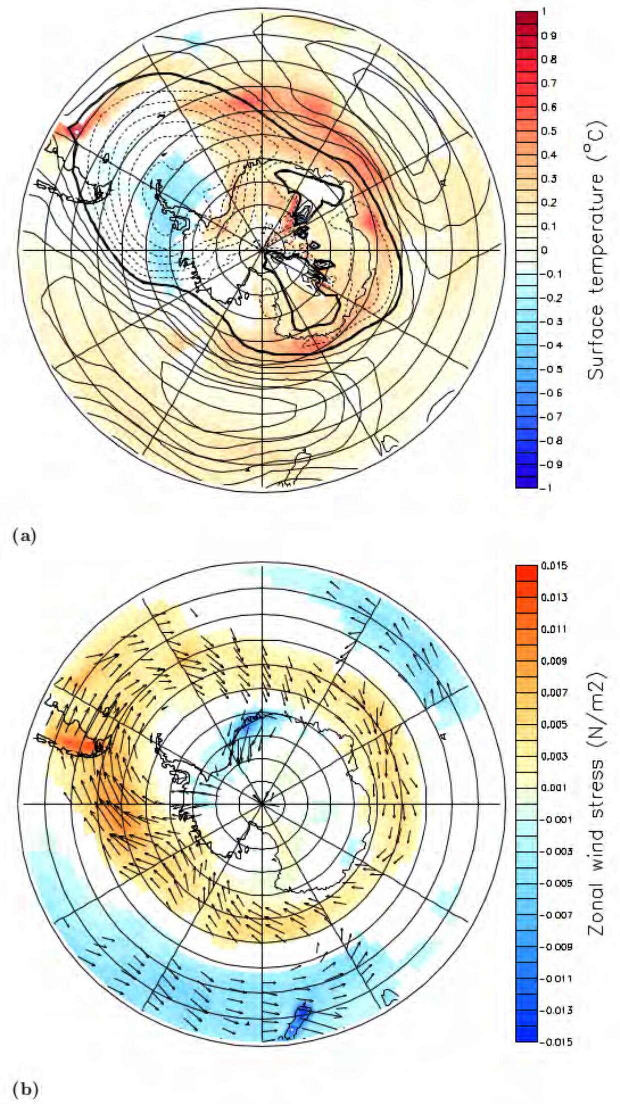

Figure 4.4.: From (Rheinlaender, 2015): (a) Surface temperature anomalies (shading; $^{\circ}C$) and SLP (contours; hPa) anomalies for the second warm phase (year 600-650) relative to the first NA cold phase (year 400-550). Contour lines are plotted in intervals of 0.1 hPa. (b) Zonal wind stress anomalies (shading; Nm^{-2}) for the same period as in (a). Vectors [Nm^{-2}] represents both zonal and meridional wind stress anomalies. Wind stress vectors are only plotted if anomalies are larger than $3 \cdot 10^{-3}$ Nm^{-2}. Changes are only plotted if they are significant on 95 % level, based on a t-test.

et al. (1999) suggest that positive feedback mechanisms between sea ice - atmosphere and the ocean mixed layer helped to maintain the Weddell Sea polynya during 1974 to 1976. An upward heat flux from an existing polynya creates local warming resulting in a low pressure system. This supports the evolution of a polynya by inducing a divergent ice drift and enhanced upwelling, due to Ekman pumping (Timmermann et al., 1999; Lemke, 1987).

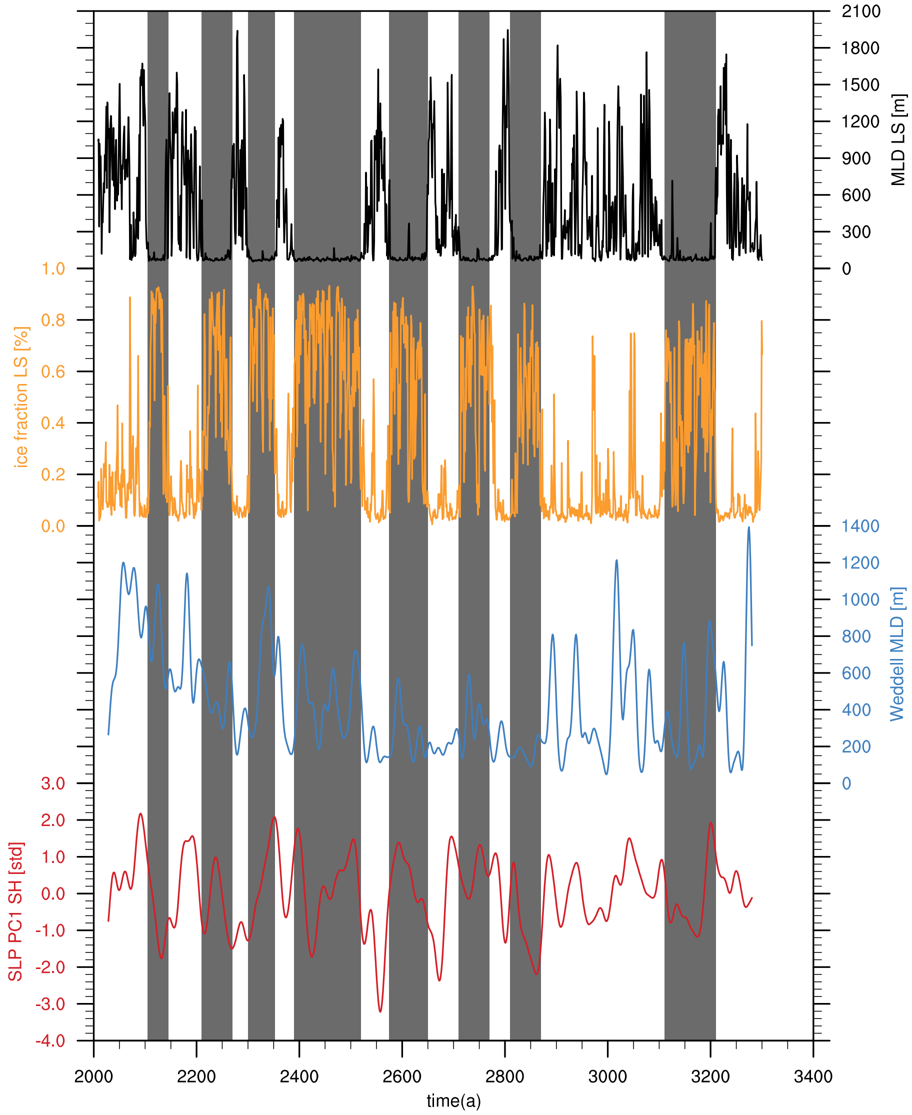

Figure 4.5.: Mixed layer depth [*m*] in the LS (black), sea ice concentration in the LS (yellow), Mixed layer depth in the Weddell Sea [*m*] (blue), smoothed by a 20 year running mean and PC 1 of 20 year LP filtered southern Hemisphere SLP anomalies [*std*] (red). The grey vertical bars indicate phases of LS deep convection cessation (corresponding to event 1-8 from left to right) and are associated with increased Weddell Sea convection for event number 1, 3, 4, 5, 6, 8 and the last event at the end of the simulation. Whereas during phases of active LS deep water formation (white areas), Weddell Sea deep water formation ceases for event 3, 4, 5, 6, 7 and 9. The period between year 2875 and 3100 is characterised by variable deep water formation in both hemispheres. Note that these are results from the FESOM model.

The cyclonic SLP anomaly over the Weddell Sea during warm NA phases could thus favour the formation of a polynya and open ocean deep water formation in the SH. This potentially provides a positive feedback mechanism, that could lend persistence to SH climate changes.

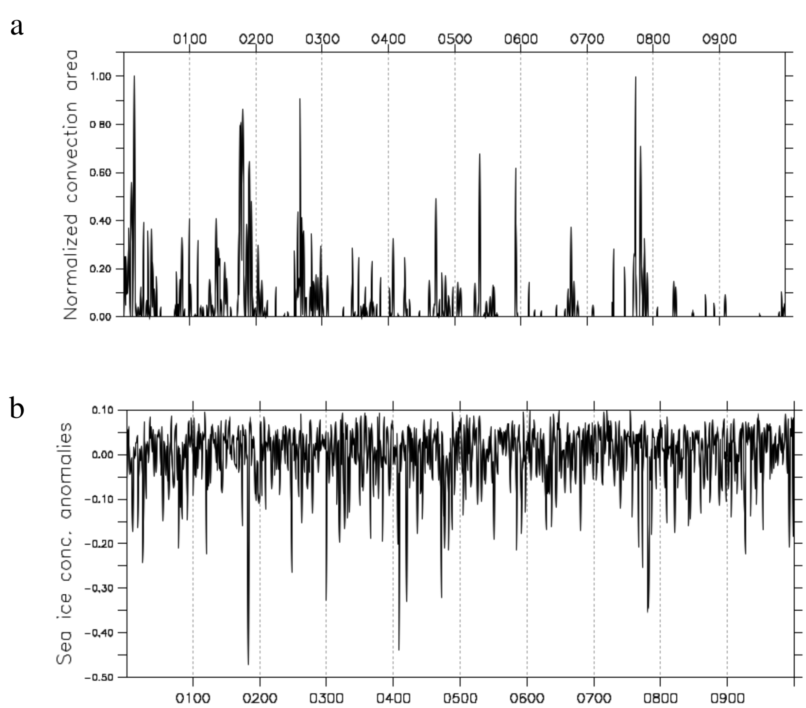

Figure 4.6.: From Rheinlaender (2015): (a) Normalized convective area for significant deep ($\geq$ 2000 m) convection in the Weddell Sea area. For each event the convective area is normalized by the maximum areal extent recorded in the entire simulation. (b) Maximum sea ice concentration anomalies in the Weddell Sea convection region.

However, no consistent changes in Weddell Sea deep water convection or sea ice anomalies occur in association with the NA warm and cold phases in CONT (Fig. 4.6). The reason for this can be manifold, since formation and maintenance of open ocean polynyas and associated deep water formation require also preconditioning of the ocean, as for example a sufficiently weak stratification. Advection of sea ice into the polynya and the subsequent melting can quickly produce a freshwater capping and hence stabilize the water column again. However, we did not investigate this scenario for SH climate changes further, but this is an interesting aspect for future research. In particular, since results from a simulation of the FESOM model (Sidorenko et al., 2014) indicate that such a relation between SLP and Weddell Sea deep water formation exists and that this changes might be linked to NA cooling events that have the same characteristics as in CONT (Fig.

4.5).

4.3 Southern Hemisphere response to increased CO_2

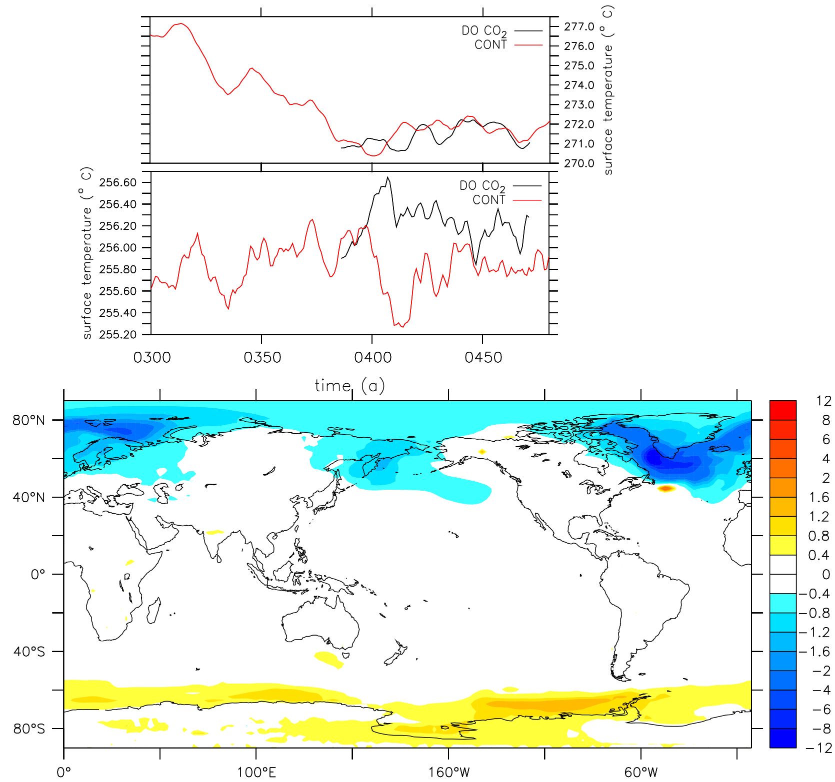

Figure 4.7.: Upper panel: Surface air temperature [$°C$] over the SPG (averaged from 60°W - 20°W and 55°N - 65°N) for CONT (red) and DO_CO_2 (black). The time series are smoothed by a 10 year running mean. Middle panel: as in the upper panel but, for the region of strongest warming response in DO_CO_2 in the southern Ocean (averaged from 100°E - 130°E and 70°S - 60°S). Lower panel: Surface air temperature anomaly [$°C$] between year 20-96 of DO_CO_2 and the second warm NA phase (year 670-720) in CONT.

In CONT solar insolation and atmospheric CO_2 concentration are constant at pre-industrial levels. However, a characteristic of D-O cycles is an increase of atmospheric CO_2 levels during GSs of 5 to 20 ppmv (e.g. Bereiter et al. (2012)). CO_2 variations associated with millennial scale climate variability during the last glacial are characterized by

a gradual increase of CO_2 in phase with AIM events. Bereiter et al. (2012) suggest a lag of the peak in atmospheric CO_2 behind D-O events (Greenland warming) of 250 ±190 years during MIS 5 and a significant longer (~ 800 *years*) lag during MIS 3. Several processes have been proposed to contribute to the millennial scale CO_2 variations. Amongst others these are dominant El Niño-like conditions (Stott et al., 2002), terrestrial and marine biosphere processes (Menviel et al., 2008) and increased Southern Ocean upwelling.
Sediment cores from the Southern Ocean show enhanced opal burial over the Younger Dryas and Heinrich event 1, indicating enhanced Southern Ocean upwelling (Anderson et al., 2009). The results of Lee et al. (2011) suggest further that NA cooling and the consequent southward migration of the ITCZ strengthen the SH mid-latitude westerlies and can result in enhanced Southern Ocean upwelling. We analysed above, why this mechanism is not present in CONT. Here we assess instead the SH temperature response to increased atmospheric CO_2. We performed an other branch experiment with increased atmospheric CO_2. The experiment DO_CO_2 is branched from initial conditions of simulation year 381 of CONT (corresponding to NA_c1). The only difference to CONT is the atmospheric CO_2 concentration that is increased by 20 ppmv to 300 ppmv.

The surface temperature difference between DO_CO_2 and the second NA warm phase reveals a distinctly clearer warming signal in the southern high latitudes (Fig. 4.7, lower panel). The maximum warming response (Fig. 4.7, middle panel) to the increased atmospheric CO_2 contributes with about $0.5°C$ to the SH warming signal in Fig. 4.7, lower panel. The maximum cooling in the NH during NA cold phases occurs over the SPG. The increased CO_2 concentration does not significantly effect the temperature evolution here (Fig. 4.7, upper panel). However, in the remaining NH the response to increased CO_2 resembles the pattern of polar amplification under global warming scenarios and surface temperatures warm, relative to the NA cold phase, by a maximum of $2°C$ along the Aleutian Arc (not shown). Together with surface temperature anomalies induced by increased atmospheric CO_2 the SH response to the NA cold phases is more consistent with reconstructions. However, we note that (a) the warming is still less than the reconstructed $1°C$ to $3°C$ (e.g., WAIS Divide Project Members et al. (2015)), in particular over land, where the maximum warm anomaly lies between $0.4°C$ and $0.8°C$ and (b) an increase of atmospheric CO_2 by 20 ppmv represents an upper limit.

4.4 Summary & Discussion

In this section we explored why a strong interhemispheric coupling is absent in CONT. We showed further that increased CO_2, as observed for GSs, amplifies the small warming of the SH during NA cold phases. We note however that an additional process is necessary for a realistic SH response. A significant correlation between the tropical Modoki mode and SLP anomalies over the Ross and Weddell Sea exist. In contrast to the NA, the SLP anomalies do not trigger ocean circulation changes that could amplify or lengthen SH climate changes. We speculate that such a positive feedback could be provided by changes in Weddell Sea deep water formation. Martin et al. (2014) show that an increase in the extent of AABW (caused by centennial scale variations in Weddell Sea deep water formation) strongly influences the AMOC and contraction and expansion of the NA SPG. We speculate further that this mechanism together with the tropical and NA climate changes in CONT could provide an important mechanism to amplify and lengthen the NA warm and cold phases.

Bibliography

Ahn, J., and E. J. Brook, 2014: Siple Dome ice reveals two modes of millennial CO2 change during the last ice age. *Nature communications*, **5**.

Anderson, R., S. Ali, L. Bradtmiller, S. Nielsen, M. Fleisher, B. Anderson, and L. Burckle, 2009: Wind-driven upwelling in the Southern Ocean and the deglacial rise in atmospheric CO2. *Science*, **323 (5920)**, 1443–1448.

Barbante, C., and Coauthors, 2006: One-to-one coupling of glacial climate variability in Greenland and Antarctica. *Nature*, **444 (7116)**, 195–198.

Bereiter, B., D. Lüthi, M. Siegrist, S. Schüpbach, T. F. Stocker, and H. Fischer, 2012: Mode change of millennial CO2 variability during the last glacial cycle associated with a bipolar marine carbon seesaw. *Proceedings of the National Academy of Sciences*, **109 (25)**, 9755–9760.

Blunier, T., and E. J. Brook, 2001: Timing of millennial-scale climate change in Antarctica and Greenland during the last glacial period. *Science*, **291 (5501)**, 109–112.

Böhm, E., and Coauthors, 2015: Strong and deep Atlantic meridional overturning circulation during the last glacial cycle. *Nature*, **517 (7532)**, 73–76.

Chiang, J. C., S.-Y. Lee, A. E. Putnam, and X. Wang, 2014: South Pacific Split Jet, ITCZ shifts, and atmospheric North–South linkages during abrupt climate changes of the last glacial period. *Earth and Planetary Science Letters*, **406**, 233–246.

Crowley, T. J., 1992: North Atlantic deep water cools the southern hemisphere. *Paleoceanography*, **7 (4)**, 489–497.

Ferrari, R., and M. Nikurashin, 2010: Suppression of eddy diffusivity across jets in the Southern Ocean. *Journal of Physical Oceanography*, **40 (7)**, 1501–1519.

Gottschalk, J., L. C. Skinner, S. Misra, C. Waelbroeck, L. Menviel, and A. Timmermann, 2015: Abrupt changes in the southern extent of North Atlantic Deep Water during Dansgaard-Oeschger events. *Nature Geoscience*.

Johnson, H. L., and D. P. Marshall, 2002: A theory for the surface Atlantic response to thermohaline variability. *Journal of Physical Oceanography*, **32 (4)**, 1121–1132.

Kageyama, M., and Coauthors, 2013: Climatic impacts of fresh water hosing under Last Glacial Maximum conditions: a multi-model study. *Climate of the Past*, **9 (2)**, 935–953.

Kawase, M., 1987: Establishment of deep ocean circulation driven by deep-water production. *Journal of Physical Oceanography*, **17 (12)**, 2294–2317.

Kissel, C., C. Laj, A. M. Piotrowski, S. L. Goldstein, and S. R. Hemming, 2008: Millennial-scale propagation of Atlantic deep waters to the glacial Southern Ocean. *Paleoceanography*, **23 (2)**.

Lee, S.-Y., J. C. Chiang, K. Matsumoto, and K. S. Tokos, 2011: Southern Ocean wind response to North Atlantic cooling and the rise in atmospheric CO2: Modeling perspective and paleoceanographic implications. *Paleoceanography*, **26 (1)**.

Lemke, P., 1987: A coupled one-dimensional sea ice-ocean model. *Journal of Geophysical Research: Oceans (1978–2012)*, **92 (C12)**, 13 164–13 172.

Liu, J., X. Yuan, D. Rind, and D. G. Martinson, 2002: Mechanism study of the ENSO and southern high latitude climate teleconnections. *Geophysical Research Letters*, **29 (14)**, 24–1.

Lynch-Stieglitz, J., M. W. Schmidt, L. G. Henry, W. B. Curry, L. C. Skinner, S. Mulitza, R. Zhang, and P. Chang, 2014: Muted change in Atlantic overturning circulation over some glacial-aged Heinrich events. *Nature Geoscience*, **7 (2)**, 144–150.

Marshall, J., E. Shuckburgh, H. Jones, and C. Hill, 2006: Estimates and implications of surface eddy diffusivity in the Southern Ocean derived from tracer transport. *Journal of physical oceanography*, **36 (9)**, 1806–1821.

Martin, T., W. Park, and M. Latif, 2014: Southern Ocean forcing of the North Atlantic at multi-centennial time scales in the Kiel Climate Model. *Deep-Sea Res. II*, doi:10.1016/j.dsr2.2014.01.018.

Menviel, L., A. Timmermann, A. Mouchet, and O. Timm, 2008: Meridional reorganizations of marine and terrestrial productivity during Heinrich events. *Paleoceanography*, **23 (1)**.

Rheinlaender, J., 2015: Interhemispheric climate variability in a pre-industrial control simulation of CCSM4. M.S. thesis, University of Copenhagen, Niels Bohr Institute, Danmark.

Rind, D., M. Chandler, J. Lerner, D. Martinson, and X. Yuan, 2001: Climate response to basin-specific changes in latitudinal temperature gradients and implications for sea ice variability. *Journal of Geophysical Research: Atmospheres (1984–2012)*, **106 (D17)**, 20 161–20 173.

Schmittner, A., O. Saenko, and A. J. Weaver, 2003: Coupling of the hemispheres in observations and simulations of glacial climate change. *Quaternary Science Reviews*, **22 (5)**, 659–671.

Sidorenko, D., and Coauthors, 2014: Towards multi-resolution global climate modeling with ECHAM6-FESOM. Part I: Model formulation and mean climate. *Clim. Dynam.*

Stocker, T. F., and S. J. Johnsen, 2003: A minimum thermodynamic model for the bipolar seesaw. *Paleoceanography*, **18 (4)**.

Stott, L., C. Poulsen, S. Lund, and R. Thunell, 2002: Super ENSO and global climate oscillations at millennial time scales. *Science*, **297 (5579)**, 222–226, doi:10.1126/science.1071627.

Timmermann, R., P. Lemke, and C. Kottmeier, 1999: Formation and maintenance of a polynya in the Weddell Sea. *Journal of physical oceanography*, **29 (6)**, 1251–1264.

Toggweiler, J., and B. Samuels, 1998: On the ocean's large-scale circulation near the limit of no vertical mixing. *Journal of Physical Oceanography*, **28 (9)**, 1832–1852.

WAIS Divide Project Members, and Coauthors, 2015: Precise interpolar phasing of abrupt climate change during the last ice age. *Nature*, **520 (7549)**, 661–665.

Wunsch, C., 2006: Abrupt climate change: An alternative view. *Quat. Res.*, **65 (2)**, 191–203, doi:10.1016/j.yqres.2005.10.006.

Yuan, X., 2004: ENSO-related impacts on Antarctic sea ice: a synthesis of phenomenon and mechanisms. *Antarctic Science*, **16 (04)**, 415–425.

5 Ocean circulation and snow accumulation changes under different orbital conditions

Milankovitch (1941) hypothesized that decreased summer insolation at high northern latitudes, caused by variations in precession, obliquity and eccentricity, allow for snow cover to persist throughout the summer. The only positive feedback necessary to cause ice sheet growth and subsequently a glaciation is the snow-albedo feedback. Even though this theory is widely accepted, there are still several challenges to it. These are amongst others the Mid-Pleistocene transition - the change from 100 kyr to 41 kyr cycles of ice ages (e.g. Mudelsee and Schulz (1997)) - and the "100 kyr problem" (e.g., Imbrie et al. (1993)), or the strong correlation between atmospheric CO_2 and Antarctic temperature evolution (Petit et al., 1999). Several possible players of the global coupled climate system have been suggested to contribute to the observed pacing of ice ages (e.g., CO_2 variations from volcanoes and mid ocean ridges (Huybers and Langmuir, 2009), or sea ice switches Gildor and Tziperman (2000)). It is beyond the scope of this study to explore all of the proposed mechanisms and the few examples given above are only meant to highlight the fact that there are still outstanding issues in the understanding of ice ages.

In the Chapter 2 we have demonstrated that the NA SPG is very sensitive to small perturbations in CCSM4. The NA SPG manifests itself in two different modes which can both occur under the same boundary conditions: a weak circulation mode, associated with colder temperatures, no deep convection and extensive sea ice cover in the LS and a strong circulation mode, associated with warmer temperatures and active deep water convection. For CONT we demonstrated that SLP anomalies and associated wind stress curl changes can trigger the initial weakening of the SPG. However, in case of a bistable system (see discussion in Sec. 2.4.3), there exist various other possible triggers which can cause a transition between the two states. Motivated by these results we investigate in this chapter whether (a) the dynamics in ocean circulation changes are comparable to orbital induced changes and (b) NA cooling can alter snow accumulation and possibly favour a glacial inception.

In the following we show that it is possible to trigger comparable changes in ocean cir-

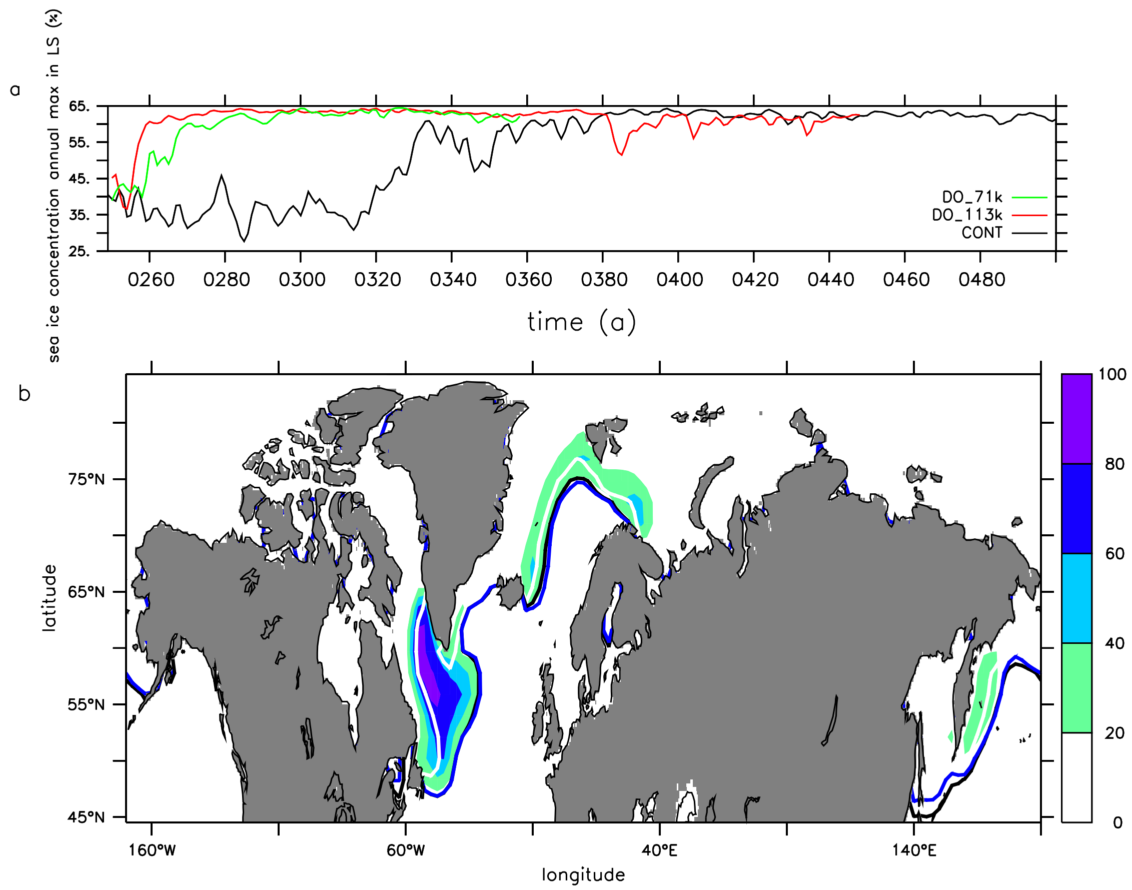

Figure 5.1.: (a) Annual maximum sea ice concentration [%] in the LS (averaged from 65° W- 45° W and 50° N- 70° N) for CONT (black), for DO_71k (green) and DO_113k (red). All time series are smoothed by a 2-year running mean. (b) Difference in annual maximum sea ice concentration between NA_w1 (CONT) and DO_113k. Overlaying contours show the averaged annual maximum sea ice extent (15%) for NA_c1 (black) and NA_w1 (white) and DO_113k (blue).

culation, LS sea ice cover and Greenland temperature by changing the summer solstice insolation in the NH with the orbital conditions from 113 *kyrs* BC and 71 *kyrs* BC. Furthermore, we show in the second part of this section (Sec. 5.3) that changes in net snow accumulation between NA_w1 and NA_c1 are comparable, in magnitude and location, to those resulting from changed orbital conditions. The presented results suggest that stochastic climate fluctuations - through the mechanism presented in Sec. 2 - have the potential to contribute to the onset of glaciations.

The section is structured as follows. The experimental set-up and the effects of changed orbital conditions are presented in Section 5.1. Section 5.2 comprises the description

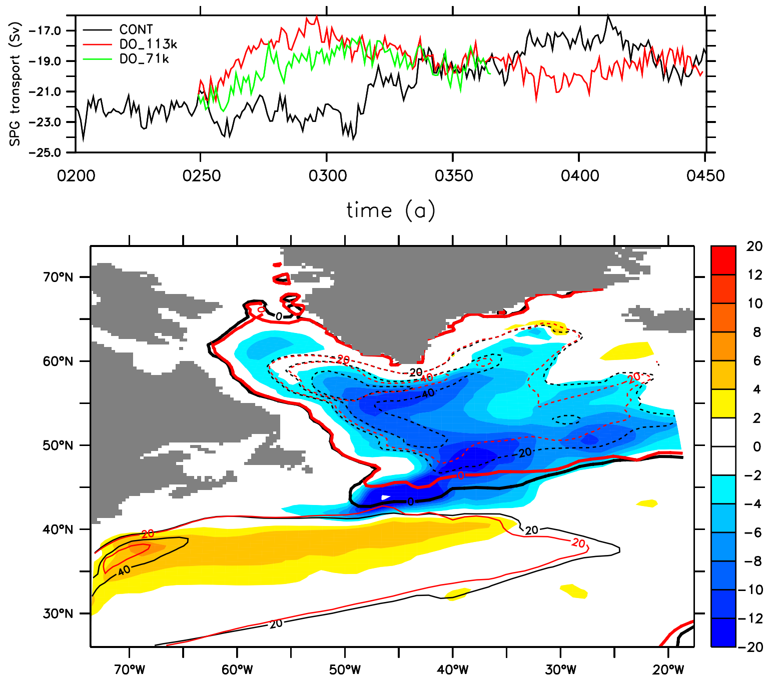

Figure 5.2.: Upper panel: Barotropic stream function [Sv] averaged over the SPG (from about $50°N$-$63°N$ and $60°W$-$26°W$) for DO_113k (red), DO_71k (green) and CONT (black). Lower panel: Barotropic stream function anomaly [Sv] in the SPG, difference between NA_w1 (year 50 to 250) and DO_113k (full length). Contours show the mean for NA_w1 (black) and for DO_113k (red). The contour interval is 20 Sv between -40 and 40, additionally the -50 Sv-contour is shown. Solid contours show anticyclonic and dashed contours cyclonic circulation.

of ocean and atmosphere circulation changes induced by the different orbital conditions. Lastly snow accumulation changes in CONT are compared to those resulting from changed orbital conditions (Section 5.3).

5.1 Experimental set-up of simulations under changed orbital conditions

Two experiments with orbital conditions corresponding to 113 kyrs BC (DO_113k) and 71 kyrs BC (DO_71k) were performed. Both experiments are branched (see Sec. 2.2) from initial conditions of simulation year 249 from CONT and integrated for 201 and 117

years, respectively.
The orbital conditions of 113 kyrs BC are chosen because they correspond to an extreme minimum in summer solstice insolation at 65°N of about 441 Wm^{-2}. Insolation at high latitudes is decreased in particular during spring and early summer and increased in fall. Overall (annual) insolation is reduced at high latitudes and slightly increased in the tropics during this period (see Fig. 1 in Jochum et al. (2010)). The reduced NH summer insolation is a consequence of obliquity and precession being at a minimum, while eccentricity is at its maximum. Based on Milankovitch (1941) these are favourable conditions for a glaciation. Observations show further that the last glacial inception occurred around 113 kyrs BC (e.g., Andrews and Mahaffy (1976) and Capron et al. (2010)). The orbital conditions from 113 kyrs BC cause a reduced summer solstice insolation at 65°N of ~ 38 Wm^{-2} with respect to present day.
The orbital conditions from 71 kyrs BC are associated with a summer solstice insolation at 65°N of 457 Wm^{-2} - a reduction of 22 Wm^{-2} - compared to present day. The onset of MIS 4 and a secondary increase of ice sheets date around this time (e.g., Mix (1992)). We focus in this section on the difference between DO_113k and CONT, the changes are however similar for DO_71k.

5.2 Changes in DO_113k compared to CONT

In DO_113k, the switch between the weak and the strong circulation mode of the SPG is triggered by a fast increase in LS sea ice associated with the insolation induced cooling. Under present day conditions strong ocean-atmosphere heat fluxes remove buoyancy in the LS, forming very dense water at the surface and thus leading to deep water convection. The sea ice increase in DO_113k (Fig. 5.1) insulates the LS from atmospheric forcing. Without the strong ocean-atmosphere heat fluxes during winter (the reduction in ocean-atmosphere heat flux due to sea ice cover during NA_c1 in CONT accounted for ~ 60 Wm^{-2}) buoyancy removal is not sufficient and LS deep water convection shuts down (Fig. 5.3). Minor compensation of deep water formation occurs in a small area south of Iceland. South of Iceland, the sea ice concentration does not increase and the solar insolation induced surface cooling destabilizes the water column and causes an increase in MLD by 50 to 200 m, similar to the changes between NA_w1 and NA_c1 in CONT. Additionally, a northward shift of the Gulf stream path (Fig. 5.2, lower) promotes subsurface warming (not shown) and contributes further to a destabilisation of the water column south of Iceland (see as well Jochum et al. (2012) and Fig. 2.9).

The shut down of LS deep water convection reduces the SPG circulation strength and

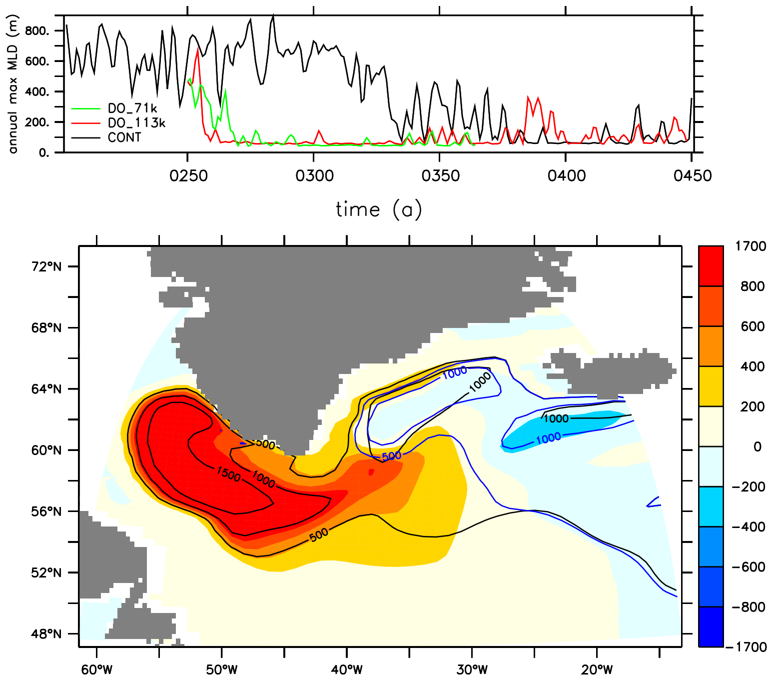

Figure 5.3.: Upper panel: annual maximum MLD in the LS (averaged from 55°N-65°N and 60°W-45°W) for CONT (black), DO_71k (green) and DO_113k (red). A 2-year running mean is applied to all time series. Lower panel: annual maximum MLD [m] anomaly between NA_w1 and DO_113k. Black contours show NA_w1 mean and blue contours the mean over DO_113k. The spacing between contours is 500 m.

causes a contraction of the SPG (Fig. 5.2). The average SPG strength reduces over the first 50 years after branching to a minimum of about -16 Sv and increases over the next 100 years to about -19 to -20 Sv, resulting in a mean SPG strength which is about 3 Sv weaker than during NA_w1. In the center of the SPG, the circulation strength is reduced by up to 10 Sv. The largest changes occur at the southern edge of the SPG (cf. black and red 0-contour in Fig. 5.2, lower panel), associated with the northward shift of the Gulf stream and the SPG contraction.
The maximum AMOC weakens as a consequence of the decreased deep water formation in the LS by about 4 Sv to a minimum of 21 Sv after about 50 years and recovers in the subsequent 100 years to about 24.5 Sv (Fig. 5.5).

The stability of the AMOC is most likely (as in CONT) a consequence of (a) no changes a b

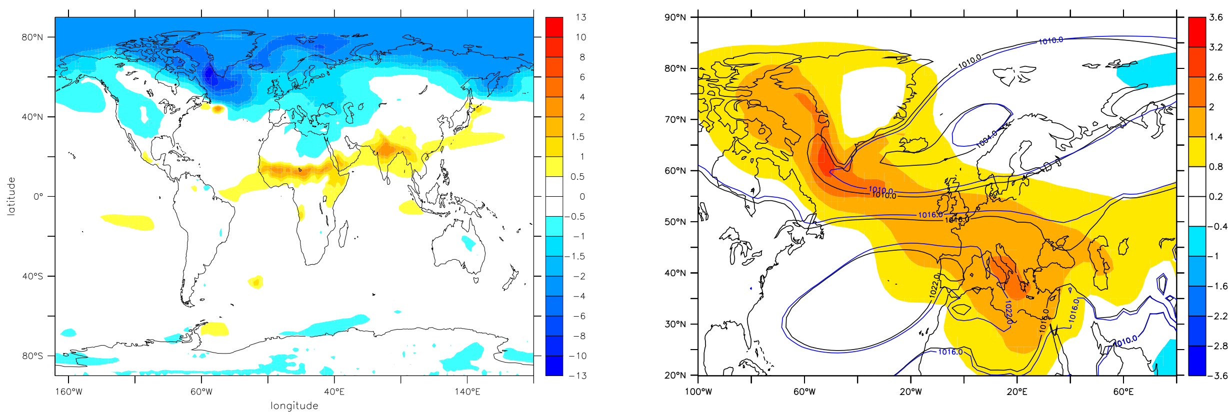

Figure 5.4.: (a) Surface temperature difference [°C] between years 50 and 250 (NA_w1) and DO_113k. (b) Sea level pressure anomaly [hPa] between NA_w1 and DO_113k. Black contours show the 1000-year mean of SLP in CONT and blue contours the 200-year mean of DO_113k.

in deep water formation in the Nordic Seas and (b) the minor compensation of deep water formation south of Iceland. Contrary to the AMOC, the SPG circulation strength does not recover completely (at least not during the 200 years of the simulation). The maximum circulation in the SPG region reduces to about -50 Sv in DO_113k within 15 to 20 years and stays constant thereafter. The maximum circulation during NA_w1 in CONT is about -56 Sv.

The different behaviour of AMOC and SPG strength can be explained by the identified positive feedbacks on the SPG circulation (Chapter 2). The first feedback is the atmospheric feedback due to the sea ice anomalies in the LS region and consists of a “cold-core high”, with increased SLP by up to 3.6 hPa (Fig. 5.4 (b), compared to 2.8 hPa in CONT). The SLP maximum occurs above the location of maximum sea ice concentration changes and then spreads with the west-ward drift far across the Eurasian continent. The anomaly spreads farther south than in CONT, most likely due to changed mean wind fields under the different orbital conditions. Associated with this change in SLP is a reduced wind stress curl forcing (not shown) of the SPG (cf. Fig. 2.5 and corresponding text). The second feedback is related to the deep convection cessation and its effect for the gyre circulation. The deep convection in the LS does not resume in DO_113k thus continuing to contribute to reduced horizontal density gradients and hence the density driven weakening of the SPG rim current.

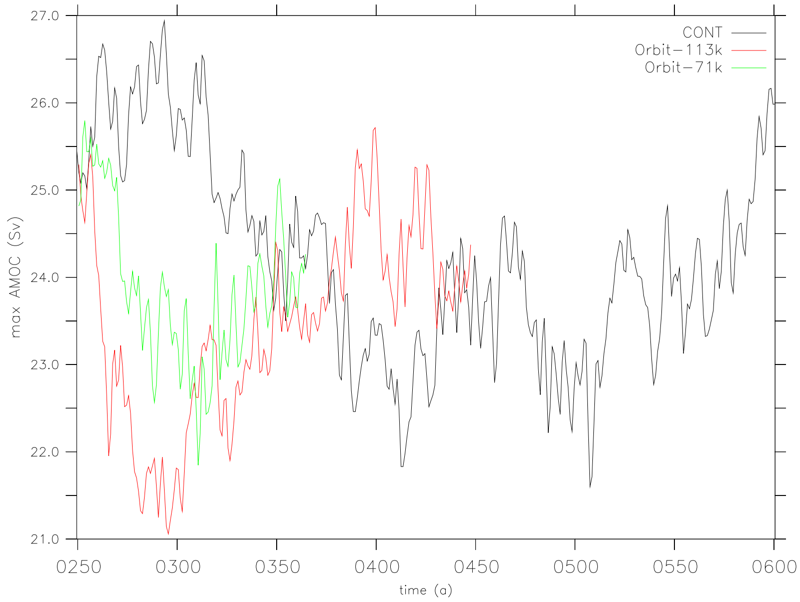

Figure 5.5.: Maximum AMOC [Sv] for CONT (black), for DO_71k (green) and for DO_113k (red).

A consequence of the reduced insolation is a stronger atmospheric surface temperature decrease than in CONT, with a relative uniform cooling of $\sim 3°C$ north of $60°N$ and $\sim 4°C$ north of $80°N$ (Fig.5.4 (a)). Strongest cooling occurs over the LS - the area of maximum sea ice changes (Fig. 5.1)- with an amplitude of 12 $°C$, identical to the changes between NA_c1 and NA_w1.
A strong warming (up to $3°C$) occurs over the African and Indian monsoon regions which is consistent with increased mean insolation in the tropics (cf. to insolation differences at the top of the atmosphere between present day and 113 kyrs BC in Fig. 1, right in Jochum et al. (2010)).

5.3 Implications for glacial inception scenario

Jochum et al. (2012) show, by comparing a pre-industrial control simulation with a simulation of the same model but with orbital conditions of 113 kyrs BC, that - as hypothesized

by Milankovitch- the only necessary feedback for a glacial inception scenario is the positive snow-albedo feedback, due to reduced snow and sea ice melt during summer. An atmospheric heat budget reveals that this positive feedback is almost compensated by increased atmospheric heat transport and reduction of low cloud cover in the Arctic (Jochum et al., 2012) . The ocean heat transport recovers after an initial weakening almost completely (both AMOC and SPG). The authors suggested that the better representation of orography in their high resolution atmosphere (finite volume 1° core) is a main reason for the realistic increase in snow accumulation compared to earlier modelling results. Given the lower atmospheric resolution (2 ° finite volume core) in CONT, DO_113k and DO_71k we first confirm the snow accumulation changes (ocean circulation changes were confirmed in the previous section) under different orbital conditions. We show further that the NA cooling in association with NA_c1 results in net snow accumaltion changes similar to the one in Jochum et al. (2012)'s study.
The colder surface temperature in DO_113k and DO_71k in high northern latitudes are linked to increased net snow accumulation of up to 0.4 $m(yr)^{-1}$ over Greenland, the Aleutian Arc, northern Siberia and the Canadian Archipelago. (Fig. 5.6 (b) and (c)). Compared to Jochum et al. (2012)'s study the snow accumulation is weaker over Greenland in DO_113k and DO_71k, but enhanced over the Chukotsky Range in eastern Siberia. In particular in northern America and the Canadian Archipelago increase in snow accumulation and the southward extension of perennial snow covered areas (red and blue shading in Fig. 5.6) are in good agreement with Jochum et al. (2012)'s findings. Jochum et al. (2012) demonstrates that the increase in net snow accumulation is almost solely the result of reduced snow melt. We assume due to model similarity and the good agreement in ocean circulation and snow accumulation changes of DO_113k and DO_71k that this is as well true for our experiments.
The changes in net snow accumulation between NA_w1 and NA_c1 in CONT are smaller in amplitude, but of the same order of magnitude as those induced by the different orbital conditions (Fig. 5.6 (a)). Net snow accumulation increases for NA_c1 at the same locations, with a maximum change of 0.25 $m(yr)^{-1}$ over the Canadian Archipelago. This is also the only increase in spatial extent of areas with a perennial minimum snow height of ≥ 1 cm during NA_c1. Areas with persistent snow cover during summer indicate where ice sheet growth would start if an ice sheet module was included. The difference between the blue and red areas and increased net snow accumulation in DO_113k, DO_71k and NA_c1 coincide with the starting location of ice sheet build up during the last glacial inception, based on ice sheet reconstructions (Svendsen et al. (2004), Kleman et al. (2010)).

5.4 Summary & Discussion

We have shown that changes in the NA climate, associated with a switch between a strong and a weak circulation mode of the SPG, can also be triggered by changes in orbital conditions. This supports the important role of the SPG circulation for climate changes in the entire NA region and its sensitivity to perturbations. The snow accumulation changes associated with the changed orbital conditions are in good agreement with the findings of Jochum et al. (2012) and are comparable in amplitude and location with snow accumulation differences between NA_c1 and NA_w1.
It is widely accepted that the main driver of glacial-interglacial transitions is the orbital forcing (Milankovitch-theory). However, as pointed out in the introduction, there are still challenges to the Milankovitch theory. Thus, the exact timing of glacial inceptions and terminations might very well be due to various other processes such as for example an internal mode of variability. The present results indicate that internal climate variability has the potential to contribute to glaciations. However, the results presented in this section need further investigation, in particular an ice sheet model response to the net snow accumulation changes would be of interest. One could imagine model simulations to determine how much the various processes contribute to ice sheet growth, by combining the snow accumulation changes from this simulation with changes from different orbital conditions in a Monte Carlo way and use them as forcing for an ice sheet model.

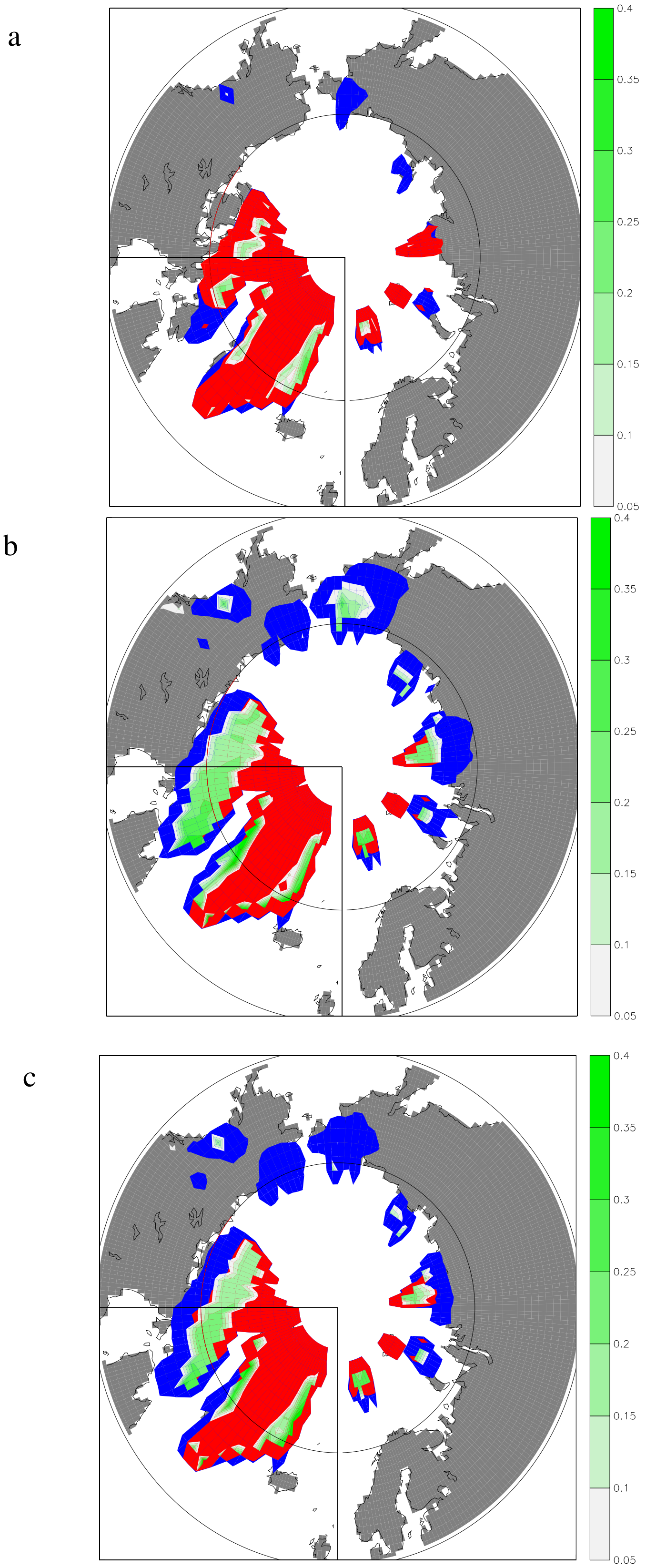

Figure 5.6.: Net snow accumulation [$m \cdot yr^{-1}$] differences are indicated by the green shading. Red and blue shadings represent areas with summer (minimum) snow height over land $\geq 1cm$. (a) Difference between cold (year 451-470, blue areas) and warm (year 51-70, red areas) phase of CONT. (b) Difference between CONT (warm, red areas) and DO_113k (blue areas). (c) Difference between CONT (warm, red areas) and DO_71k (blue areas).

Bibliography

Andrews, J., and M. Mahaffy, 1976: Growth rate of the Laurentide Ice Sheet and sea level lowering (with emphasis on the 115,000 BP sea level low). *Quaternary Research*, **6 (2)**, 167–183.

Capron, E., and Coauthors, 2010: Synchronising EDML and NorthGRIP ice cores using $\delta^{18}O$ of atmospheric oxygen ($\delta^{18}O_{atm}$) and CH_4 measurements over MIS5 (80–123 kyr). *Quaternary Science Reviews*, **29 (1)**, 222–234.

Gildor, H., and E. Tziperman, 2000: Sea ice as the glacial cycles' climate switch: Role of seasonal and orbital forcing. *Paleoceanography*, **15 (6)**, 605–615.

Huybers, P., and C. Langmuir, 2009: Feedback between deglaciation, volcanism, and atmospheric CO_2. *Earth and Planetary Science Letters*, **286 (3)**, 479–491.

Imbrie, J., and Coauthors, 1993: On the structure and origin of major glaciation cycles 2. The 100,000-year cycle. *Paleoceanography*, **8**, 699–735.

Jochum, M., A. Jahn, S. Peacock, D. A. Bailey, J. T. Fasullo, J. Kay, S. Levis, and B. Otto-Bliesner, 2012: True to Milankovitch: Glacial Inception in the new Community Climate System Model. *J. Climate*, **25 (7)**, 2226–2239, doi:10.1175/JCLI-D-11-000.44.1.

Jochum, M., S. Peacock, K. Moore, and K. Lindsay, 2010: Response of air-sea carbon fluxes and climate to orbital forcing changes in the Community Climate System Model. *Paleoceanography*, **25 (3)**, 1944–9186, doi:10.1029/2009PA001856, URL http://dx.doi.org/10.1029/2009PA001856.

Kleman, J., K. Jansson, H. De Angelis, A. P. Stroeven, C. Hättestrand, G. Alm, and N. Glasser, 2010: North American ice sheet build-up during the last glacial cycle, 115–21kyr. *Quaternary Science Reviews*, **29 (17)**, 2036–2051.

Milankovitch, M., 1941: *Kanon der Erdebestrahlung und seine Anwendung auf das Eiszeitenproblem*. Königlich Serbische Akademie.

Mix, A. C., 1992: The marine oxygen isotope record: constraints on timing and extent of ice-growth events (120–65 ka). *Geological Society of America Special Papers*, **270**, 19–30.

Mudelsee, M., and M. Schulz, 1997: The Mid-Pleistocene climate transition: onset of 100 ka cycle lags ice volume build-up by 280 ka. *Earth and Planetary Science Letters*, **151 (1)**, 117–123.

Petit, J.-R., and Coauthors, 1999: Climate and atmospheric history of the past 420,000 years from the Vostok ice core, Antarctica. *Nature*, **399 (6735)**, 429–436.

Svendsen, J. I., and Coauthors, 2004: Late Quaternary ice sheet history of northern Eurasia. *Quaternary Science Reviews*, **23 (11)**, 1229–1271.

6 Discussion & Conclusion

The prevailing view attributes D-O events to a severe reduction in AMOC strength, thought to be triggered by fresh water capping of the NA deep water formation sites. However, there exist several challenges to this hypothesis. The most important ones are likely (a) the ambiguous evidence for fresh water input in the NA during D-O events and the open question what could have caused them (b) the ongoing debate about severe changes in AMOC during D-O events and (c) the different responses that are simulated by various GCMs, dependent on model details, the location and timing of the fresh water input. Recently, an increased number of coupled climate models showed spontaneously arising climate transitions (see Chapter 1).
Motivated by this results we raised the question whether internal climate variability can account for aspects of millennial scale climate variability.

A satisfying hypothesis for D-O cycles should be capable to explain the characteristic global scale changes that are associated with D-O cycles. We presented evidence for changes in CONT in the NA region that feature several important aspects of D-O cycles. These are namely the sawtooth shaped temperature changes in Greenland, high amplitude SST changes in the LS and the northern NA, atmospheric rearrangements previous to or simultaneously with Greenland temperature changes as well as a cooling of the entire northern high latitudes. Furthermore, the shift in the tropical Pacific towards predominant El Niño-like conditions and the associated increase in ENSO variance agree with reconstructions. However, several characteristic aspects of D-O cycles are absent in CONT or present but have to small amplitudes compared to reconstructions. These are:

- amplitude and spatial extent of NA temperature changes
- pronounced ITCZ shifts over all ocean basins and closely related to this, changes in the global monsoon system
- SH warming

Although the said shortcomings are most likely linked to each other - for example a pronounced SH warming can also promote a southward migration of the ITCZ (Cvijanovic et al., 2013) - we follow the general structure of this thesis and discuss the discrepancies between the climate transitions in CONT and D-O cycles separately for the NH and the tropics. Since a clear temperature signal in the SH is absent in CONT nothing specific can be said here and we do not address the SH in the discussion.

It has been often suggested that the Holocene climate is stable and that the underlying dynamics of millennial scale climate variability thus require glacial boundary conditions as for example the presence of the Laurentide and Fennoscandian ice sheets (see e.g. Wunsch (2006)). However, Bond et al. (1997) suggest “mini-D-O events ” during the Holocene based on IRD changes in two marine sediment cores from the NA. Moy et al. (2002) suggest further that millennial scale ENSO variability is linked to these “mini-D-O events ” during the Holocene. An alternative hypothesis could thus be that the underlying dynamics of Holocene and last glacial climate variability are the same, but the amplitude and time scales are dependent on boundary conditions.

Therefore the main focus of the discussion in each section lies on how dependent the proposed mechanism is on background conditions and how glacial boundary conditions could alter them.

6.1 Northern hemisphere

The amplitude in Greenland temperature change is smaller by about a factor of 2 to 3 compared to reconstructions of Greenland temperature over a D-O cycle. Locally, over the LS and parts of the subpolar gyre the temperature anomaly amounts to $\sim 12°C$, owed to the direct effect of sea ice anomalies that insulate the atmosphere from the ocean heat content. Li et al. (2010) demonstrate that sea ice anomalies in the Nordic seas effect Greenland temperatures more efficiently than sea ice anomalies in the western NA. The simplest scenario for higher amplitude changes in Greenland and the entire northern high latitudes is hence a more extensive sea ice anomaly in association with the NA cold phases, extending into the Nordic Seas. Changes of up to 50% in sea ice concentration occur during NA cold phases off the coast of northern Norway, but are confined to the sea ice edge.

6.1.1 Background dependence

Under glacial boundary conditions the sea ice edge in the NA extends farther south than under pre-industrial conditions in CONT (e.g., De Vernal et al. (2006)). SST anomalies in association with the NA cold phases extend with amplitudes of $2°C$ to $4°C$ far into the Nordic seas. It seems plausible that sea ice anomalies linked to the mode switch of

SPG circulation could extend farther, when SSTs are generally colder as it is the case for glacial boundary conditions. Together with the aforementioned results of Li et al. (2010) this could provide a means by which our identified mechanism could attain higher amplitude temperature anomalies.

In CONT only minor changes in the thermohaline structure of the Nordic Seas occur. This is likely linked to the fact that deep water formation in the Nordic Seas persists also during the cold NA phase. Under glacial boundary conditions modeling studies suggest that the sinking branch of the AMOC is shifted southward, away from the Nordic Seas associated with a distinct lower heat transport (Brandefelt and Otto-Bliesner, 2009). The ocean heat transport in the subpolar NA is dominated by the horizontal component of the AMOC - the gyre circulation (Rhein et al., 2011). A sudden switch of the SPG to a strong circulation mode - as seen in CONT during the transition to the second NA warm phase - could revive a stronger ocean heat flux into the Nordic Seas and trigger more extensive sea ice anomalies. Additionally Chiang and Bitz (2005) have shown that extensive sea ice anomalies in the Nordic Seas, the LS and the north western Pacific cause an ITCZ response comparable, spatially and in amplitude, to fresh water hosing experiments with the associated AMOC shut down. If the sea ice anomalies between cold and warm NA phases were more extensive under glacial boundary conditions, they could trigger an adequate ITCZ response. This is also relevant for a more pronounced response in the SH through the surface ocean-atmosphere interhemispheric coupling mechanism described by Chiang et al. (2014) and Lee et al. (2011).

However, we demonstrated by comparison of CONT and HI that the sensitivity of the SPG to small perturbations depends itself crucially on the mean background climate, which is also likely to change under glacial boundary conditions. The weak SLP gradient between Azore high and Iceland low in CONT result in a smaller SLP anomaly that is necessary to weaken the gradients sufficiently to trigger said ocean circulation changes. Under glacial boundary conditions this gradient is however expected to strengthen compared to a pre-industrial climate with important effects for the strength of the atmospheric jets and atmospheric meridional heat transport (e.g., Pausata et al. (2011); Li and Battisti (2008)). The combined effect of these distinct differences between pre-industrial and glacial boundary conditions are to complex to predict whether the proposed mechanism provides also a plausible scenario for glacial climates. In Section 6.3 we propose a simple box model that could be used to address the question of background dependence, instead of computational costly GCM simulations.

6.2 Tropics

A pronounced southward migration of the ITCZ is absent in CONT. Changes in the global monsoon system in association with D-O cycles are closely linked to ITCZ migration and therefore we did not further examine, whether any minor monsoonal changes occurred during the NA cold and warm phases.
We attributed the absence of the Atlantic ITCZ migration mainly to (a) the relatively regional confined high amplitude cooling compared to fresh water hosing simulations (cf. Fig. 2.3 to Fig. 2 in Kageyama et al. (2013)) and (b) the absence of a distinct warming in the South Atlantic in association with a weak AMOC reduction ($\sim 4\,Sv$) during NA cold phases.
Support for this argument comes from a study of a multi-model ensemble of fresh water perturbed simulations under LGM boundary conditions (Kageyama et al., 2013). The authors find an almost linear relationship between simulated NA cooling amplitude and precipitation anomalies in the equatorial Atlantic.
During present El Niño events the SST pattern in the tropical Pacific becomes more symmetric around the equator, resulting also in a mean southward migration of the ITCZ in the Pacific (Fedorov and Philander, 2000). However, the dominant El Niño-like conditions during NA cold phases in CONT did not cause any significant changes in the Pacific ITCZ. We speculate that this is also attributable to a relative small amplitude of the mean changes in the tropical Pacific in CONT.

6.2.1 Background dependence

Orbital conditions - mainly through variations in precession - effect the seasonal cycle in the tropics. ENSO amplitude, period and irregularity are largely set by the seasonal cycle (e.g., Tziperman et al. (1997)). Further Timmermann et al. (2007) and Clement et al. (2001) have shown in modeling studies that abrupt changes in ENSO behaviour can occur in response to the slowly varying orbital forcing. How such forced changes in ENSO characteristics interact with internal variability of the ENSO system on decadal to centennial time scales remains to be investigated. For a mid- Holocene simulation Karamperidou et al. (2015) show that the frequency of strong EP ENSO flavours decreases significantly by about 50 % relative to a pre-industrial control simulation, this is accompanied by a decrease in EP ENSO variance by 30 %. In contrast no change in variance of the CP flavour occurs and the frequency of CP ENSO events increases slightly. The authors attribute the different trends in CP versus EP flavours to their differing response to the seasonality of the cold-tongue. Orbital induced changes in the seasonality of western Pacific wind

forcing, which acts to deepen the eastern Pacific thermocline, reduce the stratification and weaken the upwelling feedback. The upwelling feedback is determining for the evolution of EP ENSO flavours, whereas the evolution of CP flavours depends on the zonal advection feedback (Karamperidou et al., 2015; Fedorov and Philander, 2000).
This study demonstrate the importance of orbital forcing for the evolution of EP versus CP ENSO flavours. The interactions between internal climate variability (the Modoki mode in CONT) and orbital induced changes in the tropical Pacific are again to complex to make any meaningful predictions on the influences of glacial boundary conditions on the Modoki mode. To address the question how the internal mode of variability - the Modoki mode - evolves under and interacts with different boundary conditions, a study similar to Karamperidou et al. (2015)'s study but under glacial boundary conditions (or better a transient simulation) could provide further insight.
Another question that deserves further attention relates to the time scales. In CONT the variations in the Modoki mode feature a centennial time scale, whereas most D-O cycles lasted for millennia-long. Timmermann et al. (2007) suggest a four-dimensional homoclinic bifurcation scenario for the generation of decadal scale variations of the Modoki mode. Higher dimension homoclinic bifurcations can generate chaotic behaviour (Glendinning and Sparrow, 1984) and therefore can exhibit very long time scales (Lorenz, 1991). However, there is still considerable debate on whether ENSO behaves as a non-linear self-sustained oscillator or a linear dampened mode, excited by stochastic forcing (see e.g., Wang et al. (2012) for a review on the different theoretical concepts of ENSO dynamics).
The changes in ENSO variance and the east-west displacement associated with the internal Modoki mode in CONT are qualitatively similar to the orbital induced changes in ENSO flavours seen in Karamperidou et al. (2015)'s study. Alternatively to our hypothesis of internal tropical variability triggering the NA cold phases, orbital induced changes provide an other means.
The results of Chapter 3 point towards a tropical trigger of the NA cold and warm phases. However, to address the question about the cause and effect relationship, targeted experiments with modified tropical Pacific SST anomalies are necessary.

We conclude, with the constraint of the aforementioned background climate dependency, that internal climate variability can account for several important aspects of millennial scale climate variability. The absence of a SH response in CONT is likely the most important deficiency and has to be addressed by future research.
If it turns out that glacial boundary conditions are not favourable for the scenario sug-

gested in this thesis, it can still be applicable for Holocene variability, such as the Little Ice age, the 1920-Greenland warming or the reconstructions of millennial scale climate variability in the Pacific and NA (Moy et al. (2002) and Bond et al. (1997), respectively).

6.3 Future prospects

6.3.1 A simple box model for SPG - sea ice - atmosphere interactions

Based on the key feedback mechanisms identified in CCSM4 we started to develop a simple box model including the dynamical interaction between the subpolar gyre, the atmosphere and sea ice. This model can then be used to examine the dependence of the proposed mechanism on background climate. A simple box model is computational efficient and it will be therefore possible to analyse a parameter space for the hysteresis behaviour in SPG transport.
The simple box model is based on a slightly modified version of a four-box model of the SPG (Born and Stocker, 2014). The box model consists of a lower and upper box in the central SPG and the rim current of the SPG. Only temperature and salinity in the inner boxes are calculated prognostically. Temperature and salinity of the rim current are constant and represent in this regard an infinitive heat and salinity reservoir. The temperature of the upper inner box is determined by solar insolation (in the modified version) and the exchange of temperature with the outer box. The salinity of the upper inner box changes, additionally to the exchange with the outer box, through a surface freshwater flux (representing the precipitation-evaporation balance). The gyre velocity consists of a density driven and a wind driven component. The former is calculated according to thermal wind from the variations in temperature and salinity in the central part of the SPG, relative to the constant temperature and salinities of the outer boxes. The salinity and temperature fluxes between the inner and outer boxes depend on the respective differences in these properties and the velocity of the outer rim current. The velocity dependence is represented as a parametrized eddy flux. Convective overturning occurs when the density of the upper box exceeds the density of the lower box and the two water masses are entirely mixed. This box model features a hysteresis behaviour of the SPG transport in response to changes in either salinity advection of the rim current of the SPG or net freshwater flux. The non-linearity arises from the interaction of the eddy driven salinity flux into the central part of the SPG and the strength of the buoyancy driven circulation (Born and Stocker, 2014). We coupled the SPG model to a simple thermodynamic zero-layer sea ice model (Semtner Jr, 1976). To allow for a partially sea ice covered SPG the sea ice concentration is assumed to vary with the sea ice height. To represent the important

atmospheric feedback to sea ice anomalies, we calculate a geopotential height anomaly dependent only on the atmospheric temperature anomaly, that is assumed to be the areal weighted temperature over sea ice and over the open ocean. The hypsometric equation is used to relate the temperature anomaly to a change in geopotential height. By assuming a constant underlying north-south gradient of geopotential height we can infer a zonal wind strength anomaly from thermal wind, using the constant background gradient and the anomaly. Calculating the geopotential height anomaly directly from the atmospheric temperature anomaly implies the assumption of no horizontal advection. The wind driven velocity is assumed to vary linearly with the strength of the wind anomaly. In a first step the hysteresis behaviour of the modified model and the effect of the sea ice -atmosphere feedback on it has to be verified and tested. In a second step the parameter space of the hysteresis has to be determined. In a third step the effect of different boundary conditions (i.e., glacial) can be tested by an offset in the north-south geopotential height gradient, different insolation and possibly a different net freshwater flux.

6.3.2 The 1920 Greenland warming - a modern analogue?

An important step for future research is to verify the proposed mechanism with observational evidence. However, reconstructions of ocean circulation are sparse and we are not aware of any study trying to reconstruct the SPG circulation strength during the last glacial. Similarly the SLP-sea ice feedback cannot be tested against reconstructions. However, as pointed out to me by Bo Vinther, during the mid-twenties an abrupt warming of several degrees is recorded in Greenland (Cappelen, 2013). The increase by about $3-4°C$ occurs over a decade, is followed by a rather gradual cooling trend over the next decades until the beginning of the 1980ies (Fig. 6.1). Giese and Ray (2011) analyse SODA 2.2.4 reanalysis data and find that from 1890 to 1920 ENSO events were as strong as during the end of the 20th century (post 1976). In between there is a period of relative weak ENSO variability and during the 1930ies even a complete absence of El Niño events. Furthermore the strong ENSO events (pre- 1920 and post 1970) show a tendency to occur farther to the east (Giese and Ray, 2011). However, Giese and Ray (2011) also note that the null hypothesis that the east-west displacement is due to a random distribution around a mean latitude cannot be rejected.

Lastly we note that the end of Greenland warming coincides with three relatively unique events of the instrumental record period, the Weddell Sea polynya in the south, the great salinity anomaly in the NA and a major shift of ENSO properties (e.g., Zhang et al. (1997); Fedorov and Philander (2000); Wang and An (2002)). Each of these phenomenons has been studied previously. We think however that it is worth revisiting these events and to analyse whether these events could support the findings of this thesis.

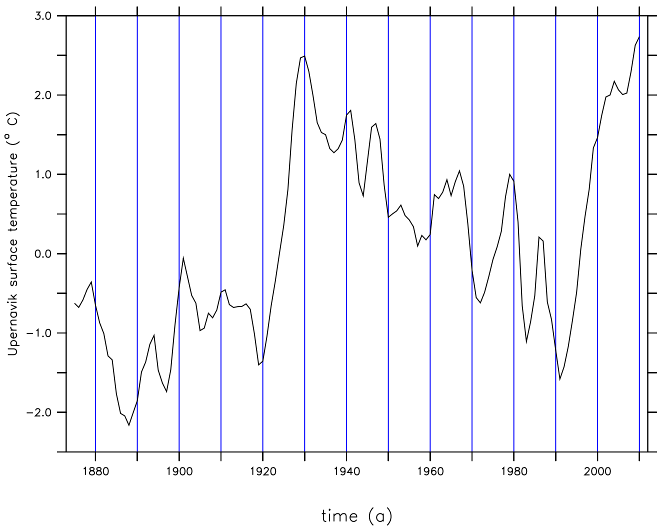

Figure 6.1.: Upernavik annual mean surface temperature anomaly from a meteorologic station in Greenland. Data are from Cappelen (2013). The time series is smoothed by a 4 year running mean.

Bibliography

Bond, G., and Coauthors, 1997: A pervasive millennial-scale cycle in North Atlantic Holocene and glacial climates. *Science*, **278 (5341)**, 1257–1266, doi:10.1126/science.278.5341.1257.

Born, A., and T. F. Stocker, 2014: Two stable equilibria of the Atlantic subpolar gyre. *J. Phys. Oceanogr.*, **44 (1)**, 246–264.

Brandefelt, J., and B. Otto-Bliesner, 2009: Equilibration and variability in a Last Glacial Maximum climate simulation with CCSM3. *Geophysical Research Letters*, **36 (19)**.

Cappelen, J., 2013: Greenland-DMI historical climate data collection 1873-2012 - with Danish abstracts. *DMI Technical Report 13-04. Copenhagen*, [http://www.dmi.dk/laer-om/generelt/dmi-publikationer/2013/].

Chiang, J. C., S.-Y. Lee, A. E. Putnam, and X. Wang, 2014: South Pacific Split Jet, ITCZ shifts, and atmospheric North–South linkages during abrupt climate changes of the last glacial period. *Earth and Planetary Science Letters*, **406**, 233–246.

Chiang, J. C. H., and C. M. Bitz, 2005: Influence of high latitude ice cover on the marine Intertropical Convergence Zone. *Clim. Dynam.*, **25 (5)**, 477–496, doi:10.1007/s00382-005-0040-5.

Clement, A. C., M. A. Cane, and R. Seager, 2001: An Orbitally Driven Tropical Source for Abrupt Climate Change. *Journal of Climate*, **14 (11)**, 2369–2375.

Cvijanovic, I., P. L. Langen, E. Kaas, and P. D. Ditlevsen, 2013: Southward intertropical convergence zone shifts and implications for an atmospheric bipolar seesaw. *Journal of Climate*, **26 (12)**, 4121–4137.

De Vernal, A., A. Rosell-Melé, M. Kucera, C. Hillaire-Marcel, F. Eynaud, M. Weinelt, T. Dokken, and M. Kageyama, 2006: Comparing proxies for the reconstruction of LGM sea-surface conditions in the northern North Atlantic. *Quaternary Science Reviews*, **25 (21)**, 2820–2834.

Fedorov, A. V., and S. G. Philander, 2000: Is El Niño changing? *Science*, **288 (5473)**, 1997–2002.

Giese, B. S., and S. Ray, 2011: El Niño variability in simple ocean data assimilation (SODA), 1871–2008. *Journal of Geophysical Research: Oceans (1978–2012)*, **116 (C2)**.

Glendinning, P., and C. Sparrow, 1984: Local and global behavior near homoclinic orbits. *Journal of Statistical Physics*, **35 (5-6)**, 645–696.

Kageyama, M., and Coauthors, 2013: Climatic impacts of fresh water hosing under Last Glacial Maximum conditions: a multi-model study. *Climate of the Past*, **9 (2)**, 935–953.

Karamperidou, C., P. N. Di Nezio, A. Timmermann, F.-F. Jin, and K. M. Cobb, 2015: The response of ENSO flavors to mid-Holocene climate: Implications for proxy interpretation. *Paleoceanography*.

Lee, S.-Y., J. C. Chiang, K. Matsumoto, and K. S. Tokos, 2011: Southern Ocean wind response to North Atlantic cooling and the rise in atmospheric CO2: Modeling perspective and paleoceanographic implications. *Paleoceanography*, **26 (1)**.

Li, C., and D. S. Battisti, 2008: Reduced Atlantic storminess during Last Glacial Maximum: Evidence from a coupled climate model. *Journal of Climate*, **21 (14)**, 3561–3579.

Li, C., D. S. Battisti, and C. M. Bitz, 2010: Can North Atlantic Sea Ice Anomalies Account for Dansgaard-Oeschger Climate Signals? *J. Climate*, **23 (20)**, 5457–5475.

Lorenz, E. N., 1991: The general circulation of the atmosphere: an evolving problem. *Tellus A*, **43 (4)**, 8–15.

Moy, C. M., G. O. Seltzer, D. T. Rodbell, and D. M. Anderson, 2002: Variability of El Niño/Southern Oscillation activity at millennial timescales during the Holocene epoch. *Nature*, **420 (6912)**, 162–165.

Pausata, F., C. Li, J. Wettstein, M. Kageyama, and K. Nisancioglu, 2011: The key role of topography in altering North Atlantic atmospheric circulation during the last glacial period. *Climate of the Past*, **7 (4)**, 1089–1101.

Rhein, M., and Coauthors, 2011: Deep water formation, the subpolar gyre, and the meridional overturning circulation in the subpolar North Atlantic. *Deep Sea Research Part II: Topical Studies in Oceanography*, **58 (17)**, 1819–1832.

Semtner Jr, A. J., 1976: A model for the thermodynamic growth of sea ice in numerical investigations of climate. *Journal of Physical Oceanography*, **6 (3)**, 379–389.

Timmermann, A., S. J. Lorenz, S.-I. An, A. Clement, and S.-P. Xie, 2007: The effect of orbital forcing on the mean climate and variability of the tropical Pacific. *J. Climate*, **20 (16)**, 4147–4159, doi:10.1175/JCLI4240.1.

Tziperman, E., S. E. Zebiak, and M. A. Cane, 1997: Mechanisms of seasonal-ENSO interaction. *Journal of the atmospheric sciences*, **54 (1)**, 61–71.

Wang, B., and S. An, 2002: A mechanism for decadal changes of ENSO behavior: Roles of background wind changes. *Climate Dynamics*, **18 (6)**, 475–486.

Wang, C., C. Deser, J.-Y. Yu, P. DiNezio, and A. Clement, 2012: El Nino and southern oscillation (ENSO): a review. *Coral Reefs of the Eastern Pacific*, 3–19.

Wunsch, C., 2006: Abrupt climate change: An alternative view. *Quat. Res.*, **65 (2)**, 191–203, doi:10.1016/j.yqres.2005.10.006.

Zhang, Y., J. M. Wallace, and D. S. Battisti, 1997: ENSO-like interdecadal variability: 1900-93. *Journal of climate*, **10 (5)**, 1004–1020.

Acknowledgments

First, I would like to thank Markus Jochum for the supervision and continuous support during my PhD studies and for introducing me to many climate scientists. It was a pleasure to work at CIC with great and supportive colleagues. Furthermore, the support over the last month from Team Ocean is greatly appreciated and I'd like to thank Jonas Blüthgen for translating the Abstract into Danish.

I learned a lot about the southern hemisphere dynamics in the bipolar seesaw reading group that Joel Pedro organized. I really enjoyed this reading group and think it added a great deal to my understanding about paleo-proxies.

I wish to thank the Ocean and Paleoclimate Working Groups at NCAR for welcoming me, discussing with me and supporting me with the CCSM simulations. A special thanks goes here to Bette Otto-Bliesner and Stephen Yeager. AK, I really enjoyed the time we spent together in Boulder.

Marlene Klockmann is greatly acknowledged for proofreading Chapter 5 and parts of the Introduction. Marlene tausend Dank, dass du mich gleich verstanden hast.

In particular during the last half year, all the motivation and moral support I needed came from my family and Corentin Reutenauer. Danke und Merci! Je sais j'étais odieuse des fois - sans toi je n'arrive pas à finir ma these.

And many more, that I fail to remember right now. I also like to acknowledge the use of Ferret (Ferret, NOAA's Pacific Marine Environmental Laboratory at http://ferret.pmel.noaa.gov/Ferret/) and NCL (The NCAR Command Language (Version 6.1.0), Boulder, Colorado: UCAR/NCAR/CISL/TDD.http://dx.doi.org/10.5065/D6WD3XH5) for analysis and graphics.

A Appendix

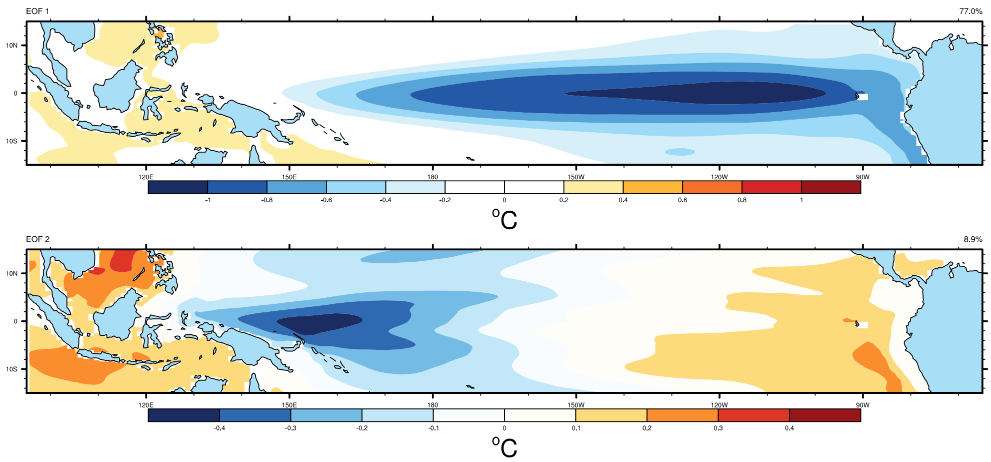

Figure A.1.: EOF 1 (77 % explained variance) and EOF 2 (8.9 % explained variance) of unfiltered SST anomalies in the tropical Pacific. EOF 2 corresponds to the Modoki mode.

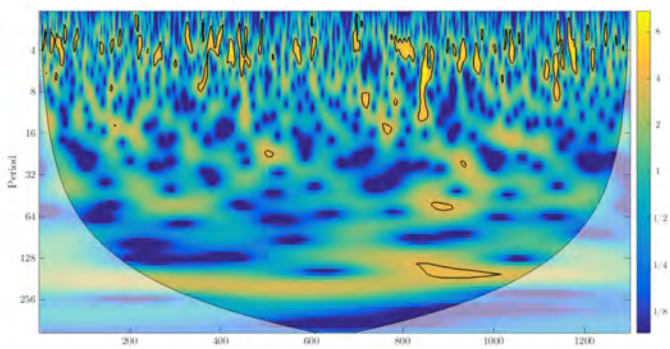

Figure A.2.: Wavenumber 6 Morlet Wavelet analysis of PC 2 of tropical Pacific SST anomalies in HI in units of normalized variance (σ^2). The black contours represent the 95%- confidence level assuming red noise. The transparent regions on the sides of the figure represent the Cone of Influence, where edge effects become important. The Figure was produced with the matlab toolbox of Grinsted et al. (2004)

a

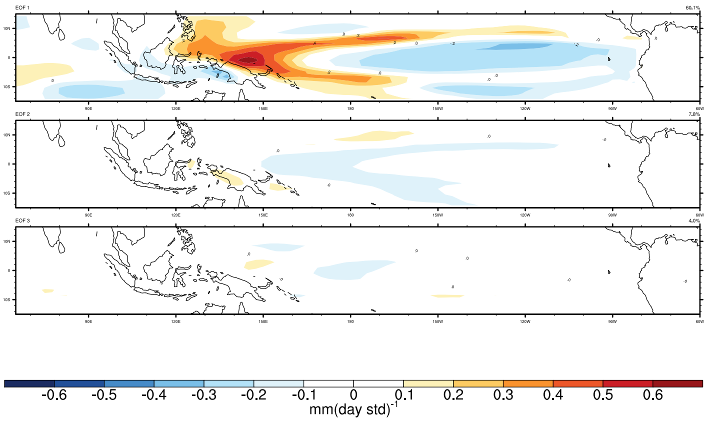

b

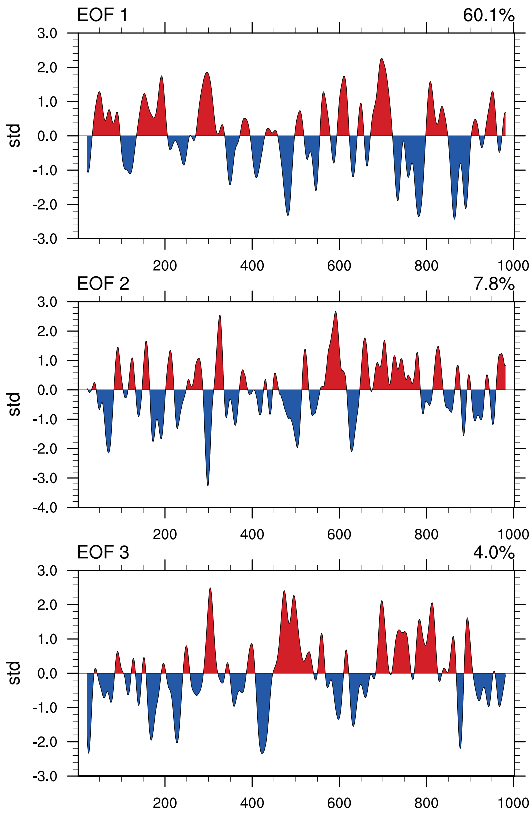

Figure A.3.: (a) Tropical Pacific EOF 1 to 3 of LP filtered precipitation anomalies in units of $mm(day \cdot std)^{-1}$. The corresponding PCs are shown in (b).

Abbreviation list

AABW	Antarctic Bottom Water
ACC	Antarctic Circumpolar Current
ADP	Antarctic Dipole Pattern
AIM	Antarctic Isotope Maximum
AMOC	Atlantic Meridional Overturning Circulation
BSF	Barotropic Stream Function
CP	Central Pacific
D-O events	Dansgaard-Oeschger events
DEAM	Decadal ENSO Amplitude Modulation
EASM	East Asian Summer Monsoon
ENSO	El Niño Southern Oscillation
EMIC	Earth System Model of Intermediate Complexity
EOF	Empirical Orthogonal function
EP	Eastern Pacific
IRD	Ice Rafted Debris
ISM	Indian Summer Monsoon
ITCZ	Intertropical Convergence Zone
GCM	General Circulation Model
GS	Greenland Stadial
GI	Greenland Interstadial
HP	High Pass
LGM	Last Glacial Maximum
LP	Low Pass
LS	Labrador Sea
MLD	Mixed Layer Depth
MIS3	Marine Isotope Stage 3
NA	North Atlantic
NADW	North Atlantic Deep Water
NAO	North Atlantic Oscillation
NH	Northern Hemisphere
PC	Principal Component
SASM	South American Summer Monsoon
SH	Southern Hemisphere
SLP	Sea Level Pressure
SPG	Subpolar Gyre
SST	Sea Surface Temperature
STG	Subtropical Gyre
WPWP	West Pacific Warm Pool